

AD-A091 858

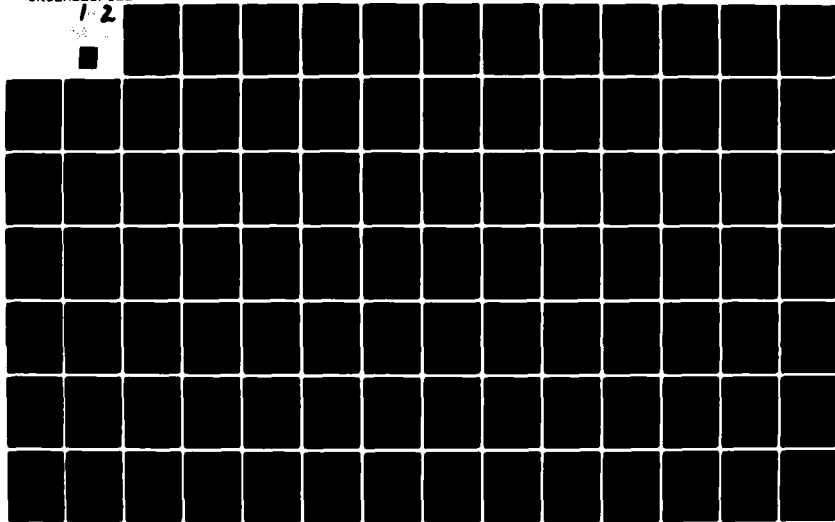
MASSACHUSETTS INST OF TECH CAMBRIDGE CENTER FOR MATE--ETC F/G 7/4  
ELECTRONIC AND OPTICAL PROPERTIES AND MODELING OF INTERCALATED --ETC(U)  
SEP 80 M S DRESSSELHAUS, G DRESSSELHAUS AFOSR-77-3391

UNCLASSIFIED

AFOSR-TR-80-1065

NL

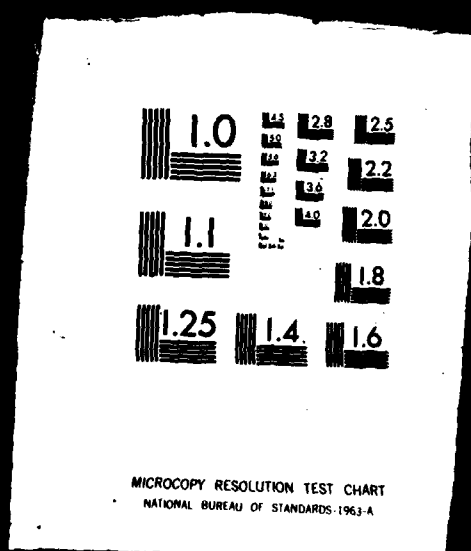
1-2



# ASSIFIE

## 1 OF 2

### AD A 091858



AFOSR-TR- 80 - 1065

LEVEL II

4

FINAL REPORT

to the

Air Force Office of Scientific Research

for research on

Electronic and Optical Properties and

Modeling of Intercalated Graphite

AFOSR-77-3391

for the years

July 15, 1977 - Sept. 30, 1980

Principal Investigator: M.S. Dresselhaus

Co-Principal Investigator: G. Dresselhaus

Room 13-2090

Massachusetts Institute of Technology

Center for Materials Science and Engineering

77 Massachusetts Avenue

Cambridge, Massachusetts 02139

Tel No. (617) 253-6864

September 30, 1980

Approved for public release;  
distribution unlimited.

80 10 21 097

AD A091858

BDC FILE COPY

UNCLASSIFIED

## REPORT DOCUMENTATION PAGE

READ INSTRUCTIONS  
BEFORE COMPLETING FORM

1. REPORT NUMBER (18) AFOSR TR-80-1065	2. GOVT ACCESSION NO. AD-A091 850	3. RECIPIENT'S CATALOG NUMBER
4. TITLE (and Subtitle) Electronic and Optical Properties and Modeling of Intercalated Graphite		5. DATE OF REPORT & PERIOD COVERED Final Rept. July 15, 1977-October 14, 1980
6. AUTHOR(s) M.S. Dresselhaus G. Dresselhaus		7. PERFORMING ORG. REPORT NUMBER JUL 77-14 OCT 80
8. CONTRACT OR GRANT NUMBER(s) AFOSR-77-3391		
9. PERFORMING ORGANIZATION NAME AND ADDRESS M.I.T. 77 Massachusetts Avenue Cambridge, Mass. 02139		10. PROGRAM ELEMENT, PROJECT, TASK AREA & WORK UNIT NUMBERS 61102F (16) 2306 (17) 82
11. CONTROLLING OFFICE NAME AND ADDRESS Air Force Office of Scientific Research Bolling AFB, DC 20032		12. REPORT DATE September 30, 1980
14. MONITORING AGENCY NAME & ADDRESS (if different from Controlling Office)		13. NUMBER OF PAGES 96
		15. SECURITY CLASS. (of this report) unclassified
		15a. DECLASSIFICATION/DOWNGRADING SCHEDULE

## 16. DISTRIBUTION STATEMENT (of this Report)

Approved for public release;  
distribution unlimited.

## 17. DISTRIBUTION STATEMENT (of the abstract entered in Block 20, if different from Report) Griffiss AFB N.Y.

## 18. SUPPLEMENTARY NOTES

## 19. KEY WORDS (Continue on reverse side if necessary and identify by block number)

Intercalated Graphite	Magnetoreflexion
Electronic Properties	Shubnikov-de Haas
Optical Properties	
Modeling	

## 20. ABSTRACT (Continue on reverse side if necessary and identify by block number)

Under this grant a study was carried out of the electronic and optical properties and modeling of intercalated graphite. A major contribution of this work has been the formulation of a model for the electronic structure, applicable to compounds of arbitrary stage and intercalant. The results of this model have been applied to the interpretation of Fermi surface and magnetoreflexion measurements also carried out under this grant. These measurements thus provide detailed information on the effect of intercalation on the electronic structure and on the Fermi surfaces of intercalated graphite.

DD FORM 1473

EDITION OF 1 NOV 65 IS OBSOLETE

UNCLASSIFIED

SECURITY CLASSIFICATION OF THIS PAGE (When Data Entered)

077400

(Cont')

20.

Results on infrared spectroscopy of intercalated graphite provide information on the lattice mode structure, complementing the findings on the electronic structure. The use of Raman spectroscopy to study adsorbed species on graphite surfaces is demonstrated.

UNCLASSIFIED

# Table of Contents

Table of Contents	1
1.0 Abstract	1
2.0 Personnel Involved with Research Program	3
2.1 Coupling Activities	3
2.2 New Discoveries, Patents or Inventions	4
3.0 Status of Research Effort	5
3.1 Studies of Shubnikov-de Haas Effect in Intercalated Graphite	5
3.2 Magnetoreflexion Studies of Intercalated Graphite	8
3.3 Calculations of the Electronic Energy Band Structure of Graphite Intercalation Compounds	11
3.4 Calculation of the Magnetic Energy Level Structure for Graphite Intercalation Compounds	12
3.5 Preparation of Review Article	13
3.6 Infrared Studies of Graphite Intercation Compounds	13
3.7 Study of Adsorbed Molecules on Graphite Surfaces Using Raman Spectroscopy	14
4.0 Publications	16

13 Accession For	
ERIC GRA&I	<input checked="" type="checkbox"/>
ERIC TAS	<input type="checkbox"/>
13 Unannounced	<input type="checkbox"/>
Justification	
14 By	
16 Distribution/	
Availability Codes	
Dist	Avail and/or Special
A	

AIR FORCE OFFICE OF SCIENTIFIC RESEARCH (AFSC)  
 NOTICE OF TRANSMISSION TO DDC  
 This technical report has been reviewed and is  
 approved for public release IAW ARK 190-12 (7b).  
 Distribution is unlimited.  
 A. D. BLOSE  
 Technical Information Officer

## 1.0 Abstract

Under this grant a study was carried out of the electronic and optical properties and modeling of intercalated graphite. Graphite intercalation compounds are synthetic metals with a density much less than that of copper. By the introduction of molecular intercalants, molecular conductors have been prepared which in some cases have room temperature electrical conductivities comparable to that of copper. In addition these materials can have an in-plane to c-axis anisotropy ratio in the electrical conductivity in excess of a million. Graphite intercalation compounds are therefore potentially useful for various applications in airborne systems. The research program carried out under this grant was directed toward gaining an increased understanding of graphite intercalation compounds in order to be able to produce better materials with more controlled physical properties. A major contribution of our work has been the formulation of a model for the electronic structure, applicable to compounds of arbitrary stage and intercalant. The model has been applied to the interpretation of our Shubnikov-de Haas measurements which probe the effect of intercalation on the Fermi surfaces of these materials. The model has also been extended to calculate for the first time the magnetic energy level structure of intercalated graphite, which is required to interpret our magnetoreflexion spectra. These spectra provide detailed and quantitative information on the effect of intercalation on the electronic structure of intercalated graphite. Both the magnetoreflexion and the Shubnikov-de Haas experiments require high magnetic fields and utilize the unique capabilities of the facilities at the Francis Bitter National Magnet Laboratory. Results on infrared spectroscopy of intercalated graphite provide

information on the lattice mode structure, complementing the findings on the electronic structure. The use of Raman spectroscopy to study adsorbed species on graphite surfaces is demonstrated.



## 2.0 Personnel Involved with Research Program

M. S. Dresselhaus, Principal Investigator

G. Dresselhaus, Co-Principal Investigator

B.L. Heflinger, Graduate Student (Surface Adsorption, left September 1979)

S.Y. Leung, Graduate Student (Infrared measurements, modeling of  
electronic dispersion relations)

S.A. Safran, Post-doctoral Student (theory; left September 1978)

C. Underhill, Research Engineer (experimental support, funded by MIT  
Mauzé Chair, left June 1980).

T.C. Chieu, Graduate Student (Magnetoreflexion experiment, Landau level  
calculation)

M. Shayegan, Graduate Student (Shubnikov-de Haas experiment and  
interpretation)

F. Hakimi, Graduate Student (preliminary Shubnikov-de Haas experiment)

## 2.1 Coupling Activities

The MIT group is strongly coupled to international activities on graphite intercalation compounds. We are frequently invited to present seminars at universities and in industry, to give invited papers at conferences, and to write review articles. We collaborate on studies of the infrared electronic properties of intercalated graphite with Professor P.C. Eklund and his group at the University of Kentucky; they have a strong experimental program and we work with them on modeling analysis of their results. We have a collaborative program with Professor J.P. Issi at the University of Louvain-la Neuve on thermal conductivity and thermopower of intercalated graphite.

with the experimental work done by Issi and his group and we contribute

to the materials preparation, modelling and interpretation of results.

A collaborative program with Professor M. Corson and his group at Boston

University has been on-going on Mössbauer studies of intercalated graphite-

$\text{FeCl}_3$  compounds. We prepare their samples, they make the Mössbauer measurements,

and we assist them with the interpretation of their results.

## 2.2 New Discoveries, Patents or Inventions

None

### 3.0 Status of Research Effort

Our research program on the electronic structure of graphite intercalation compounds has three major components. With the magnetoreflexion technique we obtain experimental information highly relevant to the form of the electronic dispersion relations and quantitative values for the band parameters. With the Shubnikov-de Haas techniques we obtain experimental information on the Fermi surface. Information from both of these experiments is utilized in our modelling calculations of the electronic structure, which is valid for any stage and intercalant. The experimental data obtained by the Shubnikov-de Haas and magnetoreflexion measurements are used to determine the parameters of the model calculations including the position of the Fermi level. Using our model for the dispersion relations, the magnetic level structure (Landau levels) has been calculated. These Landau levels are now being applied to a self-consistent interpretation of the magnetoreflexion and Shubnikov-de Haas experiments. We present below a brief summary of our accomplishments on each of these topics during the grant period.

#### 3.1 Studies of the Shubnikov-de Haas Effect in Intercalated Graphite

Study of the Shubnikov-de Haas (SdH) effect in graphite intercalation compounds provides information on the Fermi surfaces associated with each of the partially occupied bands. During the present grant period, a system was constructed to make Shubnikov-de Haas measurements on graphite intercalation compounds. Detailed measurements have been carried out on a series of alkali metal compounds with the intercalants potassium and rubidium and these results have been interpreted in terms of a model calculation for the electronic structure. This model calculation is described in Section 3.4.

The experimental system developed for carrying out these studies is based on the four-point method which was set up in a geometry which measures the in-plane transverse magnetoresistance. The system was set up to operate in the temperature range  $1.4 < T < 4.2 \text{ K}$  and in magnetic fields up to 15 Tesla. The system was set up so that the angular dependence of the SdH oscillations could be measured by rotating the sample around the direction of the current  $\vec{I}$ , with  $\vec{I} \perp \vec{H}$  for all rotation angles, and hence transverse magnetoresistance was always measured. Data acquisition was by computer using a MINC system and the data were manipulated to obtain a Fourier power spectrum of resistance vs.  $1/H$ , thereby yielding directly the frequencies of SdH oscillations. These frequencies are related to the extremal cross sections of the Fermi surface, and represent the final experimental output of the measurements.

During the course of these studies, a great deal of care was given to ensure the reproducibility of the data. For this reason, the experiment was performed on four potassium stage 5 samples and on one of these, the measurements were repeated several weeks later after attaching new leads.

The samples were prepared using the two-zone intercalation method with HOPG as the host material. Because of the instability of alkali-metal samples in the presence of air and moisture, a great deal of attention was given to sample handling and sample encapsulation. The stage of the samples was determined using (00 $l$ ) x-ray diffraction profiles both before and after the SdH experiments, confirming that the samples were single-staged and that no desorption had occurred during the measurements.

Our results show that measurements made on potassium samples with different stages yield distinctly different SdH frequencies. Different SdH frequencies were also obtained with another intercalant, in this

case rubidium. Hence our conclusion is that there is a unique set of SdH frequencies associated with each stage and for each donor intercalant (K,Rb). Suematsu et al. have also shown stage-dependent de Haas-van Alphen frequencies in stage 3 and 4 potassium compounds, and these authors have also reported stage and intercalant-dependent SdH frequencies. In contrast, several authors have reported stage-independent de Haas-van Alphen type frequencies in acceptor compounds, which is inconsistent with our interpretation of the Shubnikov-de Haas results for the alkali metal compounds.

Detailed results have been obtained for graphite-potassium with stages 4, 5 and 8. These spectra have been interpreted using our model for the electronic dispersion relations. Particular emphasis has been given to the interpretation of the results for stage 5 graphite-potassium, where we have the most complete experimental results. Our model for the electronic dispersion relations gives five valence and five conduction bands for a stage 5 compound. These bands are associated with the graphite  $\pi$ -bands, and arise from the  $k_z$ -axis zone folding procedure. The empirical position of the Fermi level  $E_F$  is determined to fit the SdH frequencies, yielding four partially occupied conduction bands and five completely filled valence bands. Various Fermi surface parameters have been calculated from this model, including the SdH frequencies, the cyclotron mass at  $E_F$ , the electron density for each carrier pocket and the anisotropy of the cross-section perpendicular to  $k_z$ . The generally good agreement of the observed SdH frequencies with the frequencies calculated on the basis of an empty intercalate layer model suggests that the effect of the intercalant-graphite bounding layer interactions can be treated as a perturbation and evaluated by fitting the model quantitatively to the observed SdH

frequencies. Although the Shubnikov-de Haas frequencies show a significant stage dependence and differ greatly from the SdH frequencies for graphite, we have shown that the stage dependence of these frequencies are compatible with electronic dispersion relations that are basically graphitic. The application of the band model to explain the observed SdH frequencies has been submitted for publication and a second paper emphasizing the interrelation between the magnetoreflexion and SdH results has also been submitted for publication.

### 3.2 Magnetoreflexion Studies of Intercalated Graphite

We have studied the electronic band structure of graphite intercalation compounds with the magnetoreflexion technique with particular reference to spectra associated with interband Landau level transitions. The magnetoreflexion technique provides detailed information on the form of the electronic dispersion relations and on the values of the band parameters describing these dispersion relations.

Magnetoreflexion measurements have now been carried out on well-staged acceptor compounds (with the intercalants  $\text{FeCl}_3$ ,  $\text{AlCl}_3$  and  $\text{Br}_2$ ) and on donor compounds (with Rb and K) in a liquid helium cold finger dewar and in magnetic fields up to 15 tesla at the National Magnet Laboratory. Careful preparation of well-characterized samples makes it possible to satisfy the condition  $\omega_c \tau \gg 1$  and to observe clear magnetoreflexion oscillations for almost all stages ( $n \geq 3$ ). The samples were characterized for stage index by (00 $l$ ) x-ray diffractograms both before and after the magnetoreflexion runs. Typical spectra consist of a dominant structure that is

identified with Landau level interband transitions near the K-point of the Brillouin zone of pure graphite. A quantitative analysis has been made of the observed magnetoreflexion spectra, showing that the Slonczewski-Weiss-McClure model for pure graphite accounts for the dominant structure observed for the graphite intercalation compounds, with changes in the band parameters that are measured as a function of intercalant and stage. Effective masses for the valence and conduction bands about the K-point have been determined and are found to be very small and similar to values obtained for pristine graphite.

We found that below a critical photon energy, which depends on the stage and the intercalant, no magnetoreflexion oscillations are observed experimentally. This effect is called the Fermi level cutoff phenomenon and is due to the raising of the Fermi level in donor compounds and to the lowering of  $E_F$  for acceptor compounds as a result of intercalation. Thus for the case of donor compounds, certain final states will no longer be unoccupied and for acceptor compounds certain initial states will no longer be occupied. The Pauli principle requires that transitions must occur from an occupied initial state to an unoccupied final state. Thus the observation of the cut-off phenomenon provides information on the position of the Fermi level relative to the K-point band edge for valence and conduction bands involved with the interband transition. Thus the cut-off phenomenon yields the dependence of the Fermi level  $E_F$  relative to the K-point band edge  $E_{3,K}^0$  as a function of stage and intercalant. We have obtained values for  $(E_F - E_{3,K}^0)$  for a number of intercalants and stages.

The magnetoreflexion results have been significant in demonstrating that the electronic bands near the Fermi level remain highly graphitic upon intercalation. This conclusion is basic to our formulation of the electronic dispersion relations for graphite intercalation compounds. This work is also significant insofar as it yields quantitative values for the change in band parameters and Fermi level with stage and intercalant. These data are of importance in obtaining band parameters for our electronic dispersion relations. Our present efforts focus on the calculation of the magnetic energy level structure (Landau levels) using our model for the electronic dispersion relations. These Landau levels will then be supplied to yield a consistent interpretation of the observed magnetoreflexion spectra, since the present analysis of the magnetoreflexion results has been on the basis of a graphite  $\pi$ -band model.

Since the magnetoreflexion results for intercalated graphite are very similar to those for pristine graphite while the Fermi surface measurements show that major changes occur in the Fermi surface upon intercalation, it was believed by some authors that the magnetoreflexion and Shubnikov-de Haas results are inconsistent. Our work however shows that the results from both experiments can be explained on the basis of energy bands that are highly graphitic, but that energy level shifts and Fermi level shifts occur as a result of intercalation. A paper showing the consistency of the magnetoreflexion and Shubnikov-de Haas results has been prepared and will appear in the Proceedings of the 15th International Conference on the Physics of Semiconductors. An invited talk summarizing the magnetoreflexion, Shubnikov-de Haas results and their interpretation based on our band model has been presented at Conference on the Application of High



Magnetic Fields to the Physics of Semiconductors at Hakone, September 1980, and will appear in the Conference Proceedings, published by Springer. We are the only group internationally that has presented results on the magnetoreflexion spectra of graphite intercalation compounds.

### 3.3 Calculations of the Electronic Energy Band Structure of Graphite Intercalation Compounds

We have calculated the electronic energy bands for graphite intercalation compounds using a model based in the well-established electronic structure of pristine graphite. In our work, we used the Hamiltonian developed by Slonczewski-Weiss-McClure (SWMcC) for the graphite  $\pi$ -bands, and have folded these bands along the  $k_z$  axis to account for the superlattice periodicity introduced by staging. The formulation can also treat an in-plane superlattice periodicity by in-plane zone folding, in cases where such periodicity is found experimentally. For convenience in introducing the perturbation due to the intercalant, the folded  $k$ -space Hamiltonian is transformed into a layer representation. To obtain the proper staging periodicity we replace one layer out of every  $(n+1)$  graphite layers by an intercalant layer. With the inclusion of an interaction between the intercalate layer and the graphite bounding layer, electronic structures appropriate to both donor and acceptor compounds can be obtained. The model is applicable to any intercalant and any stage, and is therefore ideally suited to the interpretation of many experiments. In our research program we have explicitly applied the model to the interpretation of the magnetoreflexion experiment, which is sensitive to the magnetic energy levels and the electronic dispersion relations, and to the Shubnikov-de Haas experiment which is sensitive to the Fermi surface. Reflectivity experiments are planned for future work to yield structure associated with

electronic transitions that can be used to test the model developed for the electronic structure on the basis of magnetoreflexion and Fermi surface measurements.

One paper on the general formulation of this model is now in press. A second paper which applies this model to the interpretation of Shubnikov-de Haas results was presented at the Provincetown Conference and will be published in Synthetic Metals. A third paper which contains details on the treatment of the in-plane superlattice symmetry was presented at the Yamada Conference on Layered Materials and will be published in Physica.

#### 3.4 Calculation of the Magnetic Energy Level Structure for Graphite Intercalation Compounds

Using the basic Hamiltonian for the electronic dispersion relations described in Section 3.3, we have for the first time calculated the magnetic energy level structure for a graphite intercalation compound. In this calculation the Luttinger transcription for the wave vector operator  $\vec{k}$  was used, and only linear terms in  $\vec{k}$  were retained in the off-diagonal terms. Trigonal warping was also neglected to simplify the calculation. With these approximations the Landau levels can be obtained in closed form. Explicit results have so far been obtained for stage 1, 3 and 5 compounds. Zone folding along  $k_z$  causes a near degeneracy of a number of bands in the vicinity of the HK axis, and this gives rise to crossings of the magnetic energy levels. Results are now being obtained for higher stage compounds for which we have detailed magnetoreflexion results so that the calculations can be applied directly to the interpretation of the experimental data. Perturbations due to higher terms in  $\vec{k}$ , trigonal warping and interaction between the intercalant and the graphite bounding layer will be

included. This will enable us to obtain information on the magnitude of these terms, which will be utilized in the model for the electronic structure.

### 3.5 Preparation of Review Article

During the period of this grant, a monograph was prepared on the general field of graphite intercalation compounds. The largest chapter of this monograph deals with the electronic properties, and was supported by this grant. This monograph, invited by Advances in Physics, has been completed and is now in the review process.

### 3.6 Infrared Studies of Graphite Intercalation Compounds

During the period July 15, 1978 - July 14, 1979, this grant supported infrared studies on intercalated graphite. During this period we studied the infrared spectra of graphite intercalated with the acceptors  $\text{FeCl}_3$  and  $\text{AlCl}_3$  and with the alkali metal donors K, Rb and Cs. The spectra were taken on a Fourier Transform Spectrometer, provided by a Central Facility of the Center for Materials Science and Engineering.

Our infrared studies of the lattice modes of graphite intercalation compounds have shown that the odd parity of the graphite modes is preserved upon intercalation and that the oscillator strength provides significant information on the dynamic effective charge and the magnitude of the dipole moments associated with the lattice mode. From analysis of the dependence of the IR-active mode frequencies on reciprocal stage, we have been able to identify modes that are associated entirely with graphite interior layers and modes which involve graphite bounding layers. For the donor compounds the infrared-active mode frequencies characteristically decrease as a function of reciprocal stage ( $1/n$ ) while for acceptor compounds, the mode frequencies

increase as a function of  $(1/n)$ . A similar behavior is found for the Raman active modes, consistent with the observed expansion of the in-plane lattice constant for donor compounds as a function of  $(1/n)$ , and suggesting that the in-plane lattice constant decreases as a function of  $(1/n)$  for acceptors. This prediction has now been confirmed experimentally in work on graphite- $\text{NiCl}_2$  compounds by Flandrois and coworkers at Bordeaux and also in work in our own group by Tania Krapchev on graphite- $\text{FeCl}_3$ .

Our infrared studies have focussed on the similarities and differences in behavior of the infrared lattice mode spectra for donors and acceptors. We have found that infrared-active modes are not observed for either donor or acceptor compounds, as expected since two layers are required to produce an infrared-active mode. For stage 2 compounds, the acceptors are infrared-active, but the donors are not. The stage-dependent frequency shift as a function of reciprocal stage is positive for the acceptors and negative for the donors. The magnitude of the frequency difference between modes involving only interior layers and modes involving bounding layers is much larger for donor compounds than for acceptors. The relative oscillator strengths of interior and bounding layer modes indicate that more charge is transferred to the graphite interior layers for the donors than for the acceptors, consistent with electrical conductivity and magnetoreflexion results.

### 3.7 Study of adsorbed Molecules on Graphite Surfaces Using Raman Spectroscopy

This study was initiated to study the connection between surface adsorption and intercalation. Bromine was chosen for the adsorbing species because  $\text{Br}_2$  is the only molecular intercalant for which Raman-active in-plane modes have been observed and because the spectra of the free molecule have been studied

extensively.

The Raman spectra at room temperature consist of numerous sharp lines in the wavenumber region  $290 < \omega < 340 \text{ cm}^{-1}$ . Extremely strong resonant Raman effects were observed when the frequency of the incident light was varied by means of a tunable dye laser. A given Raman spectrum changes radically by varying the laser energy by as little as  $1 \text{ cm}^{-1}$ . These complex spectra can be understood by a resonant Raman process involving vibrational-rotational levels of a free  $\text{Br}_2$  molecule in the ground or first excited electronic state.

The Raman spectra observed on a low temperature  $99 < T < 230 \text{ K}$  graphite surface were distinctly different from the resonantly-enhanced free molecular spectrum. The low temperature spectra showed two or more very broad lines distinctly different from either those for the free molecule or for the intercalated  $\text{Br}_2$  molecule. The low temperature Raman spectra were thus attributed to adsorbed bromine species. The Ph.D. thesis of Bruce Heflinger was based on this work.

#### 4.0 Publications

- (1) "Raman Study of Adsorbed Br<sub>2</sub> on Graphite", B.L. Heflinger, M.S. Dresselhaus and G. Dresselhaus, Bull. Am. Phys. Soc. 23, 218 (1978).
- (2) "Fermi Surface Model for Graphite-FeCl<sub>3</sub>", G. Dresselhaus and S.Y. Leung, Bull. Am. Phys. Soc. 24, 373 (1979).
- (3) "Infrared Spectroscopy of Graphite-Alkali Metal Intercalation Compounds", S.Y. Leung, C. Underhill and G. Dresselhaus, Bull. Am. Phys. Soc. 24, 374 (1979).
- (4) "Direct Determination of Charge Transfer in Graphite Intercalation Compounds", M.S. Dresselhaus, S.Y. Leung, C. Underhill and G. Dresselhaus, Bull. Am. Phys. Soc. 24, 410 (1979).
- (5) "Lattice Mode Spectra of Graphite Intercalation Compounds", C. Underhill, S.Y. Leung, G. Dresselhaus and M.S. Dresselhaus, Extended Abstracts, 14th Biennial Carbon Conference, Pennsylvania State University (1979), p. 266.
- (6) "Electronic Energy Band Structure of Graphite Intercalation Compounds", G. Dresselhaus and S.Y. Leung, Extended Abstracts, 14th Biennial Carbon Conference, Pennsylvania State University (1979), p. 498.
- (7) "Model for Electrical Conductivity of Graphite Intercalation Compounds", M.S. Dresselhaus and S.Y. Leung, Extended Abstracts, 14th Biennial Carbon Conference, Pennsylvania State University (1979), p. 496.
- (8) "Infrared and Raman Spectroscopy of Graphite-FeCl<sub>3</sub>", C. Underhill S.Y. Leung, G. Dresselhaus and M.S. Dresselhaus, Solid State Commun. 29, 769 (1979).
- (9) "Intercalation Compounds of Graphite", M.S. Dresselhaus and G. Dresselhaus, submitted (invited) to Advances in Physics.
- (10) "Phenomenological Electronic Energy Bands in Graphite Intercalation Compounds", G. Dresselhaus and S.Y. Leung, Solid State Commun. (accepted for Publication).
- (11) "Electronic Structure of Graphite-Alkali Metal Compounds", G. Dresselhaus, S.Y. Leung, M. Shayegan and T.C. Chieu, Synthetic Metals, accepted for publication.
- (12) "Phenomenological Model for the Electronic Structure of Graphite Intercalation Compounds", G. Dresselhaus and S.Y. Leung, Physica, accepted for publication.
- (13) "The Interrelation of Shubnikov-de Haas, Magnetoreflexion, and Transport Properties of Alkali Metal Donor Intercalation Compounds", M.S. Dresselhaus, G. Dresselhaus, M. Shayegan and T.C. Chieu, Proceedings of the Fifteenth International Conference on the Physics of Semiconductors, Kyoto, 1980.

- (14) "Infrared-Active Lattice Modes in Graphite-Alkali Metal Compounds", S.Y. Leung, C. Underhill, G. Dresselhaus and M.S. Dresselhaus, Solid State Commun. 33, 285 (1980).
- (15) "Electronic Energy Bands and Fermi Surfaces in Graphite Intercalation Compounds", G. Dresselhaus, S. Y. Leung and M. Shayegan, Bull. Am. Phys. Soc. 25, 298 (1980).
- (16) "Angular Dependence of SdH Frequencies in Alkali-Metal Graphite Intercalation Compounds", M. Shayegan and G. Dresselhaus, Bull. Am. Phys. Soc. 25, 299 (1980).
- (17) "A Raman Study of Bromine Adsorption on Graphite", B.L. Heflinger, Ph.D. thesis (unpublished), November, 1979.
- (18) "Magnetoreflexion and Shubnikov-de Haas Experiments on Graphite Intercalation Compounds", M.S. Dresselhaus, G. Dresselhaus, M. Shayegan and T.C. Chieu, Proceedings of the Oji International Seminar on the Application of High Magnetic Fields in the Physics of Semiconductors and Magnetic Materials, Hakone, September, 1980

12  
Abstract Submitted  
for the Washington Meeting of the  
American Physical Society  
March 27-31, 1978

Physical Review  
Classification Scheme  
Number 78.30

Bulletin Subject Heading  
Graphite Intercalation  
Compounds

Raman Study of Adsorbed Br<sub>2</sub> on Graphite.\* B.L.  
HEFLINGER, M.S. DRESSELHAUS and G. DRESSELHAUS†, MIT--  
Bromine intercalates into graphite above a threshold  
vapor pressure of 18 Torr at room temp.<sup>1</sup> At lower  
pressure bromine uptake is by surface adsorption. We  
report Raman spectra from high surface area forms of  
graphite (Grafoil and exfoliated graphite) at vapor  
pressures ranging between 10<sup>-3</sup> Torr and 20 Torr, where  
the transition from surface adsorption to bulk inter-  
calation occurs. We find the Raman spectra to be  
sensitive to both surface and bulk lattice modes. The  
surface-specific modes are shifted 60 cm<sup>-1</sup> higher in  
frequency than the bulk graphite modes (1580 cm<sup>-1</sup> and  
1600 cm<sup>-1</sup>) found in the intercalation compounds. We  
also report the frequency dependence of the bromine  
stretch mode as a function of surface coverage.

\* Sponsored under AFOSR Contract #77-3391

† Natl. Magnet Lab, supported by NSF

<sup>1</sup> J.G. Hooley, Chem. Phys. of Carbon 5, 321 (1969).

Prefer Regular Session

Submitted by

*M.S. Dresselhaus*

M.S. Dresselhaus  
Room 13-2090, M.I.T.  
Cambridge, MA 02139

Note: To be presented after paper by P.C. Eklund, N. Kambe, G. Dresselhaus  
and M.S. Dresselhaus entitled "Resonant Raman Scattering From Br<sub>2</sub>  
in Graphite Intercalation Compounds".



Abstract Submitted

for the Chicago Meeting of the

American Physical Society

Physical Review  
Classification Scheme  
Number 78.20

Bulletin Subject Heading  
Graphite Intercalation  
Compounds

Fermi Surface Model for Graphite  $\text{FeCl}_3$ .† G.

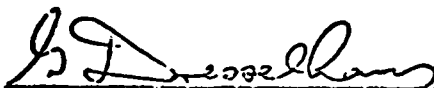
DRESSELHAUS and S.Y. LEUNG, M.I.T.--The angular dependence of the various Shubnikov-de Haas (SdH) periods on stage is interpreted in terms of fluted graphitic ellipsoidal Fermi surfaces which have extremal cross-sectional areas resulting from the staging of the intercalation compounds. The structure factor calculations indicate, in agreement with the interpretation of 0-20 x-ray spectra, that although the folded Brillouin zone for the dilute compounds is very small (indicating many extremal areas) only the Bragg reflections near those for pristine graphite have structure factor sufficiently large to yield observable SdH periods. This model accounts for (1) the observed angular dependence and cut-off phenomena for the slow and fast periods, (2) the weak stage dependence of the fast periods and (3) the larger stage dependence of the slow periods. The model also explains why the anisotropy of the Fermi surface is independent of stage and of the volume enclosed by the constant energy surfaces and is similar to that for pristine graphite.

† Supported by AFOSR Grant #77-3391.

\* Nat'l Magnet Lab, supported by NSF.

refer Regular Session

Submitted by



G. Dresselhaus  
Room 13-3017, M.I.T.  
Cambridge, MA 02139

for the Chicago Meeting of the  
American Physical Society  
March 19-23, 1979

Physics and Astronomy  
Classification Scheme  
Number 78.20.Gc

Suggested Title of Session  
in which Paper Should be Placed  
Graphite Intercalation Compounds

Infrared Spectroscopy of Graphite-Alkali Metal Intercalation Compounds† S.Y. LEUNG, C. UNDERHILL, G. DRESSELHAUS‡, M.I.T.--For the first time, infrared spectra of graphite-alkali metal donor compounds are reported. Of significance is the large ( $\approx 30\text{cm}^{-1}$ ) downshift of the infrared-active optic modes from the  $E_{1u}$  mode in graphite at  $1587\text{cm}^{-1}$ , in contrast with results observed for the acceptor compounds where the stage dependent frequency shift is smaller in magnitude and opposite in sign. Results are reported for the IR-active mode frequencies, linewidths and oscillator strengths for K, Rb, and Cs compounds as a function of stage. Analysis of the oscillator strengths permits independent determination of the charge transfer to the interior and bounding graphite layer modes vs. stage for K, Rb and Cs donor compounds. Analysis of the stage dependence of the mode frequencies indicates an in-plane lattice expansion due to the intercalation process, in agreement with direct x-ray measurements.<sup>1</sup>

<sup>1</sup>D.E. Nixon and G.S. Parry, J. Phys. C. 2, 1732 (1969).

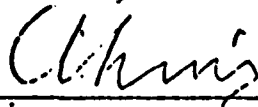
†Supported by AFOSR Grant #77-3391.

\*Nat'l Magnet Lab, supported by NSF.

‡Submitted by A. Linz.

Prefer Regular Session

Submitted by

  
A. Linz  
Room 13-3154, M.I.T.  
Cambridge, MA 02139

## Abstract Submitted

for the Chicago Meeting of the

American Physical Society

March 19-23, 1979

Physical Review  
Analytical Subject Index  
Number 78.20, 78.30

Bulletin Subject Heading  
Graphite Intercalation  
Compounds

Direct Determination of Charge Transfer in Graphite Intercalation Compounds.\* M.S. DRESSELHAUS, S.Y. LEUNG, C. UNDERHILL and G. DRESSELHAUS<sup>†</sup>, MIT -- Although charge transfer in graphite acceptor compounds has been discussed by many authors, only recently, using infrared spectroscopy, has the charge on the graphite bounding and interior layers been determined independently. This determination is possible because the IR modes associated with the interior and bounding layers occur at different frequencies, and a lineshape analysis of the IR spectra yields the dipole moment and hence charge associated with each mode. For example, the results for graphite-FeCl<sub>3</sub> show that there is a 70% charge transfer to the bounding layers (essentially independent of stage), and for stage  $n \geq 3$  an additional 30% transfer is made to the interior layers collectively. The small charge transfer to graphite interior layers is corroborated by magnetoreflexion results on graphite-FeCl<sub>3</sub> which probe primarily the graphite interior layers. We also discuss the relation of this determination of the charge transfer to Shubnikov-de Haas data, which yield fluted Fermi surface ellipsoids associated with both graphite interior and graphite bounding layers.

<sup>†</sup>Nat'l Magnet Lab, supported by NSF.

\*Supported by AFOSR Grant #77-3391.

Prefer Regular Session

Submitted by

---

M.S. Dresselhaus  
Room 13-2090, M.I.T.  
Cambridge, MA 02139

# LATTICE MODE SPECTRA OF GRAPHITE INTERCALATION COMPOUNDS<sup>1</sup>

C. Underhill\*, S.Y. Leung\*, G. Dresselhaus† and M.S. Dresselhaus\*

Massachusetts Institute of Technology  
Cambridge, Massachusetts 02139

Infrared and Raman active modes in graphite intercalation compounds can be classified into three categories: those arising from (1) the intercalant; (2) the graphite bounding layers (the graphite layer that is adjacent to the intercalant) and (3) the interior graphite layers.<sup>1-7</sup> Since the lattice modes of the intercalant, graphite bounding and interior layers occur at different frequencies, these techniques can investigate each of the different types of layers separately. The present study focusses on two important ideas in the understanding of graphite intercalation compounds: strain field and effective charge. We have measured the stage dependence of the frequency upshift of the graphitic optic  $E_{2g_2}$  and  $E_{1u}$  modes (arising from both the bounding and interior graphite layers). A similar stage dependent frequency upshift is observed in graphite ferric chloride for all the infrared-active and Raman-active lattice modes. This stage-dependent upshift of the lattice modes can be interpreted via a strain field intercalation mechanism. Analysis of the infrared spectra gives the stage dependence of the effective charge associated with the graphitic bounding and interior layers. An effective charge ratio of 7/3 was measured between the bounding and interior layers for graphite-ferric chloride.

Using highly oriented pyrolytic graphite (HOPG) as a host material and employing the conventional two-zone technique<sup>9</sup> we have been able to grow a series of essentially single-staged graphite-ferric chloride samples including stages: 1, 2, 3, 4, 5, 6, and 11. The stage of the compound was determined using a conventional  $\theta$ - $2\theta$  x-ray diffractometer scan employing  $\text{MoK}\alpha$  as the incident radiation. Admixtures of secondary stage material appear as additional peaks in the x-ray spectra and these additional peaks can easily be identified.

Room temperature Raman spectra were taken using an argon-ion laser operating at 4880Å in the back-scattering geometry. With the incident beam along the c-axis of the crystal, the Raman-active in-plane  $E_{2g_2}$  modes are excited. Intercalant desorption associated with laser heating was avoided by using a low laser power level ( $\leq 50$  mw). Infrared reflectivity spectra were taken using a Fourier transform spectrometer. Room temperature spectra covering the energy range  $400 \leq \omega \leq 4000 \text{ cm}^{-1}$  were taken with the sample c-axis parallel to the incident beam.

Raman and infrared spectra of graphite-ferric chloride are consistent with the identification of the lattice modes with the graphite bounding and interior layers.<sup>7</sup> In the Raman spectra a single Lorentzian line is found for both stage 1 and 2 compounds and two Lorentzian lines for compounds with  $n \geq 3$ . For the infrared spectra, fitting the data in terms of a Drude background and Lorentzian oscillators also yields a single Lorentzian oscillator

for stages 1 and 2 and two Lorentzian oscillators for stages  $n \geq 3$ . The higher frequency component in the Raman spectrum ( $E_{2g_2}$ ) is identified with the bounding graphitic layer because it exists in all stages (including 1 and 2) but not in pristine graphite, while the lower frequency component ( $E_{2g_2}$ ) is identified with the interior graphite layer because its frequency extrapolates to that for pristine graphite in the limit of very dilute compounds. Furthermore, there is no evidence of the lower frequency component in stages 1 and 2. Identification of the infrared-active modes with the bounding and interior layers follows a similar line of reasoning. The difference is that for the infrared spectra the high frequency component ( $E_{1u}$ ) is identified with the interior layer and the lower frequency component ( $E_{1u}$ ) is identified with the bounding graphite layer.

The dependence of the lattice mode frequency  $\omega$  on reciprocal stage ( $1/n$ ) for both the infrared-active and Raman-active modes is shown in Fig. 1. We observe that all the lattice mode frequencies (infrared and Raman) for  $n \geq 3$  exhibit the same linear dependence on reciprocal stage whether the mode is associated with graphite bounding or interior layer.

The frequency upshift of the modes shown in Fig. 1 is interpreted as a lattice stiffening upon intercalation. As the number of graphite layers between successive intercalate layers increases, the strain experienced per graphite layer is decreased and thus a smaller shift in the lattice mode frequency results. The slope of the dependence of the mode frequency on reciprocal stage has the same sign in graphite- $\text{AlCl}_3$ <sup>10</sup>, a compound similar in structure to graphite- $\text{FeCl}_3$  (i.e. for both types of acceptor compounds the mode frequencies increase as a function of  $1/n$ ). In contrast, for both the infrared-active modes<sup>11</sup> and Raman-active<sup>3</sup> modes in the graphite-alkali metal compounds, the slope of a plot of the mode frequency vs reciprocal stage has a sign opposite to that for graphite-ferric chloride (i.e. the mode frequencies decrease as a function of  $1/n$ ). This interpretation of the mode frequency shift is consistent with the observation that in graphite-potassium compounds there is a contraction in the graphite in-plane lattice constant ( $a_0$ ) upon intercalation.<sup>12</sup>

Infrared spectroscopy is useful for the study of lattice modes and electronic properties of graphite intercalation compounds in the following two ways: (1) infrared spectroscopy probes odd-parity modes while Raman spectroscopy probes even-parity modes in these compounds. (2) Determination of the oscillator strengths provides important information concerning electronic properties such as the dipole moments and effective charges. The dipole moment associated with the infrared-active

<sup>1</sup>The Raman and infrared studies were respectively supported by the Office of Naval Research (ONR N00014-77-0005) and the Air Force Office of Scientific Research (877-3391).

<sup>†</sup>Department of Electrical Engineering and Computer Science and Center for Materials Science and Engineering.

<sup>\*</sup>Francis Bitter National Magnet Laboratory, supported by the NSF.

as a function of reciprocal stage is shown as an inset to Fig. 1 for bounding and interior graphite layers. Since different types of graphite layers can be probed independently, we have determined the effective charge associated with the bounding and interior layers separately. Analysis of the dipole moment in terms of an effective charge<sup>6</sup> shows that for the graphite-FeCl<sub>3</sub> system the charge distribution is divided such that 70% of the charge resides on the two bounding layers and the remaining 30% is shared among the n-2 interior layers. These charge distributions will be related to (1) Fermi surface measurements on the same compounds using the Shubnikov-de Haas Effect (reported by Woollam et al at this conference) (2) the Fermi level shift in the graphite interior layers as a result of intercalation with FeCl<sub>3</sub> as measured by the magnetoreflexion technique (reported by Mendez et al at this conference) and (3) the dependence of the electrical conductivity on reciprocal stage.

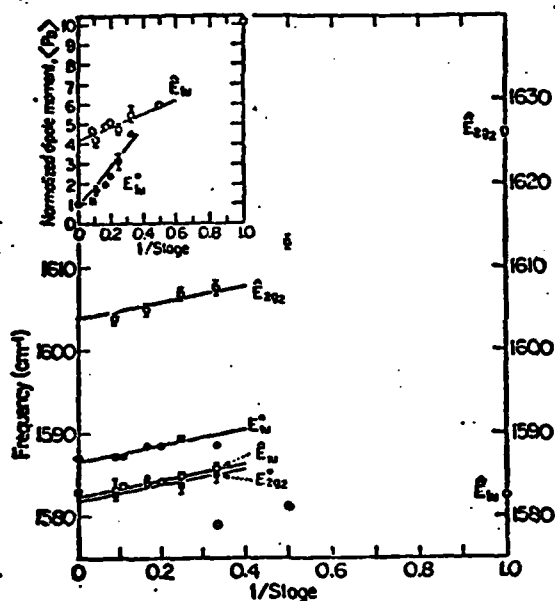


Fig. 1 The inverse stage dependence of the mode frequencies for Raman  $E_{2g2}$  and  $E_{2g2}$  (squares) and IR  $E_{1u}$  and  $E_{1u}$  (circles) modes in graphite-ferric chloride compounds. The <sup>o</sup> and <sup>i</sup> superscripts refer respectively to graphite interior and bounding layers. The solid lines represent a least squares fit to the experimental points for  $n \geq 3$  and indicate a similar strain dependence for all observed modes. The  $E_{2g2}$  and  $E_{1u}$  mode frequencies for pristine graphite are given at  $(1/n)=0$ . The inset shows the  $(1/n)$  dependence of the dipole moment for the infrared  $E_{1u}$  and  $E_{1u}$  modes normalized to that for the  $E_{1u}$  mode in pristine graphite. The Raman and IR frequencies for the lowest stages  $n=1$  and  $n=2$  compounds labeled  $E_{2g2}$  and  $E_{1u}$  depart from the behavior observed for the  $n \geq 3$  compounds.

24

#### References

1. Dresselhaus, M.S., Dresselhaus, G., Eklund, P.C. and Chung, D.D.L., *Mat. Sci. Eng.* **31**, 41 (1977).
2. Nemanich, R.C., Solin, S.A., Guerard, D., *Phys. Rev.* **B16**, 2965 (1977).
3. Solin, S.A., *Mat. Sci. Eng.* **31**, 153 (1977).
4. Song, J.J., Chung, D.D.L., Eklund, P.C. and Dresselhaus, M.S., *Solid State Comm.* **20**, 1111 (1976).
5. Eklund, P.C., Kambe, N., Dresselhaus, G. and Dresselhaus, M.S., *Phys. Rev.* **B17**, 7069 (1978).
6. Underhill, C., Leung, S.Y., Dresselhaus, G. and Dresselhaus, M.S., *Solid State Comm.* (to be published).
7. Caswell, N. and Solin, S.A., *Solid State Comm.* **27**, 961 (1978).
8. Kittel, C., *Solid State Comm.* **25**, 519 (1978).
9. Hooley, J.G. and Soniassy, R.N., *Carbon* **8**, 191 (1970); Hooley, J.G. and Bartlett, M., *Carbon* **5**, 417 (1967).
10. Gualberto, G., Underhill, C., Dresselhaus, G. and Dresselhaus, M.S., *Bull. Am. Phys. Soc.* **24**, (1979).
11. Leung, S.Y., Underhill, C., Dresselhaus, G. and Dresselhaus, M.S., *Bull. Am. Phys. Soc.* **24** (1979).
12. Nixon, D.E. and Parry, G.S., *J. Phys.* **D1**, 291 (1968).

## ELECTRONIC ENERGY BAND STRUCTURE OF GRAPHITE INTERCALATION COMPOUNDS\*

G. Dresselhaus<sup>b</sup> and S.Y. Leung<sup>c</sup>Massachusetts Institute of Technology  
Cambridge, Massachusetts 02139

Recent experimental results on the electronic structure of graphite intercalation compounds such as those reported at this conference using the Shubnikov-de Haas effect<sup>1</sup> and the magneto-reflection technique<sup>2</sup> show that the electronic levels near the Fermi level are mainly derived from graphite  $\pi$ -bands. These experimental programs are currently generating large amounts of experimental data relevant to the dependence of the electronic structure on intercalate species and stage, and there is consequently a pressing need for energy band models which can be used to interpret these data quantitatively. First principles calculations exist for the stage 1 alkali metal compounds  $C_6Li$ <sup>3</sup> and  $C_8K$ <sup>4</sup>, and these calculations confirm that the significant energy bands near the Fermi level originate from the graphite  $\pi$ -bands. On the other hand, an extensive amount of work is required to determine  $E(k)$  from a first principles calculation for each intercalate species and stage, and the calculations become more difficult with increasing stage. Because of the success of phenomenological models based on symmetry (e.g. the Slonczewski-Weiss-McClure (S-W-McC) model)<sup>5,6,7</sup> for the interpretation of experimental data for graphite, it would seem that useful phenomenological models based on the symmetry of the intercalation compounds could also play an important role in the interpretation of experimental data for these materials.

We present here a phenomenological model for the calculation of the electronic dispersion relations for graphite intercalation compounds based on the symmetry properties of the graphite structure upon which the superlattice symmetry of the intercalation compounds is superimposed. The model is readily applicable to intercalated graphite for any intercalate species and stage. In the limit of the stage 1 alkali metal compounds  $C_6Li$  and  $C_8K$ , the dispersion relations calculated on the basis of the phenomenological model are in good agreement with those reported using a first-principles calculation. In the limit of very high stage, the S-W-McC graphite model is recovered for  $k$  points near the edges HKH of the Brillouin zone. The basic features of this band structure model are determined directly from the band parameters of pristine graphite (which are known) and the superlattice periodicity (which is deduced from x-ray data). A quantitative fit of the model to the experimental data now emerging from the Fermi surface and magnetoreflection spectra will determine the band parameters representing interaction between the graphite and intercalate layers.

The phenomenological model presented here makes use of the 3-dimensional Fourier expansion of the graphite  $\pi$ -bands previously developed by Johnson and Dresselhaus<sup>8</sup> to account for the optical properties of pristine graphite. This model is an

extension of the S-W-McC model which is based on a Fourier expansion of the energy bands along  $k_z$  and a  $k$ -p expansion about the HKH axes. Thus, by carrying out the Fourier expansion in 3-dimensions, a model is obtained for  $E(k)$  throughout the Brillouin zone. This extension is necessary for the interpretation of the optical data which involves contributions from a larger volume of the Brillouin zone than does Fermi surface data. To carry out the zone folding procedures outlined below, such an extension is also necessary for application to the intercalation compounds. It should be emphasized that the use of the 3-dimensional Fourier expansion for graphite does not introduce any parameters other than those already evaluated by Johnson and Dresselhaus in their interpretation of the optical data for graphite.<sup>8</sup>

The present phenomenological model adds to the basic graphite symmetry the superlattice periodicity appropriate to the intercalation compounds through suitable zone folding of the basic graphite Brillouin zone. The in-plane intercalate order gives rise to zone folding of the in-plane wave vectors and in this way is sensitive to the intercalate species. The staging phenomenon introduces a c-axis superlattice structure which is incorporated into the calculation by c-axis zone-folding. The zone folded representation is then transformed into a layer representation and the interaction between graphite bounding layers and the intercalate layer is treated as a perturbation. This perturbation is dependent on band parameters that are related to the overlap between the graphite  $\pi$ -band  $p_z$  orbitals and orbitals on the intercalate layer. These band parameters can be evaluated by comparison with either first principles calculations or experimental Fermi surface, optical and magneto-optical data. It should be noted that once these interaction band parameters are evaluated for a specific intercalant, the phenomenological bands for that intercalant are determined for all stages that have the same in-plane ordering.

The results for  $E(k)$  for the phenomenological model for stage 1 compounds with the  $C_6X$  and  $C_8X$  are shown in Figs. 1 and 2 using no adjustable parameters. In this form, the bands are broadly applicable to all compounds with the indicated structures. For each figure the results are compared with the pertinent first-principles calculations for  $C_6Li$ <sup>3</sup> and  $C_8K$ <sup>4</sup> and very good agreement is obtained for the bands related to the graphite  $\pi$ -bands. To obtain agreement for the hybridized metal s and p bands, it is necessary to fit the phenomenological bands to the first principles hybridized s-bands to determine the overlap band parameters between the graphite  $p_z$   $\pi$ -orbitals and the intercalate orbitals. One attractive feature of the phenomenological model is

\*Supported by the Air Force Office of Scientific Research (477-3391).

<sup>b</sup>Francis Bitter National Magnet Laboratory, supported by NSF.

<sup>c</sup>Department of Electrical Engineering & Computer Science and Center for Materials Science & Engineering.

that once the band parameters are determined for any low stage compound (where the graphite-intercalate interactions are important), the dispersion relations for all stages can then be evaluated without introduction of additional band parameters. The phenomenological model thus provides a useful tool for the calculation of the electronic structure for high stage compounds where first principles calculations are difficult to make and the phenomenological model is expected to be most convergent.

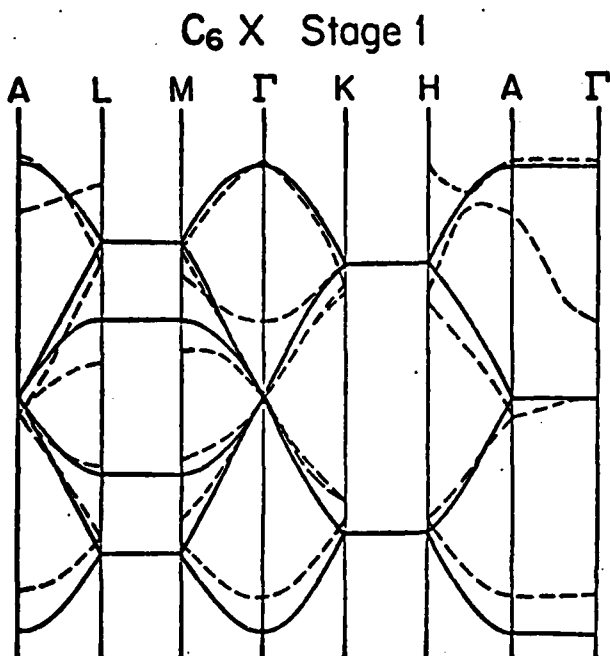


Fig. 1 Comparison of the 3-dimensional-zone-folded Fourier expansion calculation (solid line) for all C<sub>6</sub>X stage 1 compounds with the first principles calculation for C<sub>6</sub>Li (dotted line).<sup>3</sup> The zero of energy is shifted to match the degenerate levels at the  $\Gamma$  point. The 2s Li band is included in the first principles calculation but the intercalate band X from the Fourier expansion calculation is not included in the figure.

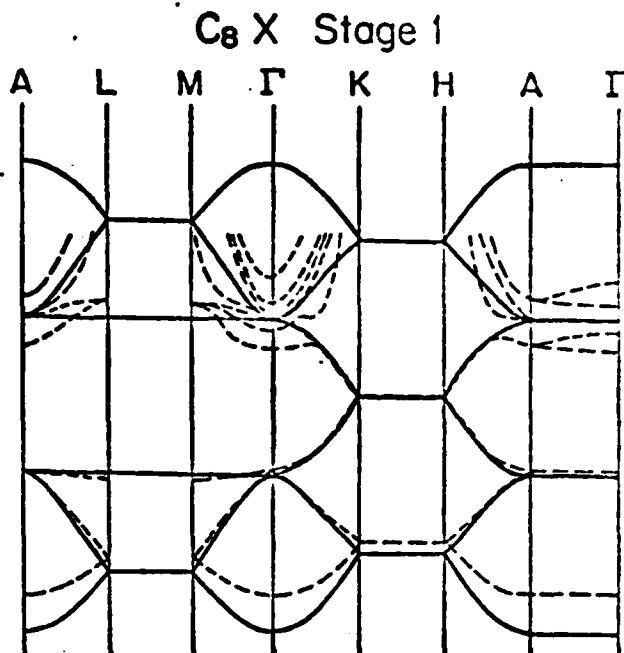


Fig. 2 Comparison of the 3-dimensional-zone-folded Fourier expansion calculation (solid line) for all C<sub>8</sub>X stage 1 compounds with the first principles calculation for C<sub>8</sub>K (dotted line).<sup>4</sup> The zero of energy is shifted to match degenerate levels at the K point. The energy scale for C<sub>8</sub>K in this figure is twice that of Ref. 4. The 4s and 4p K bands are included in the first principles calculation, but the intercalate band X from the Fourier expansion calculation is not included in the figure.

#### References

1. Wooliam, J.A., Haugland, E., Dowell, M.B., Kambe, N., Mendez, E. and Hakimi, F., Extended Abstracts, this conference.
2. Mendez, E., Kambe, N., Dresselhaus, M.S. and Dresselhaus, G., Extended Abstracts, this conference.
3. Holzwarth, N.A.W. and Rabi, S., Mat. Sci. & Eng. **31**, 195 (1977).
4. Inoshita, T., Nakao, K. and Kamimura, H., J. Phys. Soc. Japan **43**, 1237 (1977).
5. Slonczewski, J.C. and Weiss, P.R., Phys. Rev. **109**, 272 (1958).
6. McClure, J.W., Phys. Rev. **108**, 612 (1957).
7. Dresselhaus, G. and Dresselhaus, M.S., Phys. Rev. **140**, A401 (1965).
8. Johnson, L.G. and Dresselhaus, G., Phys. Rev. **37**, 2275 (1973).

## MODEL FOR ELECTRICAL CONDUCTIVITY OF GRAPHITE INTERCALATION COMPOUNDS\*

M.S. Dresselhaus<sup>†</sup> and S.Y. Leung<sup>‡</sup>Massachusetts Institute of Technology  
Cambridge, Massachusetts 02139

The property of graphite intercalation compounds that may be of greatest commercial interest is the high electrical conductivity resulting from the intercalation process.<sup>1</sup> Graphite offers a host material with high in-plane mobility (room temperature mobility =  $13,000 \text{ cm}^2/\text{V-sec}$  as compared to Cu with  $35 \text{ cm}^2/\text{V-sec}$  and to Si with  $1600 \text{ cm}^2/\text{V-sec}$ ).<sup>2,3</sup> Nevertheless, graphite is a material with modest conductivity because of its low carrier concentration ( $2 \times 10^{-4}$  carriers/atom at room temperature).<sup>2</sup> If we consider the intercalate layer as a source for the introduction of carriers into the graphite host (electrons for donor compounds and holes for acceptor compounds), then the intercalation process provides a mechanism for producing high conductivity materials by greatly increasing the intrinsic carrier concentration in a high mobility host without significant loss of carrier mobility. We present here a simple model for the electrical conductivity which accounts for the characteristic features of the dependence of the in-plane conductivity on intercalate concentration. On the basis of this model we can draw several conclusions about characteristics that may lead to increased in-plane electrical conductivity.

The simple phenomenological model for the electrical conductivity is based on the observation that the total conductance per unit cell of length  $l_c$  is equal to the sum of the conductances of the constituent layers contained within the unit cell (see Fig. 1). In this model we distinguish between the graphite bounding layers adjacent to an intercalate layer and the graphite interior layers that are fully surrounded by other graphite layers. According to this model, the conductance equation is

$$I_c(\sigma_a/\sigma_g) = d_1(\sigma_i/\sigma_g) + 2c_0(\sigma_{gb}/\sigma_g) + (n-2)c_0(\sigma_{gi}/\sigma_g)$$

in which  $n$  is the stage of the sample,  $c_0$  is the graphite interlayer separation, and  $(d_1+c_0)$  is the separation of two graphite bounding layers between which the intercalate layer is sandwiched. In a conductivity experiment we measure the conductivity  $\sigma_a$  which is here conveniently normalized to the in-plane conductivity of pristine graphite  $\sigma_g$ . Of the various layers within the unit cell, the conductivity of the graphite bounding layers  $\sigma_{gb}$  is dominant because of the high carrier density in these layers relative to the graphite interior layers<sup>4,5</sup> and because of the much higher mobility of the graphite bounding layers relative to the intercalate layer. Though smaller, the contribution of the graphite interior layers  $\sigma_{gi}$  is significant, particularly for certain intercalate species such as the alkali metals. For most intercalants, it is believed that the contribution from the intercalate layer  $\sigma_i$  is negligibly small because the Fermi level generally lies below the intercalant conduction bands and

above the intercalant valence levels,<sup>6</sup> and because ionic mobilities tend to be very low.

At low intercalate concentrations, the conductivity  $\sigma_a$  is dominated by the fraction of the unit cell occupied by the highly conducting graphite bounding layers  $2c_0/(nc_0+d_1)$ , thereby yielding an approximately linear dependence of  $(\sigma_a/\sigma_g)$  on  $(1/n)$  in good agreement with much of the published experimental data<sup>7,8,9</sup> (see Fig. 2).

In the low stage limit where the semi-insulating intercalate layer occupies a significant fraction of the unit cell,  $d_1/(nc_0+d_1)$ , saturation behavior in the  $(\sigma_a/\sigma_g)$  vs  $(1/n)$  curve results, leading eventually to a decrease in  $(\sigma_a/\sigma_g)$  for the lowest stage compounds, in agreement with experimental observations. This saturation and fall-off effect at low stage is more important for intercalants with large  $d_1$  values (e.g.  $\text{HNO}_3$ ) and less important when  $d_1$  is small (e.g.  $\text{Li}$ ), also in agreement with experimental observations.

Contributions from the graphite interior layers are significant when the charge transfer to these layers is appreciable and the carrier mobility on the graphite interior layers is significantly higher than on the graphite bounding layers. Evidence for significant contributions from the graphite interior layers is the observation of an enhanced initial rise in  $(\sigma_a/\sigma_g)$  vs  $(1/n)$  or alternatively as a shift in the peak or the onset of saturation of  $(\sigma_a/\sigma_g)$  to lower  $(1/n)$  values.

Fits of this phenomenological model have been made to conductivity data for the donor intercalant K and the acceptors  $\text{HNO}_3$  and  $\text{FeCl}_3$ . Results of this analysis show that the contribution from the graphite interior layers is more pronounced for the K compounds than for these acceptor compounds. This conclusion is in good agreement with magneto-reflection results on the stage dependence of the Fermi level for the donor Rb and the acceptors  $\text{FeCl}_3$ ,  $\text{AlCl}_3$  and  $\text{Br}_2$ .<sup>10</sup> Also of significance is the supporting evidence obtained from determination of the dynamic charge associated with the graphite bounding and graphite interior layers from measurement of the strength of the corresponding infrared oscillator strengths. Infrared measurements show in agreement with results on the static charge that the effective dynamic charge for the interior layers is relatively larger for the alkali metal donor compounds than for the  $\text{FeCl}_3$  acceptor compounds.<sup>10</sup>

The phenomenological conductivity model suggests that for further enhancement of the electrical conductivity of graphite intercalation compounds, it is important to maximize the charge density in the graphite layers through increased charge transfer. Attention to increasing the

\*Supported by the Air Force Office of Scientific Research (877-3391).

<sup>†</sup>Department of Electrical Engineering & Computer Science and Center for Materials Science & Engineering.



sample perfection for increased carrier mobility in the graphite bounding layer could also be of significance. To exploit the high conductivity in the graphite bounding layers for the low stage compounds, the intercalate layer thickness  $d_i$  should be minimized. The interpretation of conductivity data using this simple phenomenological model thereby suggests some characteristic factors that could be utilized in further increasing the electrical conductivity of these materials.

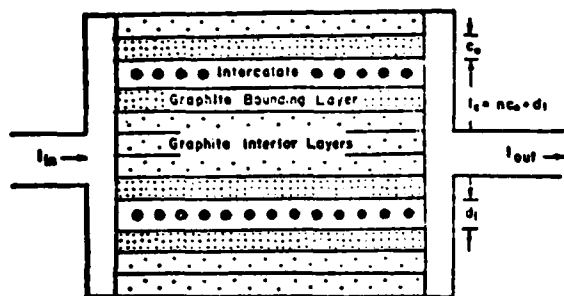


Fig. 1 Geometrical view of conductance model

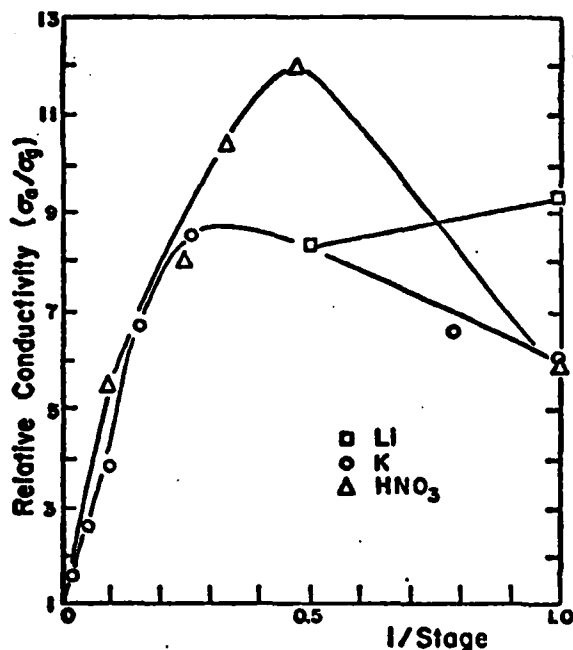


Fig. 2 Relative conductivity ( $\sigma_a/\sigma_g$ ) vs reciprocal stage ( $1/n$ ) for several intercalants. (See refs. 6-8).

## References

1. This subject is discussed in several articles contained in: Proceedings of the International Conference on Intercalation Compounds of Graphite. Materials Science and Engineering Vol. 31, December 1977. F.L. Vogel and A. Hérol, editors, Elsevier Sequoia S.A. (Lausanne).
2. Spain, I.L. in Chemistry and Physics of Carbon, Vol. 8, P.L. Walker, ed., Marcel Dekker, New York, p. 105,110.
3. Kittel, C., Introduction to Solid State Physics (2nd edition), John Wiley, New York, p. 240, 352.
4. Pietronero, L., Strässler, S., Zeller, H.R. and Rice, M.J., Phys. Rev. Lett. 41, 763 (1978).
5. Bok, J., to be published in the Proceedings of the International Conference on High Magnetic Fields in Semiconductors, Oxford, September 1978.
6. Holzwarth, N.A.W. and Rabi, S., Mat. Sci. & Eng. 31, 195 (1977).
7. Basu, S., Zeller, C., Flanders, P., Fuerst, C.J., Johnson, W.D. and Fischer, J.E., Mat. Sci. & Eng. (accepted for publication).
8. Blackman, L.C.F., Mathews, J.F. and Ubbelohde, A.R., Proc. Roy. Soc. A256, 15 (1960).
9. Vogel, F.L., Fuzellier, H., Zeller, C. and McRae, E.J. (to be published).
10. Mendez, E., Kambe, N., Dresselhaus, M.S. and Dresselhaus, G., Extended Abstracts, this conference.
11. Underhill, C., Leung, S.Y., Dresselhaus, G. and Dresselhaus, M.S., Solid State Comm. 29, 769 (1979), and to be published.



# INFRARED AND RAMAN SPECTROSCOPY OF GRAPHITE-FERRIC CHLORIDE

C. Underhill,<sup>\*</sup> S.Y. Leung,<sup>\*</sup> G. Dresselhaus<sup>†</sup> and M.S. Dresselhaus<sup>\*</sup>

Massachusetts Institute of Technology, Cambridge, MA 02139

(Received 30 November 1978 and in revised form 18 January 1979 by R.H. Silsbee)

We present the first detailed study of the stage dependence of the IR- and Raman-active optic graphitic modes in a graphite acceptor intercalation compound. The general frequency upshift observed with increasing  $\text{FeCl}_3$  concentration for all optic modes is interpreted to indicate an in-plane compression within the graphitic layers. An identification of the IR-active modes with bounding and interior graphite layers is made. A lineshape analysis of the IR spectra implies IR dipole moments corresponding to  $\sim 70\%$  of the effective charge in the graphite bounding layers, independent of stage, and  $\sim 30\%$  distributed among the graphite interior layers for stage  $n \geq 3$  compounds.

## 1. INTRODUCTION

It is established [1-5] that the Raman-active lattice modes for graphite intercalation compounds can be identified with (i) the intercalate layer, (ii) the graphite layers adjacent to the intercalate layer (the graphite bounding layers) or (iii) the graphite interior layers. Graphitic Raman modes in the vicinity of  $1600 \text{ cm}^{-1}$  have been observed for a variety of intercalate species as doublet structures separated by approximately  $20 \text{ cm}^{-1}$ . The lower frequency component (denoted by  $E_{2g2}^*$ ) is associated with the interior graphite layers, and the upper component (denoted by  $E_{2g2}^*$ ) with bounding graphite layers. Previous work focussed on the relative intensities of these components as a function of intercalate concentration [1-5] or alternatively as a function of stage, where the stage index  $n$  is the number of graphite layers between consecutive intercalate layers. The present Raman study on well-characterized graphite-ferric chloride samples, while supporting previous findings on the intercalate concentration-dependence of the doublet separation and the relative intensity of the doublet components, represents the first systematic analysis of the graphitic optic mode frequencies of an acceptor system over a wide intercalate concentration range. The present work also represents the first systematic study of the infrared (IR) spectra of a graphite intercalation compound. The complementary information obtained from the Raman and infrared spectra has important implications on the interaction between intercalate and host layers in these compounds.

## 2. EXPERIMENTAL DETAILS

When highly oriented pyrolytic graphite (HOPG) is employed as a host material, staging conditions change with respect to those of single crystal or flake graphite [6-8]. However, in agreement with

previously reported results for alkali metal [9] and halogen intercalants [10] it is possible to produce a series of well staged, homogeneous crystals over a wide range of intercalate concentration. We report here, for the first time, results on essentially single staged  $n = 1, 2, 3, 4, 5, 6$  and 11 compounds prepared from HOPG and anhydrous ferric chloride (made in situ) using the now conventional two zone system [11]. Improved sample homogeneity has been achieved by using graphite of approximately  $20 \mu\text{m}$  initial thickness. For the growth process employed, the graphite temperature was maintained throughout at  $350^\circ\text{C}$  and the temperature (and hence vapor pressure) of the ferric chloride was varied: stage 2 ( $300^\circ\text{C}$ ), stage 3 ( $227^\circ\text{C}$ ), stage 4 ( $216^\circ\text{C}$ ), stage 5 ( $202^\circ\text{C}$ ), stage 6 ( $216^\circ\text{C}$ ) [12] and stage 11 ( $192^\circ\text{C}$ ). For all stages a chlorine atmosphere of 600 torr was employed. Using a single crystal x-ray diffractometer, conventional  $\theta$ - $2\theta$  scans were taken to characterize the samples. By employing a Si(Li) detector and a single channel analyzer to provide discrimination of incident photon energy, small concentrations of admixed stages were identified [13]. X-ray spectra for stages  $n=1, 2, 3$  and 4 are shown in Fig. 1, together with the corresponding intercalant repeat distances  $l_c$  determined using the  $\text{MoK}\alpha$  x-ray line. The preparation of single staged  $n=1$  material proved difficult because of the tendency for inclusion of either regions of pristine graphite or stage  $n \geq 1$  material. Spectra for all compounds used in this study showed the samples with stage  $n \geq 2$  to be essentially single-staged. Only small secondary-phase x-ray diffraction peaks (indicated by \* in Fig. 1) are observed. The relative intensities of the diffraction peaks can be related to the structure factor for the intercalation compounds [13].

For the light scattering measurements, laser excitation was provided by an argon-ion laser operating at  $4880 \text{ \AA}$  in the back-scattering geometry. Unpolarized room temperature Raman spectra were

- \* Department of Electrical Engineering and Computer Science and Center for Materials Science and Engineering.
- † Francis Bitter National Magnet Laboratory, supported by the NSF.

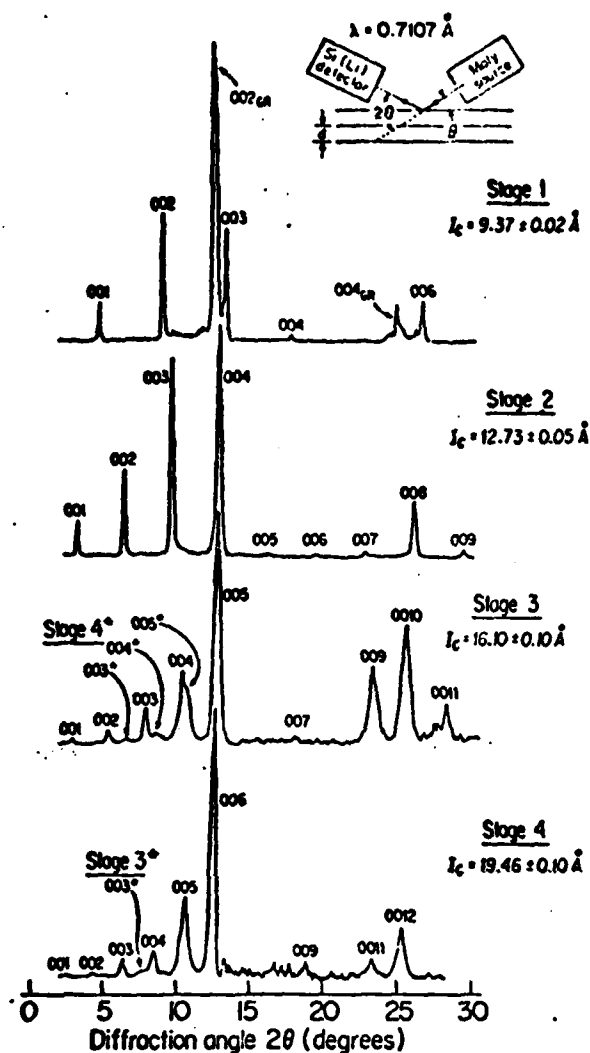


Fig. 1. X-ray stage characterization for stages  $n = 1, 2, 3$  and  $4$  graphite-ferric chloride compounds. The intercalant repeat distance  $I_c$  and stage indices are given on the right. Reflections due to admixed stages are indicated by \*. The peaks labeled 004cr in the stage  $n = 1$  trace refer to pristine graphite reflections. A schematic of the X-ray system incorporating a Si(Li) detector and a Mo X-ray source is shown in the inset.

taken from the sample c-faces and correspond to the excitation of in-plane Raman-active modes. To avoid intercalate desorption effects associated with laser heating, these spectra were taken at low (<50mW) laser power levels.

Infrared reflectivity spectra were obtained using a Fourier transform spectrophotometer operating with a globar source and a TGS detector with a KBr window. Room temperature spectra, covering the energy range  $800\text{ cm}^{-1}$  to  $4000\text{ cm}^{-1}$  with a resolution of  $2\text{ cm}^{-1}$  were taken with the c-axis approximately parallel to the beam path. The spectrophotometer was purged with an atmosphere of

dried air and no spectral interference from water vapor absorption lines was detected in the region of interest.

To check that the reported x-ray results are compatible with the Raman and IR results, x-ray measurements were also made on very thin samples and on freshly-cleaved samples. Similar results were obtained in all cases. We have confidence that our Raman and IR spectra are representative of the indicated stage.

### 3. RESULTS

Raman spectra for graphite ferric chloride are shown in Fig. 2 for essentially single-staged  $n = 2, 3, 4, 6, 11$  and for our purest stage 1 compounds.

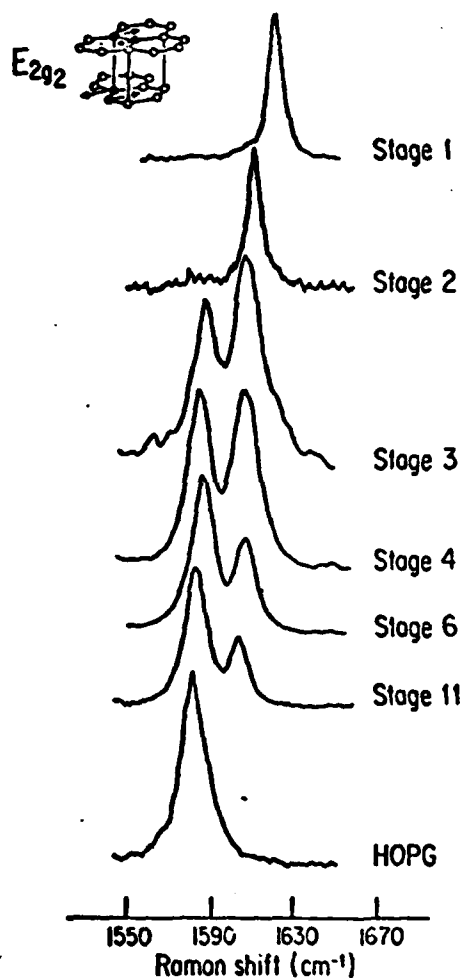


Fig. 2. Unpolarized room temperature Raman spectra taken in the backscattering geometry ( $E 1 c$ ) for stage  $n = 1, 2, 3, 4, 6$  and  $11$  graphite-ferric chloride compounds and for pristine graphite (HOPG). Laser excitation at  $4880\text{ Å}$  and a power level  $< 50\text{ mW}$  were used to excite in-plane Raman-active  $E_{2g2}$  modes (see inset). The upper frequency component ( $E_{2g2}$ ) is identified with the bounding layer mode and the lower component ( $E'_{2g2}$ ) with the interior graphitic mode.

Raman results were previously reported in a preliminary form for most of these stages [14] and by Caswell and Solin for stages  $n=1$  and  $n=2$  [15]. Included for comparison is the spectrum for pristine graphite ( $n=\infty$ ), showing a single line at the  $E_{2g_2}$  mode frequency. (See inset to Fig. 2). Of particular significance is the large intercalate concentration-dependent upshift of the  $E_{2g_2}$  bounding layer mode. The spectra for stages  $n=1$  and  $n=2$  exhibit only a single peak, consistent with the absence of interior graphite layers for these stages. Samples for  $n \geq 3$  however show both  $E_{2g_2}$  and  $E_{1u}$  modes, the latter mode associated with interior graphite layers. For stage  $n=4$ , where the number of bounding and interior layers is equal, the two peaks have approximately equal intensity. As the intercalate concentration decreases and the stage index increases, the doublet separation remains constant while the relative intensities of the  $E_{2g_2}$  and  $E_{1u}$  features exhibit a dependence on intercalate concentration (or  $1/n$ ) in qualitative agreement with previous work on other intercalate species [3,4]. Accurate fits to the Raman spectra have been achieved with a single Lorentzian line for stages  $n=1$  and 2 and two Lorentzians for stage  $n \geq 3$ . In the lineshape analysis, the Lorentzian lines were convolved with the measured instrument function and the results for the central frequency, linewidth and peak intensity for the spectra in Fig. 2 are given in Table 1.

Infrared reflectivity spectra for stages  $n=1, 2, 4, 6$  and 11 compounds and for graphite are shown in Fig. 3. Because of the increased free-carrier concentration in the intercalation compounds compared to that of graphite, the baseline reflectivity in the vicinity of  $1600 \text{ cm}^{-1}$  is increased from  $\sim 70\%$  in graphite to  $\sim 80\%$  for stage  $n=11$ , and to  $\sim 95\%$  for stages  $n=1, 2, 4$  and 6. Free carrier effects are also responsible for the major changes in lineshape exhibited by these traces. Three typical lineshapes occur, and these are shown for HOPG, stage  $n=11$  and stage  $n \leq 6$ . To extract the lattice mode frequency, linewidth and oscillator strength, a lineshape analysis was performed and results for these parameters are given in Table 1. The computed reflectivity using these parameters is shown in Fig. 3 by the dotted curves. In this analysis, the form for the free-carrier and electronic interband contributions is largely determined by the IR spectra observed over the frequency range  $800 < \omega < 4000 \text{ cm}^{-1}$  [16]. For stages  $n=1$  and 2, the spectra are fitted with a single IR-active lattice mode at  $1584$  and  $1581 \text{ cm}^{-1}$ , respectively. However, for stage  $n \geq 3$  two modes (labeled  $E_{1u}^*$  and  $E_{1u}$ ) of comparable linewidth are required (see Table 1).

The dependence on reciprocal stage ( $1/n$ ) of the frequencies for the Raman-active modes (Fig. 2) and for the IR-active modes (Fig. 3) is given in Fig. 4. It is noteworthy that the  $E_{2g_2}$ ,  $E_{2g_2}^*$ ,  $E_{1u}$  and  $E_{1u}^*$  mode frequencies for stage  $n \geq 3$  all exhibit

TABLE 1 Optic Mode Parameters for Graphite-Ferric Chloride Intercalation Compounds (Central frequency ( $\omega_0$ ), linewidth ( $\Gamma$ ) and strength ( $F$ ) of Raman- and IR-active modes) resulting from analysis of the data shown in Figs. 2 and 3.

Stage	Raman						Infrared					
	(a)			(b)			(a)			(b)		
	Interior Layer			Bounding Layer			Interior Layer			Bounding Layer		
	$\omega_0$	$\Gamma$ (c)	$F_R$ (d)	$\omega_0$	$\Gamma$ (c)	$F_R$ (d)	$\omega_0$	$\Gamma$ (c)	$F_{IR}$ (e)	$\omega_0$	$\Gamma$ (c)	$F_{IR}$ (e)
1				1626.0	3	4.0				1582.5	8	0.220
2				1612.9	3	4.0				1581.2	3	0.110
3	1585.0	13	3.6	1607.5	13	4.3	1588.5	6	0.025	1585.8	4	0.074
4	1583.7	12	4.2	1606.7	12	4.2	1589.4	6	0.020	1585.0	4	0.047
5							1588.6	8	0.015	1584.2	6	0.045
6	1584.4	10	4.2	1604.9	9	2.2	1588.5	7	0.012	1584.0	7	0.037
9							1587.3	4	0.008	1583.0	10	0.020
11	1582.8	10	4.4	1603.8	6	2.0	1587.3	5	0.004	1583.2	10	0.020
$\infty$	1581.5	11	4.8				1587.5	2	0.006 <sup>(f)</sup>			

(a) Raman- and IR-active graphite interior layer modes are respectively denoted as  $E_{2g_2}^*$  and  $E_{1u}^*$ .

(b) Raman- and IR-active graphite bounding layer modes are respectively denoted as  $E_{2g_2}$  ( $E_{2g_2}^*$ ) and  $E_{1u}$  ( $E_{1u}^*$ ).

(c) Central frequency  $\omega_0$  and full-width half-maximum linewidth  $\Gamma$  are in  $\text{cm}^{-1}$ .

(d) Peak intensities (arbitrary units), accurate to  $\pm 10\%$  except for stage 3 where the uncertainty is  $\sim \pm 20\%$ .

(e) The IR spectra are analyzed by  $\epsilon(\omega) = \epsilon_\infty + \epsilon_{\text{Drude}} + \sum F_{IR} \omega_0^2 / (\omega_0^2 - \omega^2 - i\Gamma\omega)$ .

(f) Value given in Ref. 17 is  $\sim 5$  times larger.

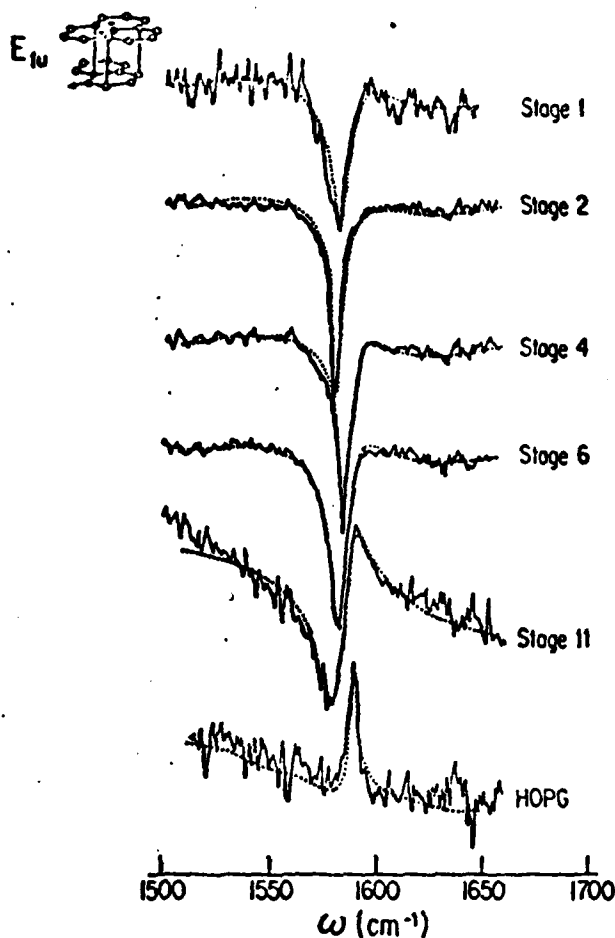


Fig. 3. Room temperature c-face infrared reflectivity spectra for the energy range  $1520 \leq \omega \leq 1650 \text{ cm}^{-1}$  for stage  $n = 1, 2, 4, 6$  and 11 graphite-ferric chloride compounds and for pristine graphite (HOPG). The fit to experimental data using parameters given in Table 1 is shown by the dotted curves. These data are analyzed in terms of the graphitic  $E_{1u}$  modes (see inset) which, in the intercalation compounds are designated as  $E_{1u}^i$  for interior graphitic layers and as  $E_{1u}^b$  for bounding graphitic layers: see text and Table 1.

a linear upshift in frequency with  $(1/n)$  as indicated by the solid lines in Fig. 4. Furthermore, all lines have similar slopes, resulting in doublet separations of  $22 \pm 2 \text{ cm}^{-1}$  for the Raman-active modes and  $4 \pm 1 \text{ cm}^{-1}$  for the IR-active modes. Also shown in Fig. 4 (see inset) is the stage dependence of  $\langle P_A \rangle$ , the in-plane dipole moment for the  $E_{1u}$  modes resulting from the lineshape analysis of the IR data. In this inset, the value of  $\langle P_A \rangle$  is normalized (i.e.  $\langle P_A \rangle \rightarrow 1$  as  $n \rightarrow \infty$ ).

#### 4. DISCUSSION

The main contributions of this work are: (1) identification of the observed IR-active modes with interior and bounding graphitic layers, (2) determination of the charge associated with the dipole moment in the bounding and interior layers,

and (3) observation of a similar stage-dependent upshift in frequency for all Raman-active and IR-active graphitic modes for stage  $n \geq 3$  compounds.

The IR mode labeled  $E_{1u}$  in Fig. 4 is identified with vibrations in the graphite interior layers for the following reasons. Firstly, the frequency of this mode extrapolates to that for the  $E_{1u}$  mode for graphite as the intercalate concentration goes to zero ( $n \rightarrow \infty$ ). Secondly, this mode is not found for stage  $n=1$  or 2 compounds (where there are no interior graphite layers), but is observed only for stage  $n \geq 3$  compounds. Furthermore, analysis of the IR lineshapes shows that the dipole moment  $\langle P_A \rangle$  (see inset to Fig. 4) for the  $E_{1u}^i$  mode in the intercalation compounds decreases with increasing stage index and extrapolates to the value for graphite. Consistent with this identification for

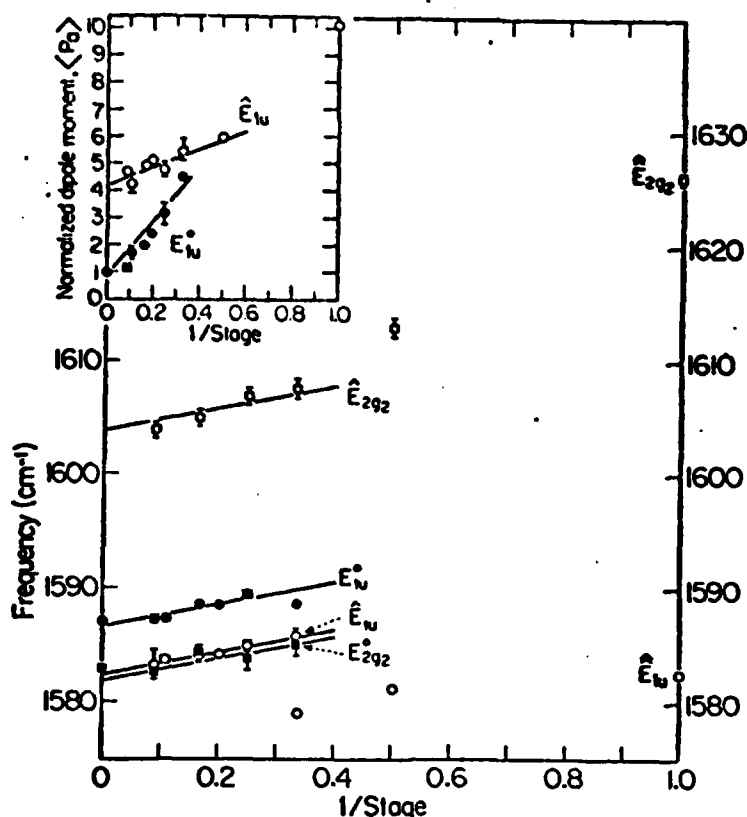


Fig. 4. The inverse stage dependence of the mode frequencies for Raman  $E_{2g2}^*$  and  $E_{2g2}$  (squares) and IR  $E_{1u}^*$  and  $E_{1u}$  (circles) modes in graphite-ferric chloride compounds. The solid lines represent a least square fit to the experimental points for  $n \geq 3$  and indicate a similar strain dependence for all observed modes. The  $E_{2g2}^*$  and  $E_{1u}$  mode frequencies for pristine graphite are given as  $(1/n) \rightarrow 0$ . The inset shows the  $(1/n)$  dependence of the dipole moment for the infrared  $E_{1u}^*$  and  $E_{1u}$  modes normalized to that for the  $E_{1u}$  mode in pristine graphite. The Raman and IR frequencies for the lowest stages  $n=1$  and  $n=2$  compounds labeled  $E_{2g2}^*$  and  $E_{1u}$  depart from the behavior observed for the  $n \geq 3$  compounds.

the  $E_{1u}$  mode is the observation that the magnitude of  $\langle Pa \rangle$  for this IR mode increases by a factor of four from its small value in graphite [17].

A second IR-active mode, absent in graphite and labeled  $E_{1u}$  in Fig. 4, is identified with the bounding layer. The dipole moment for this mode has a much weaker stage dependence and tends to be large compared with  $\langle Pa \rangle$  for the  $E_{1u}$  mode for high stage compounds (see inset to Fig. 4). The approximate equality of  $\langle Pa \rangle$  for the  $E_{1u}$  and  $E_{1u}$  modes at stage 3 is also consistent with this identification. The single IR mode for the lowest stage  $n \leq 2$  compounds is clearly due to bounding layer vibrations. The frequencies of the bounding layer modes are anomalously low for stages  $n=1$  and  $n=2$ , while the corresponding frequencies of the Raman-active modes are anomalously high. For stage 2, the bounding layer lies between another bounding layer and an intercalate layer,

while for stage 1 the bounding layer lies between two intercalate layers. In both cases therefore, the interplanar coupling is different from the situation for stage  $n \geq 3$  where the bounding layer is adjacent to an interior graphite and an intercalate layer. Analysis of the IR-mode intensity provides values for the effective charge  $e^*$  associated with the dipole moment [17]. Since the  $E_{1u}$  and  $E_{1u}$  occur at different frequencies, the relative charge associated with the graphite interior and bounding layers [18,19] can be determined independently. The data in Table 1 were analyzed using the Szegedi effective charge model [20], assuming that per unit cell there is one oscillator per bounding layer and  $(n-2)$  oscillators distributed among the interior layers. With these assumptions the data yield reasonable values for the effective charge  $e^*$  per unit cell:  $e^* \sim 0.75e$  for stages  $n=1$  and 2 and  $e^* \sim 0.95e$  for

stage  $n\frac{1}{2}$ ). In addition, analysis shows that  $\epsilon^*$  on each bounding graphite layer is approximately stage independent. For stage  $n\frac{1}{2}$ , the effective charge distributed among the interior graphite layers is essentially constant at 10%, with the remaining 70% residing on the bounding layers. Assuming the same charge in each graphite interior layer then the charge per interior layer is stage dependent.

The upshift of the  $E_{1u}$  and  $E_{2u}$  modes with increasing intercalate concentration for stage  $n\frac{1}{2}$  is in good agreement with the upshift observed for the  $E_{2g2}$  and  $E_{2g2}$  Raman-active modes. We attribute the stiffening of these lattice modes to a strain which decreases the in-plane graphite lattice constant [21]. The constancy of the linewidth for the  $E_{2g2}$  interior layer mode as a function of intercalate concentration and an identical frequency upshift for both interior and bounding Raman and IR-active modes suggests that an identical strain exists within both the bounding and interior graphitic layers for a given compound. On the other hand, the magnitude of the

strain increases as the number of interior graphite layers decreases, consistent with the idea that the stress introduced by intercalation must be shared by fewer layers as  $n$  decreases [22]. The coincidence in the  $E_{1u}$  and  $E_{2g2}$  mode frequencies, the relatively small linewidth of the Raman-active bounding layer mode, and the anomalous Raman and IR mode frequencies for stage  $n=1$  and 2 compounds present important characteristics which must be explained by a theory for the lattice mode spectra of graphite intercalation compounds.

#### ACKNOWLEDGEMENTS

We wish to thank Dr. A.W. Moore of Union Carbide for his generous contribution of HOPG material, G. Calabrese for help with sample preparation and Dr. S. Safran for numerous discussions on lattice strain effects. The Raman and IR measurements were supported respectively through ONR Grant # N00014-77-C-0053 and AFOSR Grant # 77-3391.

#### REFERENCES

1. DRESSELHAUS, M.S., DRESSELHAUS, G., EKLUND, P.C., CHUNG, D.D.L., *Mat. Sci. Eng.* **31**, 41 (1977).
2. NEMANICH, R.G., SOLIN, S.A., GUERARD, D., *Phys. Rev.* **B16**, 2965 (1977).
3. SOLIN, S.A., *Mat. Sci. Eng.* **31**, 153 (1977).
4. SONG, J.J., CHUNG, D.D.L., EKLUND, P.C., DRESSELHAUS, M.S., *Solid State Commun.* **20**, 111 (1976).
5. EKLUND, P.C., KAMBE, N., DRESSELHAUS, G. and DRESSELHAUS, M.S., *Phys. Rev.* **B17**, 7069 (1978).
6. METZ, W. and HOHLWEIN, D., *Carbon* **13**, 87 (1975).
7. METZ, W., and SIEMSGLUSS, L., *Mat. Sci. Eng.* **31**, 119 (1977).
8. SCHOPPEN, G., MEYER-SPASCHKE, L., SIEMSGLUSS, L., and METZ, W., *Mat. Sci. Eng.* **31**, 115 (1977).
9. NIXON, D.E. and PARRY, G.S., *J. Phys.* **D1**, 291 (1968).
10. SASA, T., TAKAHASHI, Y., MUKAIBO, T., *Carbon* **9**, 407 (1971).
11. HOOLEY, J.G., SONIASSY, R.N., *Carbon* **8**, 191 (1970); HOOLEY, J.G. and BARTLETT, M., *Carbon* **5**, 417 (1967).
12. Different growth conditions were necessary for samples of different initial thickness. For a sample initially 1mm thick a temperature of 216°C for the  $FeCl_3$  resulted in a well staged  $n=6$  compound, although excess ferric chloride remained in the ampoule. Further experimental details of the growth technique are to be found in P. Maki B.S. Thesis, MIT 1978 (unpublished).
13. UNDERHILL, C., LEUNG, S.Y., OGILVIE, R.E., (to be published).
14. UNDERHILL, C., LEUNG, S.Y., DRESSELHAUS, G., DRESSELHAUS, M.S., *Proc. Int. Conf. Physics of Semiconductors*, September 1978, Edinburgh, Scotland.
15. CASWELL, N and SOLIN, S.A., *Solid State Commun.* **27**, 961 (1978).
16. The observed background reflectivity was fit using several broad oscillators to represent electronic interband and multiphonon absorption processes and a free electron plasma term given by  $\omega_p(eV) = (0.09 + 2.16/n)^{1/2}$ . The precise form and interpretation of this background reflectivity is not critical to the analysis yielding the parameters of Table 1.
17. NEMANICH, R.J., LUCOVSKY, G., SOLIN, S.A., *Solid State Commun.* **23**, 117 (1977).
18. FISCHER, J.E., *Mat. Sci. Eng.* **31**, 211 (1977).
19. PIETRONERO, L., STRASSLER, S., ZELLER, H.R., RICE, M.J., *Phys. Rev. Lett.* **41**, 763 (1978).
20. SZIGETI, B., *Trans. Faraday Soc.* **45**, 155 (1949).
21. Further work using x-ray and electron diffraction techniques are in progress to test the implications of this strain model.
22. KITTEL, C., *Solid State Commun.* **25**, 519 (1978).

ELECTRONIC STRUCTURE OF GRAPHITE-ALKALI METAL COMPOUNDS

G. Dresselhaus\*, S.Y. Leung†, M. Shayegan†, T.C. Chieu†

Massachusetts Institute of Technology  
Cambridge, Massachusetts 02139

ABSTRACT

A theoretical model for the electronic structure of the graphite intercalation compounds based on the  $k_z$  axis zone folding of the pristine graphite  $\pi$ -bands is applied to explain the experimental results obtained in magneto-reflection and in Shubnikov-de Haas experiments on donor compounds. The detailed fit to the observed Shubnikov-de Haas frequencies for stage 5 graphite-potassium supports the model and suggests that the dominant interactions that determine the Fermi surfaces are closely related to those involving the  $\pi$ -bands for pristine graphite.



## I. Introduction

The recent development of theoretical models for the electronic structure of graphite intercalation compounds gives promise for new advances in our understanding of this important class of compounds. These models include first principles calculations for stage 1 alkali metal compounds [1,2], modified two dimensional graphite layer models [3], and models based on the three dimensional graphitic Slonczewski-Weiss-McClure (SWMcC) model using the band parameters for pristine graphite [4].

A common feature of all of these approaches is that the  $\pi$ -bands derived from pristine graphite are the dominant electronic states in the intercalation compound within an eV of the Fermi level. This paper focusses on the models which are directly related to the three-dimensional pristine graphite model Hamiltonian of SWMcC and demonstrates that a phenomenological energy band structure can be developed which is consistent with a number of experimental magneto-optical and magneto-transport measurements on these compounds. Since a large number of intercalation compounds have been prepared, much work remains to be done to fully establish the parameters of the present model or indeed whether some alternate model gives a more convergent treatment for a particular class of graphite intercalation compounds.

The c-axis zone folded model considered here [4] is a simple extension of the dilute limit model proposed earlier and used by Suematsu et al. [5] to interpret de Haas-van Alphen (DHVA) data and by Mendez et al. [6] to interpret magnetoreflexion data. Since these two experiments played a dominant role in the evaluation of the SWMcC parameters in pristine graphite, they will be the experiments which are the focus of this paper for the intercalation compounds. This paper will show that without introduction of additional parameters (i.e. the intercalate layer is approximated as an

empty layer between two graphite bounding layers) a model Hamiltonian is developed which accounts for the main features of the Shubnikov-de Haas (SdH) and magnetoreflexion spectra obtained for alkali metal donor compounds.

## II. Band Model

To obtain electronic dispersion relations  $E(\vec{k})$  for graphite intercalation compounds, a Hamiltonian is developed based on the SWMcC three-dimensional model for the graphite  $\pi$ -bands. As a first step, the c-axis superlattice periodicity is included and an "empty intercalate lattice" for the intercalation compounds is introduced, depending only on the graphite band parameters that are already known. Intercalant-specific interactions between the intercalant and the graphite bounding layer can then be introduced to obtain the final dispersion relations. The main features of this model, presented elsewhere [4], are summarized below.

The 4x4 SWMcC Hamiltonian for the graphite  $\pi$ -bands  $H_0(k_z)$  is zone folded along  $k_z$  to account for the staging periodicity as

$$H_{\text{folded}}(\vec{k}_s) = \begin{vmatrix} H_0(\vec{k}_s) & 0 & \dots & \dots \\ 0 & H_0(\vec{k}_s + \frac{\pi}{lc} \hat{z}) & & \\ \vdots & & \ddots & \\ \vdots & & & H_0(\vec{k}_s + \frac{l-1}{l} \frac{\pi}{c} \hat{z}) \end{vmatrix} \quad (1)$$

in which  $\vec{k}_s$  is the wave vector near the HK axis, each of the blocks is the 4x4 SWMcC Hamiltonian and  $l = n+1$  for even stage or  $(n+1)/2$  for odd stage compounds, where  $n$  is the stage index.

In order to consider explicitly the effect of intercalation, the

Hamiltonian given by Eq. (1) must be transformed to a layer representation which is written explicitly by

$$H_{\text{layer}}(\vec{k}_s) = U H_{\text{folded}}(\vec{k}_s) U^{-1} \quad (2)$$

where the unitary transformation is derived from the basis functions, yielding

$$H_{\text{layer}}^{(2\ell)}(\vec{k}_s) = \begin{vmatrix} H_{AA}^{(1)} & H_{AB}^{(1)} & \dots \\ H_{AB}^{(1)\dagger} & H_{BB}^{(1)} & \\ \vdots & \ddots & H_{AA}^{(\ell)} & H_{AB}^{(\ell)} \\ \vdots & & H_{AB}^{(\ell)\dagger} & H_{BB}^{(\ell)} \end{vmatrix} \quad (3)$$

The intercalation process is modelled by substitution of an intercalate layer for one or more of the graphite layers in the layer Hamiltonian. The "empty intercalate lattice" model for a graphite intercalation compound is then obtained by treating the intercalate layer as an empty layer, neglecting interactions within the layer and between this layer and the other  $(2\ell-1)$  layers. The "empty intercalate lattice" model thus requires no band parameters other than those for graphite which are already well established [7]. To obtain the full model for the dispersion relations, interactions between the intercalate layer and the graphite bounding layers are introduced and the pertinent band parameters evaluated by a fit to experimental data. In the present work the two experiments that are emphasized are the Shubnikov-de Haas and magnetoreflexion experiments which are respectively sensitive to the Fermi surface and the energy band structure near the Fermi level.

In Fig. 1 results for  $E(\vec{k})$  for the "empty intercalate lattice" model for stage 1,2 and 3 graphite intercalation compounds are given. These "empty intercalate lattice" bands are derived for an in-plane  $2 \times 2$  superlattice

and for no intercalate-graphite bounding layer interaction. Only the graphite  $\pi$ -bands are shown and these bands are also plotted on an expanded scale along and near the H-K axis of the folded hexagonal Brillouin zone. For this empty intercalate lattice model, the  $\pi$ -bands near the H-K axis are independent of in-plane folding and in the limit of  $\infty$  stage these dispersion curves reduce exactly to the SWMcC  $\pi$ -bands. Comparison of the stage 1 results [8] with the band structure of Inoshita et al. [9] gives good agreement for the graphitic bands between the two methods. The H and K points in the Brillouin zone are high symmetry points and show extremal cross sectional areas which are expected to give rise to de Haas-van Alphen oscillations. Since the H and K points are in general non-degenerate, a three-dimensional calculation is needed to obtain different DHVA frequencies for K and H point extremal cross sectional areas.

### III. Magnetoreflexion Results

The magnetoreflexion experiment is important in providing detailed information on the form of  $E(\vec{k})$  for the nearly degenerate bands near the K-point in the Brillouin zone (see Fig. 1). In the magnetoreflexion experiment, resonant behavior is observed in the magnetic field dependence of the reflectivity and these resonances are identified with Landau level transitions associated with these nearly degenerate bands from occupied valence magnetic subbands to unoccupied conduction subbands above the Fermi level. To relate these results to band models, the experiments are carried out on well-staged samples and changes in the magnetoreflexion spectra are studied as a function of stage and intercalant. Typical magnetoreflexion results [6] are given in Fig. 2 for an acceptor compound (stage 7 graphite- $\text{FeCl}_3$ ) and for a donor compound (stage 6 graphite-Rb). Resonances identified

with K-point Landau level transitions are indicated by arrows and the quantum numbers for the initial valence and final conduction magnetic subbands are given in the figure. Experimental results on a variety of acceptor and donor compounds indicate that the form for the dispersion relations  $E(\vec{k})$  for bands close to the K-point degeneracy remains similar to that in graphite, consistent with the model for  $E(\vec{k})$  presented in Section II. On the other hand, small but measurable changes in the graphite band parameters are obtained and evaluated quantitatively. Results for several representative compounds are given in Table 1 in terms of valence and conduction band effective masses  $m_v^*$  and  $m_c^*$  and the ratio of SWMcC band parameters  $(\gamma_0^2/\gamma_1)$  which sensitively determine the Landau level separation. Furthermore, analysis of magnetoreflexion structure which in the case of pristine graphite is associated with H-point Landau level transitions indicates that  $\gamma_0$ , the nearest neighbor overlap integral is changed by less than 5% for all the intercalate species and stages that have been studied [6]. Since the SWMcC band parameters are not strongly perturbed by intercalation, the fit to the Fermi surface measurements, discussed in the next section, is made as a first approximation assuming the full set of SWMcC parameters appropriate to pristine graphite.

#### IV. Shubnikov-de Haas Results

Study of the Shubnikov-de Haas effect in graphite intercalation compounds provides information on the Fermi surfaces associated with each of the partially occupied bands. To obtain quantitative information on the stage dependence of these Fermi surfaces it is important to work with well-staged and characterized samples. Results obtained for the alkali metal compounds with the intercalants K and Rb show stage-dependent Fermi surfaces, so that staging fidelity was essential for obtaining reproducible

experimental results for different samples of the same stage index.

The samples were prepared using the conventional two-zone technique with HOPG (highly oriented pyrolytic graphite) as the host material. The sample dimensions were typically (5x6x0.5 mm). Because of the instability of alkali-metal samples in the presence of air and moisture, the samples were encapsulated in ampoules and sample handling was done in an Argon-filled dry box ( $\sim 1$  ppm oxygen content). The stage of the samples was determined using (00 $\ell$ ) x-ray diffraction profiles both before and after the SdH experiments, confirming that the samples were single-staged and that no desorption had occurred during the measurements.

The four-point method was used to study the a-plane transverse magnetoresistance in the temperature range  $1.4 < T < 4.2\text{K}$  and in magnetic fields up to 15 Tesla. The leads were attached to the sample using conducting epoxy. The sample was then inserted in a helium-filled ampoule and stycast was used to seal the ampoule. The angular dependence of the SdH oscillations could thus be measured by rotating the sample around the direction of the current  $\vec{I}$  such that  $\vec{I} \perp \vec{H}$  for all angles, and hence transverse magnetoresistance was always measured. Data acquisition was by computer, and the data were manipulated to obtain a Fourier power spectrum of resistance vs.  $1/H$ , thereby yielding the frequencies of SdH oscillations. These frequencies are related to the extremal cross sections of the Fermi surface. The Fourier power spectra for the SdH frequencies for Rb stages 2,8 and K stages 2,5,8 are presented in Figs. 3 and 4, respectively.

During the course of these studies, a great deal of care was given to ensure the fidelity and reproducibility of the data. For this reason, the experiment was performed on two potassium stage 5 samples and on one of these, the measurements were repeated several weeks later after attaching

new leads. While x-ray profiles after each step of the experiment confirmed that the samples retained their single stage identity, the magnetoresistance oscillations and the relevant Fourier power spectra revealed identical traces for these stage 5 samples. Measurements done on potassium samples with different stages or on rubidium samples, however, showed distinctly different SdH frequencies. Hence our conclusion is that there is a unique set of SdH frequencies associated with each stage and donor intercalant (K,Rb). Suematsu et al. [5] have also shown stage dependent de Haas-van Alphen frequencies in stages 3 and 4 potassium compounds.

The model for  $E(\vec{k})$  described above is now applied to the interpretation of the observed SdH frequencies. Specific application is here made for stage 5 graphite-K, and in this connection the energy band model for  $n=5$  is shown in Fig. 5, for the five valence and five conduction  $\pi$ -bands. In order to calculate the SdH frequencies the Fermi level  $E_F$  must be determined. The empirical position of  $E_F$  shown in Fig. 5 yields four partially occupied conduction bands with the Fermi surface parameters listed in Table 2, including calculated and observed SdH frequencies, the cyclotron mass at  $E_F$ , the trigonal warping anisotropy listed as  $k_1/k_2$ , and the electron density for each carrier pocket. The values for  $k_1/k_2$  in Table 2 suggest that trigonal warping is important for the larger cross-sectional areas with heavier masses, whereas the smaller light mass cross-sections are circular. The generally good agreement of the observed SdH frequencies with the empty intercalate layer model of Fig. 5 suggests that the effect of intercalant-graphite bounding layer interactions can be treated as a perturbation and evaluated by fitting the model quantitatively to the observed SdH frequencies. It should be noted that the volumes of the carrier pockets for the four occupied bands in Fig. 5 correspond to a charge transfer of  $\sim 0.3$  electron per intercalant into these carrier pockets.

## V. Concluding Remarks

The mathematical technique used here to obtain the electronic dispersion relations can also be applied to obtain phonon dispersion relations for graphite intercalation compounds [10]. A major strength of this general approach is the proper treatment of symmetry in the Fourier expansion of the dispersion relations for the intercalation compounds.

A three-dimensional Fourier expansion of the electronic energy bands for intercalated graphite based on a  $k_z$ -axis folded SWMcC structure has been developed. An "empty intercalate layer" limit of this model has been applied to interpret the observed SdH frequencies in stage 5 graphite-potassium. Using only the SWMcC parameters for pristine graphite, and no other parameters, the model is able to account for most of the observed SdH frequencies. The good agreement with the magnetoreflexion results is built into the model by using the basic SWMcC Hamiltonian in which the band parameters were originally evaluated to fit the observed magnetoreflexion spectra for graphite. Further tests of the  $k_z$ -axis folded SWMcC model are now in progress by applying the model to the SdH spectra for other stages in the graphite-potassium system and for compounds with the intercalant Rb. The model is also being tested by an application to the interpretation of measured optical reflectivity spectra.

## Acknowledgments

We gratefully acknowledge Prof. M.S. Dresselhaus for numerous suggestions and Mr. L. Rubin of the Francis Bitter National Magnet Laboratory for technical assistance and AFOSR Grant #77-3391 for support of this research.



## REFERENCES

- \* Staff Member, Francis Bitter National Magnet Laboratory, supported by NSF.
- † Department of Electrical Engineering and Computer Science and Center for Materials Science and Engineering.
- [1] T. Ohno, K. Nakao, and H. Kamimura, J. Phys. Soc. Japan 47, 1125 (1979).
- [2] N.A.W. Holzwarth, S. Rabi and L.A. Girifalco, Phys. Rev. B18, 5190 (1978).
- [3] J. Blinowski, H.H. Nguyen, C. Rigaux, J.P. Vieren, LeToullec, G. Furdin, A. Herold, J. Melin, J. Physique 41, 47 (1980) and J. Blinowski and C. Rigaux (proceedings of this conference).
- [4] G. Dresselhaus and S.Y. Leung, Solid State Commun. (to be published).
- [5] H. Suematsu, K. Higuchi, and S. Tanuma, J. Phys. Soc. Japan 48, 1541 (1980).
- [6] E. Mendez, T.C. Chieu, N. Kambe, and M.S. Dresselhaus, Solid State Commun. 33, 837 (1980).
- [7] E. Mendez, A. Misu, and M.S. Dresselhaus, Phys. Rev. B21, 827 (1980).
- [8] G. Dresselhaus and S.Y. Leung, Extended Abstract of the 14th Biennial Conference on Carbon, Penn State University, p. 497 (1979).
- [9] T. Inoshita, K. Nakao, and H. Kamimura, J. Phys. Soc. Japan 43, 1237 (1977).
- [10] S.Y. Leung, G. Dresselhaus and M.S. Dresselhaus (Proceedings of this conference).

## FIGURE CAPTIONS

- Fig. 1 Electronic energy levels derived by  $k_z$ -axis zone-folding of the 3 dimensional Fourier expansion of the pristine graphite  $\pi$ -band Hamiltonian for a primitive (2x2) superlattice. An empty intercalate layer is assumed and the expansion parameters are based on the SWMcC parameters along the HK axis. On the right an expanded scale is used to plot the levels on and near the HK axis.
- Fig. 2 Magnetoreflexion spectrum using (+) circular polarization for an acceptor compound ( $\text{FeCl}_3$  stage 7) at a photon energy  $\hbar\omega = 0.295$  eV and for a donor compound (Rb stage 6) at  $\hbar\omega = 0.335$  eV. For comparison, traces for graphite are shown at comparable photon energies. The resonances are specified by the quantum numbers for the initial and final states. (From the work of Mendez et al. Ref. 6).
- Fig. 3 Shubnikov-de Haas Fourier Transform Power Spectra for stage 2 and 8 graphite-Rb. These power spectra were obtained by a Fourier transform of an experimental resistivity vs  $1/H$  trace for magnetic fields  $H < 15$  Tesla. The peaks in the power spectra correspond to SdH frequencies, which are given in Tesla and the same scale is used for each stage.
- Fig. 4 Shubnikov-de Haas Fourier Transform Power Spectra for stage 2, 5 and 8 graphite-K. (See Fig. 3).
- Fig. 5 Electronic band structure in the vicinity of the HK axis near the Fermi level for a stage 5 "empty intercalate layer" model for a graphite intercalation compound. The Fermi level is determined to fit the observed SdH frequencies. For the indicated Fermi level four of the conduction bands are partially occupied and give rise to Fermi surfaces and carrier pockets.

Table 2 Fermi Surface Parameters Associated with Stage 5 Graphite-Potassium

Fermi Surface Parameters	Band Designation							
	$K_1$	$H_1$	$K_2$	$H_2$	$K_3$	$H_3$	$K_4$	$H_4$
Trigonal Warping $k_1/k_2$	0.68	0.68	0.77	0.78	0.91	0.91	1.00	1.00
Effective Mass $m^*/m_0$	0.143	0.138	0.115	0.115	0.0828	0.0828	0.0511	0.0488
Electron Density Per Pocket ( $\times 10^{20} \text{ cm}^{-3}$ )	2.36		1.76		0.975		0.138	
Calculated SdH Frequencies (Tesla)	401	401	300	299	163	168	26.7	20.2
Observed SdH Frequencies (Tesla)	453,430		290,267,243		191,152,135		24,18	

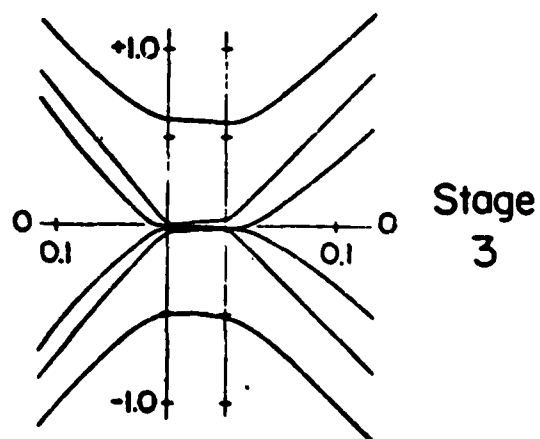
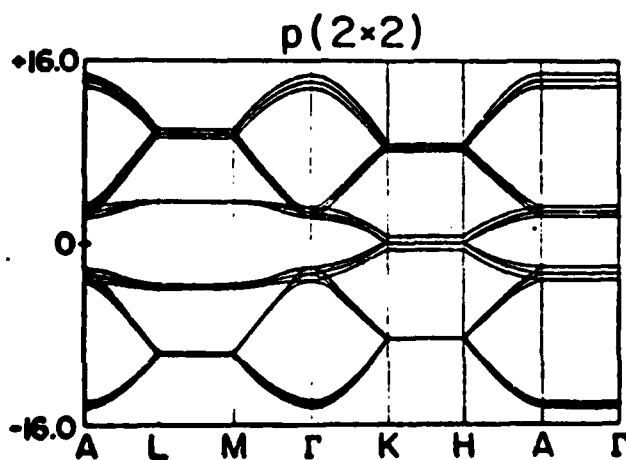
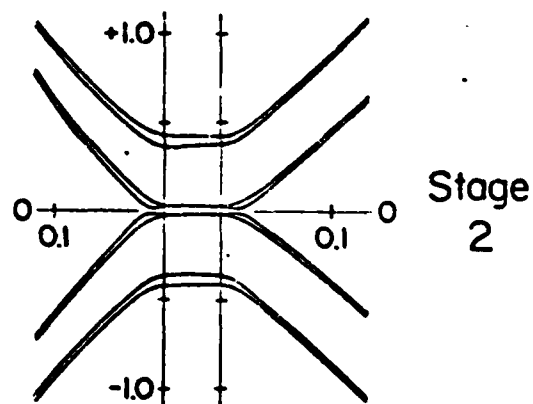
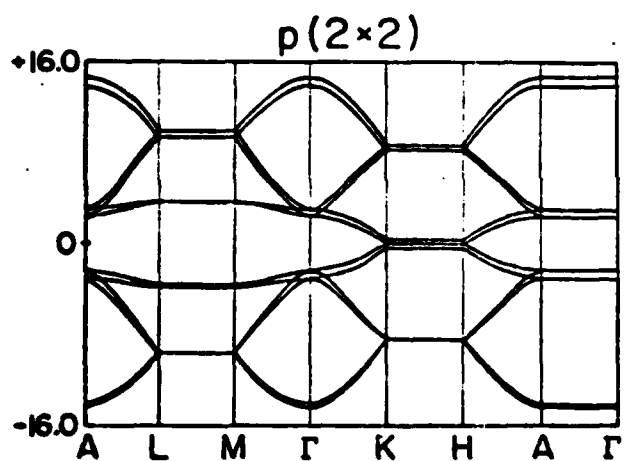
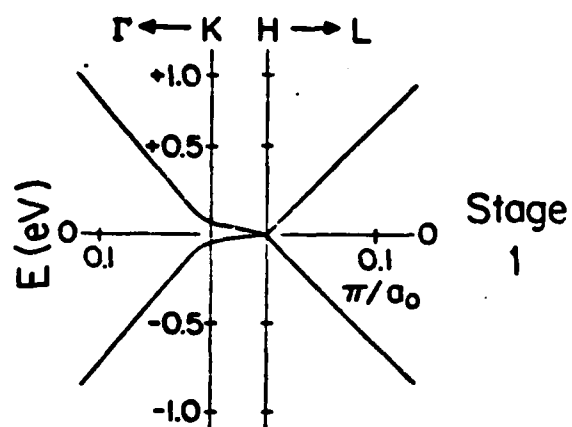
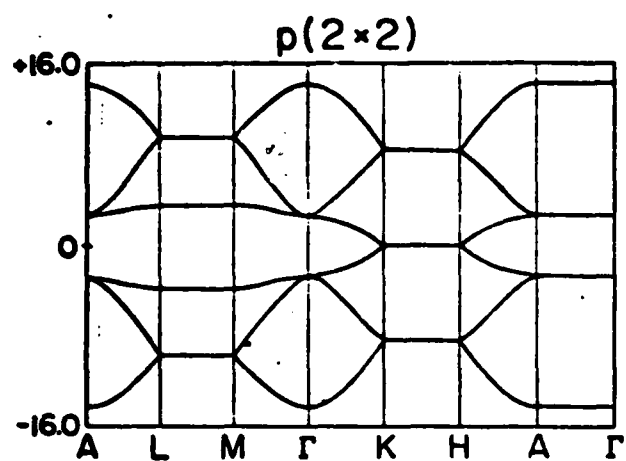


Fig. 1

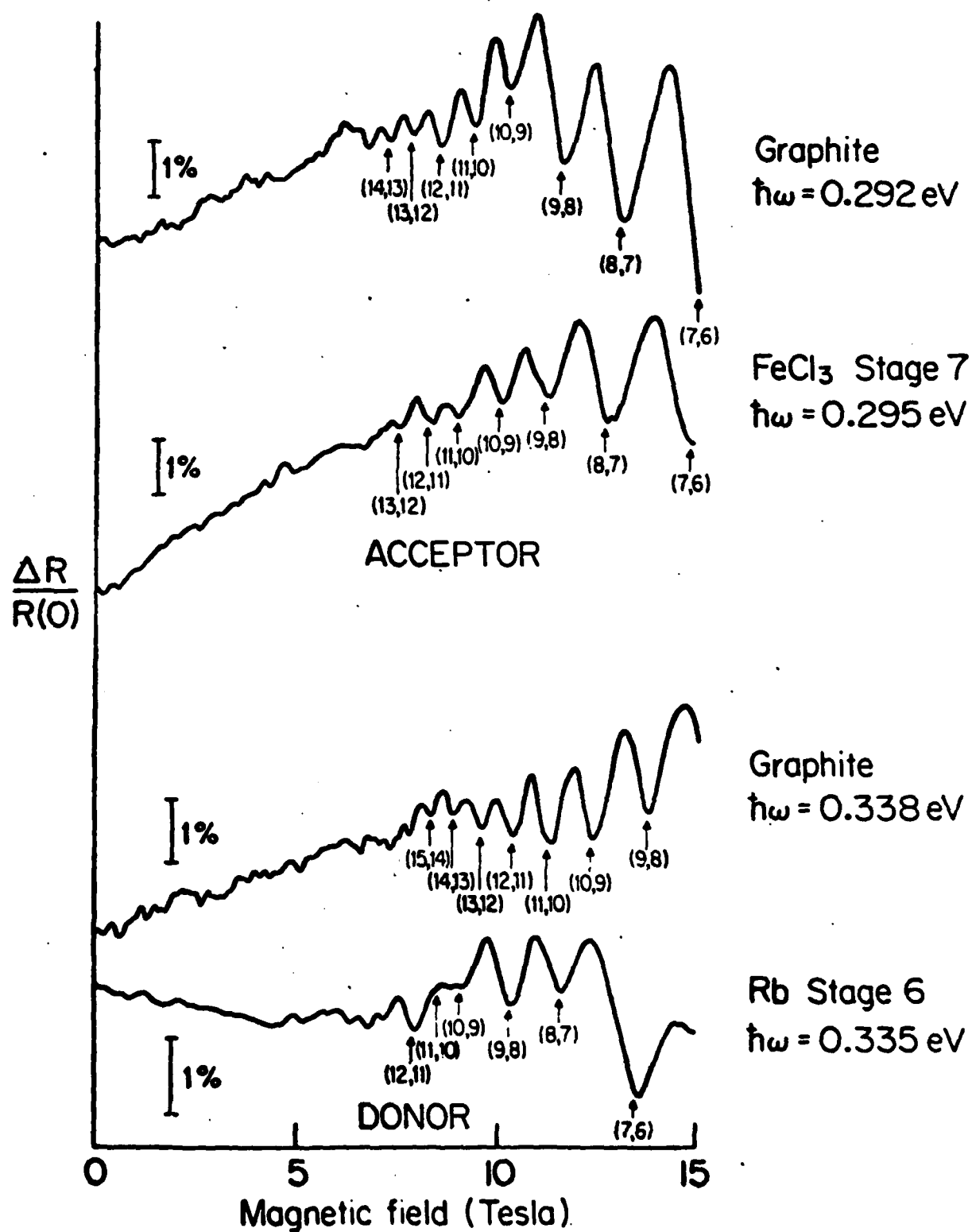
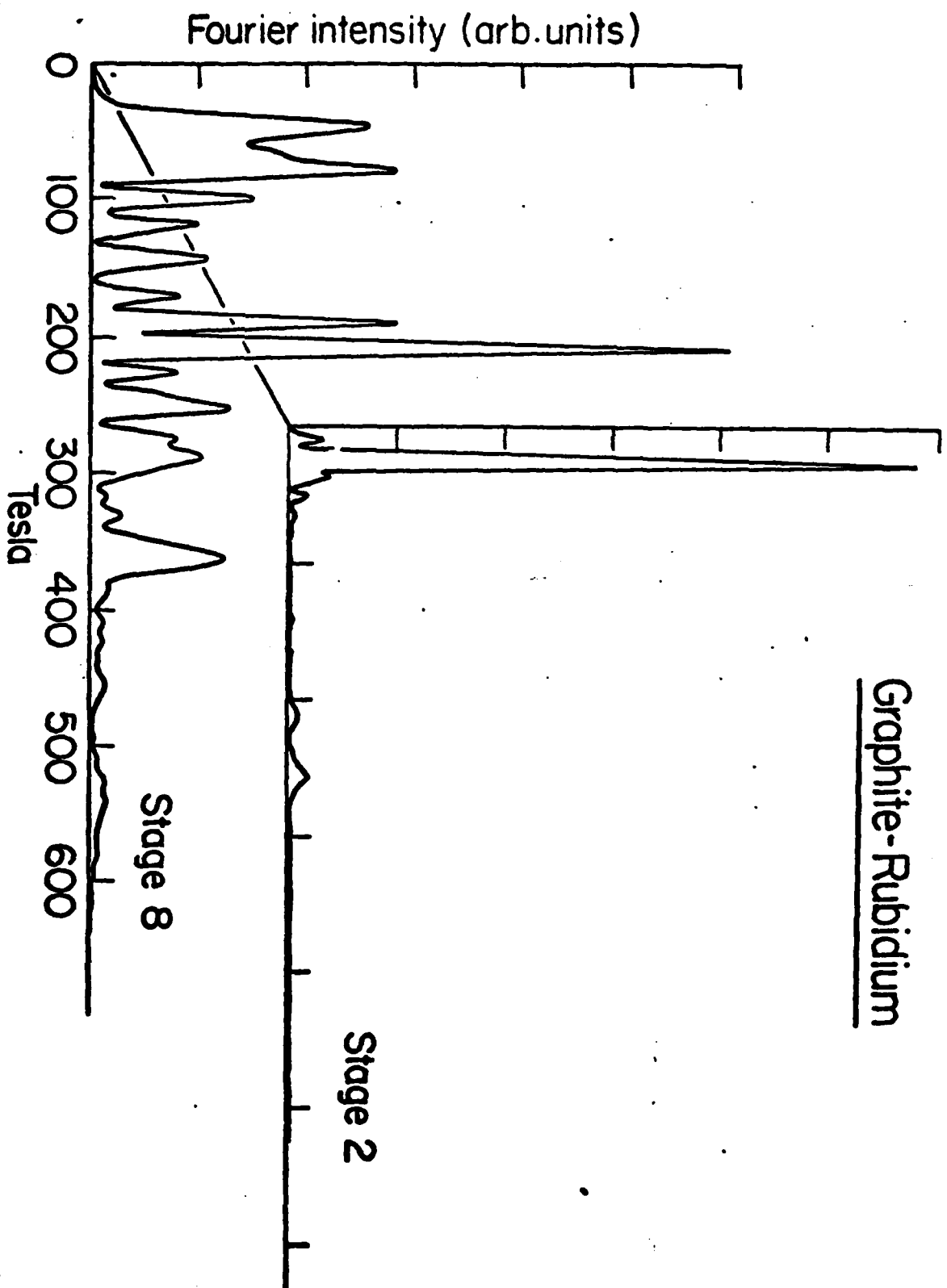


Fig. 2

Graphite-Rubidium



Graphite-Potassium

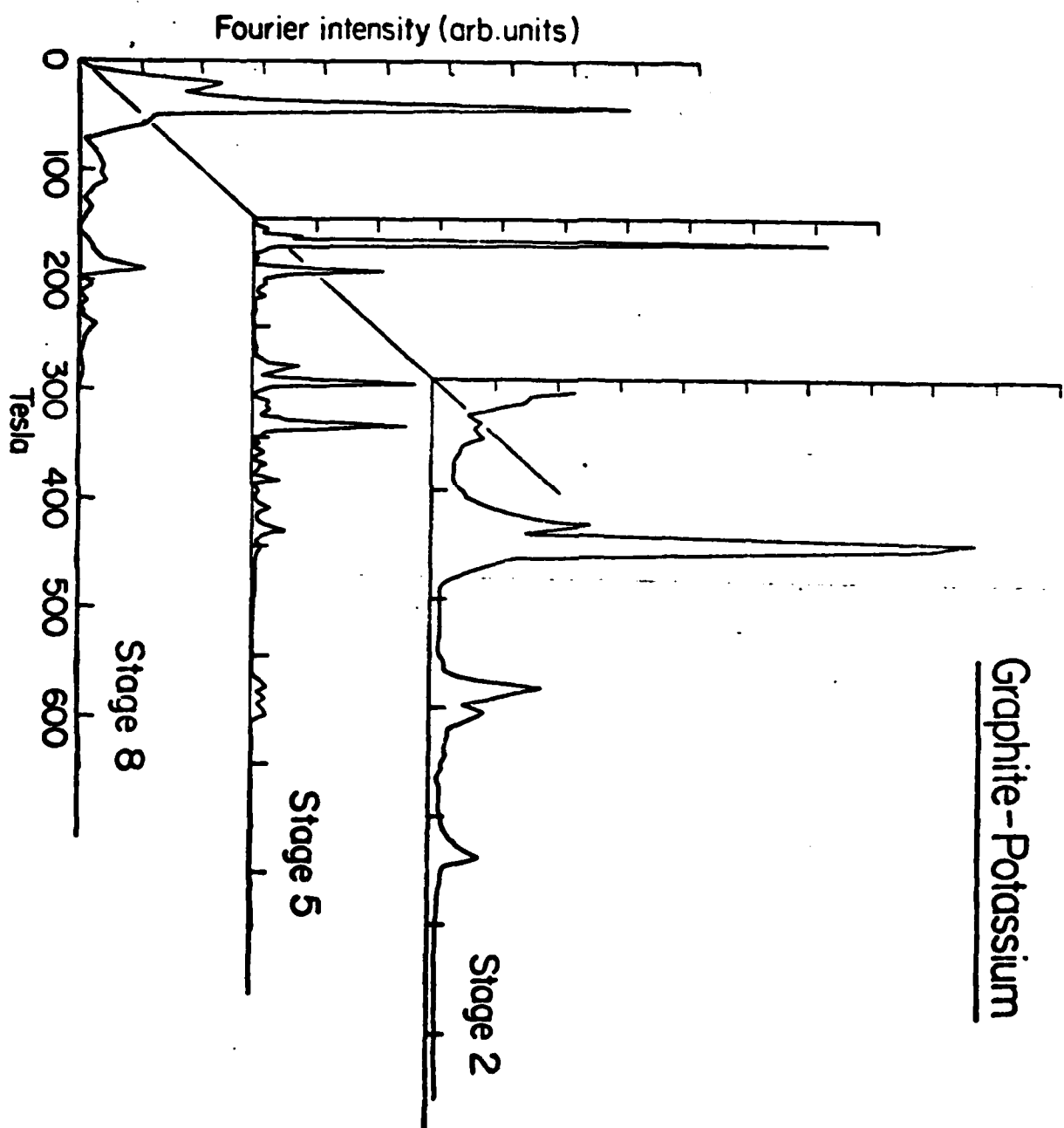


Fig. 4

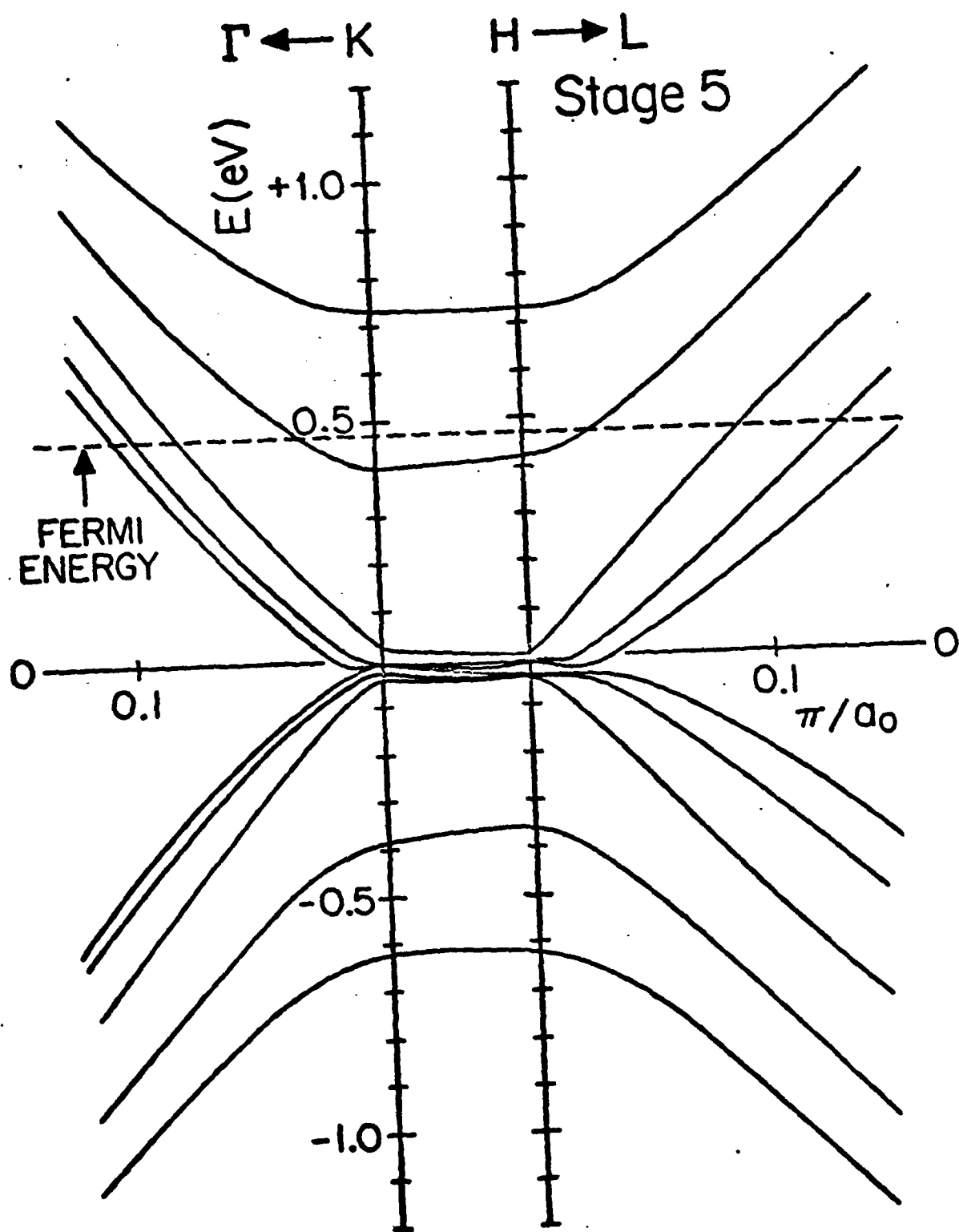


Fig. 5



PHENOMENOLOGICAL MODEL FOR THE ELECTRONIC STRUCTURE  
OF GRAPHITE INTERCALATION COMPOUNDS

G. Dresselhaus<sup>\*</sup> and S.Y. Leung<sup>+</sup>

Massachusetts Institute of Technology  
Cambridge, Massachusetts 02139, USA

ABSTRACT

The electron energy bands for graphite intercalation compounds are calculated using a model based on the well-established electronic structure of pristine graphite. The  $\pi$ -band Hamiltonian for graphite is folded in  $k$ -space appropriate to the intercalant superlattice which includes  $k_z$ -axis and in-plane zone folding. The folded  $k$ -space Hamiltonian is transformed into a layer representation and modifications are incorporated into the Hamiltonian to properly account for the perturbations due to the intercalate layer. With the inclusion of an interaction between the intercalate layer and the graphite bounding layer, electronic structures appropriate to both donor and acceptor compounds can be deduced. The model is applicable to any intercalant and stage, and predicts stage dependent Shubnikov-de Haas and optical spectra.

## I. Introduction

The intercalate symmetry imposes a superlattice periodicity on the crystal structure of graphite intercalation compounds which is reflected in the electronic structure. This intercalate symmetry can be conveniently modeled by Brillouin zone folding of the electronic dispersion relations  $E(k)$  of pristine graphite [1]. The staging periodicity is the dominant symmetry of intercalated graphite, and can be found in most donor and acceptor compounds that have been prepared to date [2]. The staging periodicity is treated mathematically in terms of a  $k_z$ -axis zone folding of  $E(k)$ . In addition, in-plane ordering appears to be well established in some compounds, such as the stage 1 alkali metal compounds [3]. The symmetry imposed by the in-plane intercalate ordering for systems where the intercalate structure is commensurate with the graphite layers is treated by an in-plane folding of the dispersion relations. Both types of zone folding are considered in this treatment of the electronic dispersion relations for intercalated graphite. By emphasizing the basic symmetry of the intercalation compounds, a model is developed which is applicable to any intercalant and stage.

The zone folding technique presented here is based on the known electronic structure of pristine graphite [4,5]. The intercalate layer is initially modeled as a periodic empty layer [6] in otherwise perfectly ordered graphite. This empty intercalate layer model simultaneously explains Fermi surface data [7], which show a pronounced stage dependence of the Fermi surfaces and major departures from the graphite Fermi surfaces, and magnetoreflexion data [8] which provide strong evidence that the energy bands near the Fermi level remain highly graphitic upon intercalation. A  $k_z$ -dependent charge distribution results from the incomplete occupation of zone edge valence or conduction bands and from the intercalant-graphite bounding layer

interactions which are introduced to obtain a quantitative fit to experimental data .

In this paper, explicit results for the electronic dispersion relations are presented for various in-plane superlattices for stage 1 compounds, and for some higher stage compounds. Calculated dispersion relations are also presented as a function of stage, and are related to experimental results relevant to the electronic structure.

## II. Brillouin Zone Folding Model

The introduction of the intercalant introduces a c-axis periodicity associated with the staging phenomenon and in some cases an additional in-plane periodicity when the intercalant is commensurate with the graphite in-plane structure. The effect of the superlattice periodicity on the electronic structure is treated by zone folding of the graphite Brillouin zone on to the smaller zone for the superlattice structure. The interaction between the intercalate and graphite is then treated in perturbation theory.

In cases where an in-plane superlattice is present, the zone folding is represented mathematically by the in-plane zone-folded Hamiltonian  $H_{lf}(k)$

$$H_{lf}(k) = \begin{vmatrix} H_0(k+K_1) & . & . & 0 \\ . & . & . & . \\ 0 & . & . & H_0(k+K_m) \end{vmatrix} \quad (1)$$

in which  $H_0(k)$  is the 4x4 Hamiltonian for the graphite  $\pi$ -bands and the reciprocal lattice vectors  $K_1 \dots K_m$  are given in Table I for the simpler in-plane structures. For a superlattice unit cell containing  $p^2$  graphite unit cells there are  $p$  reciprocal lattice vectors and  $H_{lf}(k)$  is a  $(4px4p)$  matrix. If there is no in-plane periodicity, then  $H_{lf}(k)$  is simply the  $(4x4)$  Slonczewski-Weiss-McClure or Fourier expansion Hamiltonian for pristine graphite.

The staging periodicity for the intercalation compound is modeled using a  $k_z$ -axis zone folding technique. The Hamiltonian is written in terms of  $l$  pairs of graphite planes ABAB...AB, where the basic repeat distance is determined by the number of planes in the  $c$ -axis repeat distance of the intercalation compound, considering for the moment the intercalate layer to be indistinguishable from graphite. The  $k_z$ -zone-folded Hamiltonian  $H_{zf}(k)$  is then written as

$$H_{zf}(k) = \begin{vmatrix} H_{\perp f}(k) & 0 & \cdots \\ 0 & H_{\perp f}(k + \frac{\pi}{lc_0} \hat{z}) & \\ \vdots & & \ddots \\ & & & H_{\perp f}(k + \frac{l-1}{l} \frac{\pi}{c_0} \hat{z}) \end{vmatrix} \quad (2)$$

where each of the blocks is the (4px4p) in-plane folded graphite Hamiltonian given by Eq. (1) and  $l = n+1$  for even stage or  $(n+1)/2$  for odd stage compounds, where  $n$  is the stage index and  $c_0 = 3.35\text{\AA}$  [1].

The effect of intercalation is easily implemented in the Hamiltonian given by Eq. (3) after making a transformation to a layer representation [1], which is written as

$$H_{\text{layer}}(k) = U H_{zf}(k) U^{-1} \quad (3)$$

where the unitary transformation transforms the basis functions of Eq. (2) to basis functions for a layer representation. The resulting layer Hamiltonian is then written as

$$H_{\text{layer}}(k) = \begin{vmatrix} H_{A_0 A_0} & H_{A_0 B_0} & \dots & \dots \\ H_{A_0 B_0}^\dagger & H_{B_0 B_0} & H_{B_0 A_1} & \dots \\ \vdots & H_{B_0 A_1}^\dagger & H_{A_1 A_1} & \dots \\ \vdots & \vdots & \vdots & \ddots \\ & & & H_{B_{l-1} B_{l-1}} \end{vmatrix} \quad (4)$$

in which the blocks  $H_{A_i A_j}$ ,  $H_{A_i B_j}$ ,  $H_{B_i B_j} \dots$  are  $2p \times 2p$  matrices having layer subscripts.

The unitary transformation of  $H_{zf}(k)$  does not change the eigenvalues of the Hamiltonian. Thus the energy bands from the folded graphite Hamiltonian in the layer representation of Eq. (4) are formally identical to the graphite energy bands. However, in the layer representation, the effect of intercalation is easily included by substitution of matrix blocks for the intercalate species in place of the appropriate graphite layer. For the odd stage  $n$  compounds, the resulting Hamiltonian is

$$H_{\text{GIC}}^{(n)} = \begin{vmatrix} H_{XX} & H_{XB_0} & H_{XA_1} & \dots & H_{XB_\lambda} \\ H_{XB_0}^\dagger & H_{B_0 B_0} & H_{B_0 A_1} & \dots & \vdots \\ H_{XA_1}^\dagger & H_{B_0 A_1}^\dagger & H_{A_1 A_1} & \dots & \vdots \\ \vdots & \vdots & \vdots & \ddots & \vdots \\ H_{XB_\lambda}^\dagger & \vdots & \vdots & \vdots & H_{B_\lambda B_\lambda} \end{vmatrix} \quad (5)$$

where  $\lambda$  is written for  $(n-1)/2$ , and  $X$  denotes an intercalate layer. For

the even stage compounds [1] both an A layer and a B layer must be replaced by an intercalate block. Explicit results for the electronic energy dispersion relations are now presented for several cases of interest.

### III. Results and Discussion

Dispersion relations for graphite and for various in-plane zone foldings, some of which are appropriate to stage 1 compounds in their low temperature phases, are shown in Fig. 1. These  $\pi$ -band dispersion relations are calculated from Eq. (5) for the case where the graphite layer is replaced by an empty intercalate layer (the "empty intercalant layer lattice"). We note that in constructing the dispersion relations in Fig. 1, only the known energy band parameters for graphite are used with no additional terms introduced to account for the intercalant-graphite bounding layer interaction. The results for the  $p(\sqrt{3} \times \sqrt{3})R30^\circ$  and  $p(2 \times 2)$  superlattices enable a comparison to be made between the phenomenological model and both experimental results and theoretical first principles calculations for stage 1 compounds.

Results are shown in Fig. 2 for such a comparison between the dispersion relations calculated for the stage 1 empty intercalate layer model for a  $p(\sqrt{3} \times \sqrt{3})R30^\circ$  and  $p(2 \times 2)R0^\circ$  superlattice and for the first principles calculations of Holzwarth et al. [9] for  $C_6Li$  and of Ohno et al. [10] for  $C_8K$ . Good agreement is obtained for the bands related to the graphite  $\pi$ -bands, showing that the perturbation of the graphite  $\pi$ -bands by the intercalant is small. To obtain agreement for the hybridized metal s-bands, it is necessary to fit the phenomenological bands to the first principles hybridized s-bands to determine the overlap band parameters between the graphite  $\pi$ -orbitals and the intercalate orbitals. One attractive feature of the phenomenological model is that once the band parameters are determined for any low stage compound (where the graphite-intercalate interactions are

important), the dispersion relations for all stages can then be evaluated without introduction of additional band parameters. The phenomenological model thus provides a useful tool for the calculation of the electronic structure for high stage compounds where first principles calculations are difficult to make and the phenomenological model is expected to be most convergent.

A comparison between the dispersion relations for zone folded graphite (Eq. 4) and for the empty intercalate layer model (Eq. 5) is shown in Fig. 3 for a stage 3 compound for both a  $p(\sqrt{3} \times \sqrt{3})R30^\circ$  and a  $p(2 \times 2)$  in-plane superlattice. Independent of the in-plane superlattice, the replacement of a graphite layer by an empty intercalate layer gives rise to only minor differences in the structure of the  $\pi$ -bands, but results in a great reduction in the  $k_z$  dispersion near the zero of energy in Fig. 3. This reduction in the  $k_z$  dispersion has major consequences on the electronic and optical properties of intercalation compounds. Inclusion of a donor or an acceptor layer does little to perturb the general features of the "empty lattice" energy band model except for the placement of the energy levels near the zero of energy.

Finally, we show in Fig. 4, dispersion relations based on the empty intercalate layer model for stage 1 to 5 compounds with a  $p(\sqrt{3} \times \sqrt{3})R30^\circ$  in-plane folding. On the left we show a plot of the energy bands on an expanded energy scale in the region of the  $\Gamma$  and A points in the hexagonal Brillouin zone. For this in-plane superlattice, the Slonczewski-Weiss-McClure bands fold into the region of the Brillouin zone about  $\Gamma$ A. A comparison with other in-plane orderings shows that the details of the band structure in the neighborhood of the Fermi level is independent of in-plane order, since no explicit intercalate-graphite bounding layer interaction has been introduced. In this figure we further note that the dispersion relations differ

as we move away from the  $\Gamma$  point in the  $\Gamma M$  and  $\Gamma K$  directions, reflecting the trigonal warping of the energy bands.

The basic model for the dispersion relations presented in this paper has been applied to fit experimental Shubnikov de Haas (SdH) [7] and magneto-reflection [8] data. In addition, structure observed in the infrared reflectivity [11,12] can be identified with transitions between energy bands that are folded back because of the  $k_z$  periodicity due to the staging phenomenon. To distinguish between donor and acceptor compounds and to obtain a quantitative fit to experimental data, it is necessary to include an explicit interaction between the intercalate and graphite bounding layers.

With regard to Shubnikov de Haas measurements, the Fermi surface cross sectional areas depend critically on the position of the Fermi level. If the Fermi level lies above the highest  $\pi$ -band along the HK axis, the SdH frequencies will group into a number of clusters equal to the stage of the compound. The splitting within the clusters is directly related to the  $k_z$ -dispersion of the energy levels. In the fit to the SdH frequencies observed for stage 5 graphite-K [7], the Fermi level was placed so that only 4 out of 5 possible electron pockets were occupied, indicating a non-uniform  $z$ -dependence of the charge distribution.

The  $z$ -dependence of the charge distribution depends critically on both the position of the Fermi level and the shift in the bounding layer potential associated with the intercalate-graphite bounding layer interaction. If the  $\pi$ -bands are fully occupied (or fully empty) or exactly half occupied (as in pristine graphite), then the  $\pi$ -electron charge distribution is uniform on the graphite layers. Since each of the energy bands corresponds to a different contribution from each of the real space layers, a partial occupation of antibonding  $\pi$ -bands, associated with raising the Fermi level through donor



intercalation, gives rise to a non-uniform charge distribution even within the empty intercalate layer model. The introduction of an intercalate-graphite bounding layer interaction further contributes to the  $z$ -dependence of the charge distribution.

The formalism developed for the electronic levels in the intercalation compounds is easily applied to the calculation of quantized Landau levels [13]. Such an analysis is needed for the detailed interpretation of the magnetoreflexion experiments [8] which show that intercalation gives rise to small changes in the graphite band parameters. These changes can be measured quantitatively over a wide range of intercalate concentrations and the resulting band parameters can be incorporated into the model of Eq. (5). The large decrease found for the  $k_z$ -dispersion of the electronic states is also observed for the Landau levels, and hence the magnetic field-induced singularities in the density of states are enhanced by intercalation. In addition,  $k_z$ -axis zone folding introduces new singularities in the density of states which are expected to give rise to new series of Landau level transitions.

A great amount of work yet remains to be done to obtain electronic dispersion relations which can quantitatively account for the large variety of detailed experimental information now becoming available for the graphite intercalation compounds.

#### Acknowledgments

We wish to gratefully acknowledge advice from Prof. M.S. Dresselhaus and support for this work from AFOSR Grant #77-3391.

## REFERENCES

- \* Francis Bitter National Magnet Laboratory, supported by NSF.
- † Center for Materials Science and Engineering and Department of Electrical Engineering and Computer Science.
- [1] G. Dresselhaus and S.Y. Leung, Solid State Commun. (to be published).
- [2] A. Hérold, Physics and Chemistry of Materials with Layered Structures (ed. F. Lévy) Reidel, Dordrecht, Holland, vol. 6, p. 323 (1979).
- [3] D.E. Nixon and G.S. Parry, J. Phys. D1 (1968) 291;  
G.S. Parry, Mat. Sci. Eng. 31 (1977) 99.
- [4] J.W. McClure, Proc. Int. Conf. on Semimetals and Narrow Gap Semiconductors, Dallas, Texas (1970), ed. D.L. Carter and R.T. Bate, Pergamon Press, New York, p. 127.
- [5] L.G. Johnson and G. Dresselhaus, Phys. Rev. B7 (1973) 2275.
- [6] G. Dresselhaus and S.Y. Leung, Extended Abstracts of the 14th Biennial Conference on Carbon, Penn. State Univ. p. 496 (1979).
- [7] G. Dresselhaus, S.Y. Leung, M. Shayegan and T.C. Chieu, Syn. Metals (to be published). H. Suematsu, K. Higuchi, and S. Tanuma, J. Phys. Soc. Jpn. 48 (1980) 1541.
- [8] E. Mendez, T.C. Chieu, N. Kambe and M.S. Dresselhaus, Solid State Commun. 33 (1980) 837.
- [9] N.A.W. Holzwarth, S. Rabi and L.A. Girifalco, Phys. Rev. B18 (1978) 5190.
- [10] T. Ohno, K. Nakao and H. Kamimura, J. Phys. Soc. Japan 47 (1979) 1125.
- [11] J. Blinowski, H.H. Nguyen, C. Rigaux, J.P. Vieren, R. LeToullec, G. Furdin, A. Hérold and J. Mélin, J. Physique 41 (1980) 47.
- [12] P.C. Eklund, D.S. Smith, and V.R.K. Murthy, Syn. Metals (to be published).
- [13] M.S. Dresselhaus, T.C. Chieu, M. Shayegan and G. Dresselhaus, Proc. of the Int. Conf. on High Magnetic Fields 1980 (Hakone).

Abbreviated Running Title: Electronic Energy Bands of GIC

Table I Points Equivalent to the  $\Gamma$  Point for Various In-Plane Zone Foldings

Superlattice		Equivalent Points	
Carbon Atoms Per Unit Cell	Notation	Label	$\underline{B}_0 \quad \frac{a}{2\pi} \underline{k} \quad (a)$
$C_2$	$p(1 \times 1)$	$\Gamma$	$(0,0,0)$
$C_6$	$p(\sqrt{3} \times \sqrt{3})R30^\circ$	$\Gamma$	$(0,0,0)$
		$K_0, K_1$	$(\frac{1}{3}, \frac{1}{\sqrt{3}}, 0)$
$C_8$	$p(2 \times 2)$	$\Gamma$	$(0,0,0)$
		$M_0, M_1, M_2$	$(\frac{1}{2}, \frac{1}{2\sqrt{3}}, 0)$
$C_{14}$	$p(\sqrt{7} \times \sqrt{7})R19.1^\circ$	$\Gamma$	$(0,0,0)$
		$W_0, W_1, \dots, W_5$	$(\frac{2}{7}, \frac{4}{7\sqrt{3}}, 0)$
$C_{18}$	$p(3 \times 3)$	$\Gamma$	$(0,0,0)$
		$K_0, K_1$	$(\frac{1}{3}, \frac{1}{\sqrt{3}}, 0)$
		$\Sigma_0, \Sigma_1, \dots, \Sigma_5$	$(0, \frac{2}{3\sqrt{3}}, 0)$
$C_{24}$	$p(\sqrt{12} \times \sqrt{12})R30^\circ$	$\Gamma$	$(0,0,0)$
		$K_0, K_1$	$(\frac{1}{3}, \frac{1}{\sqrt{3}}, 0)$
		$M_0, M_1, M_2$	$(\frac{1}{2}, \frac{1}{2\sqrt{3}}, 0)$
		$T_0, T_1, \dots, T_5$	$(\frac{1}{3}, 0, 0)$

(a) The equivalent reciprocal space vectors  $\underline{B}_n$  are given by a rotation of  $\underline{B}_0$  by  $n60^\circ$  around the  $k_z$ -axis.

# FIGURE CAPTIONS

- Fig. 1** Electronic dispersion curves for  $\pi$ -bands in graphite and in an empty intercalate layer model for a stage 1 intercalation compound with various in-plane zone foldings, each corresponding to the indicated commensurate ordered intercalate superlattice.
- Fig. 2** Comparison between the stage 1 empty intercalate layer model for a  $p(\sqrt{3} \times \sqrt{3})R30^\circ$  superlattice (solid curves) and the band structure calculation (dashed curves) for  $C_6Li$  by Holzwarth et al. (Ref. 9). The  $p(2 \times 2)$  structure (solid curves) is compared to the band calculation (dashed curves) for  $C_8K$  by Ohno et al. (Ref. 10). The first principles calculations (dashed curves) also show alkali metal s and p bands and consider explicitly the  $\alpha\beta\gamma\delta$  intercalate stacking order in the case of  $C_8K$ ; these features are not considered in the present calculation.
- Fig. 3** Electronic dispersion relations for a stage 3 compound assuming both a  $p(\sqrt{3} \times \sqrt{3})R30^\circ$  and a  $p(2 \times 2)$  in-plane ordering. For the dispersion relations labeled 'folded graphite',  $k_z$ -axis zone folding appropriate to a stage 3 compound has been carried out while the curves labeled 'stage 3' correspond to the replacement of a graphite layer by an empty intercalate layer, thereby reducing the number of energy levels and reducing the  $k_z$  dispersion of the energy bands.
- Fig. 4** Empty intercalate layer  $\pi$ -band model applied to a  $p(\sqrt{3} \times \sqrt{3})R30^\circ$  superlattice for stage  $1 \leq n \leq 5$  compounds. On the left is shown an expanded energy scale plot of the bands which occur near the Fermi level for each intercalation compound.

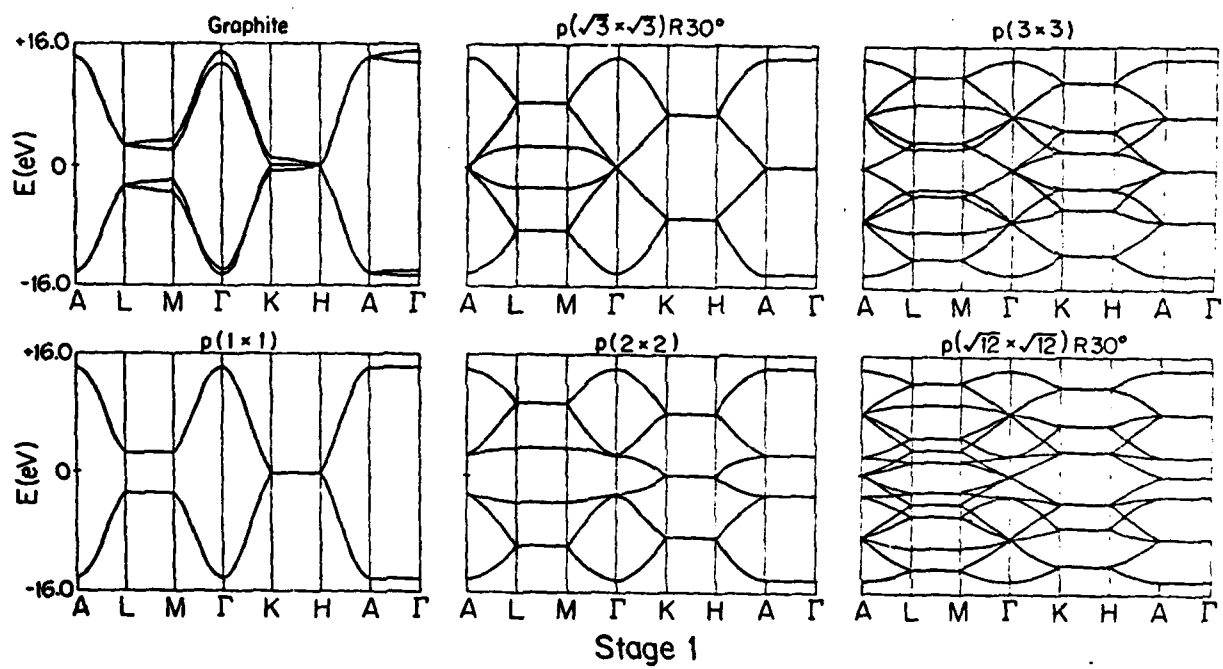


Fig. 1

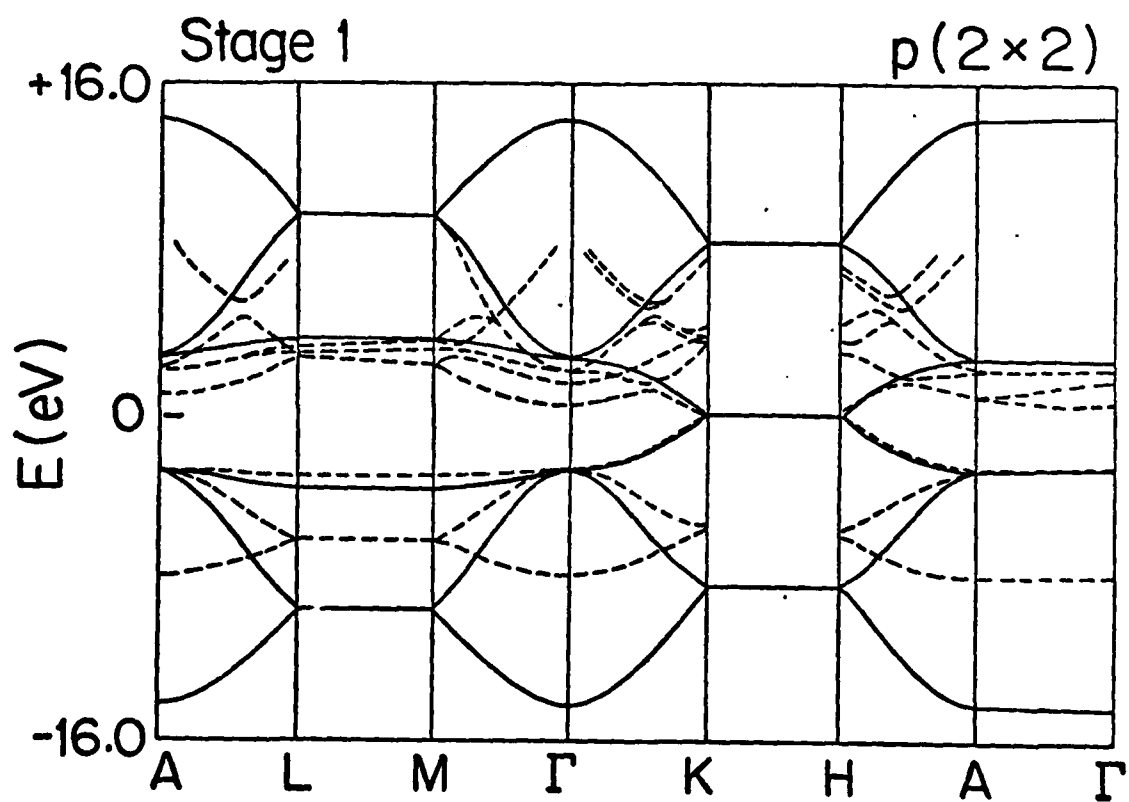
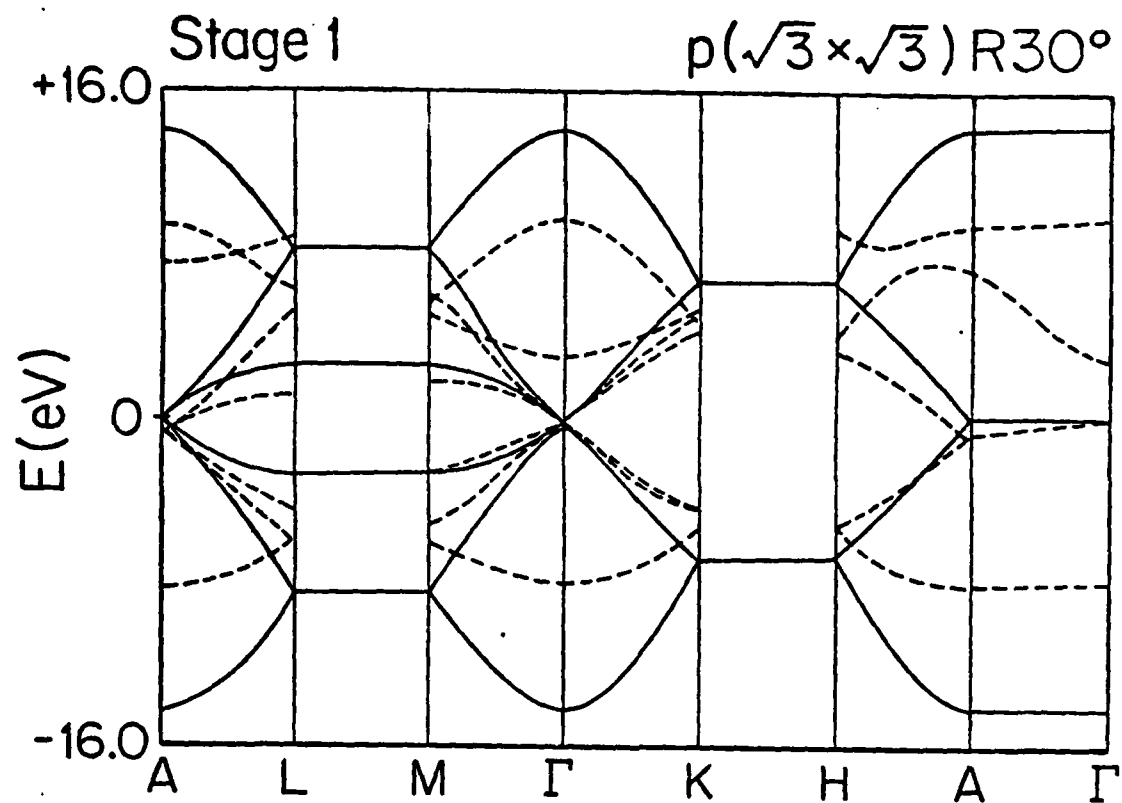


Fig. 2

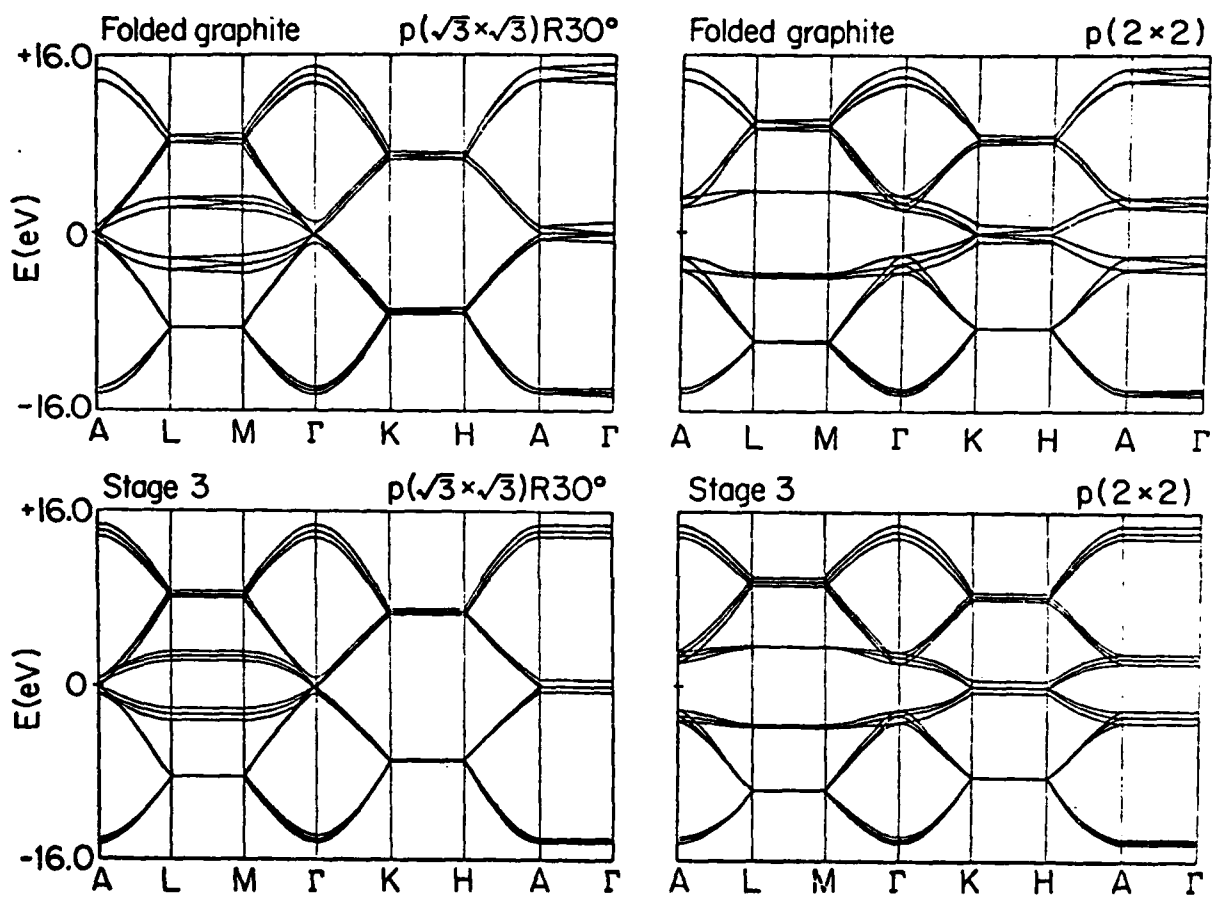


Fig. 3

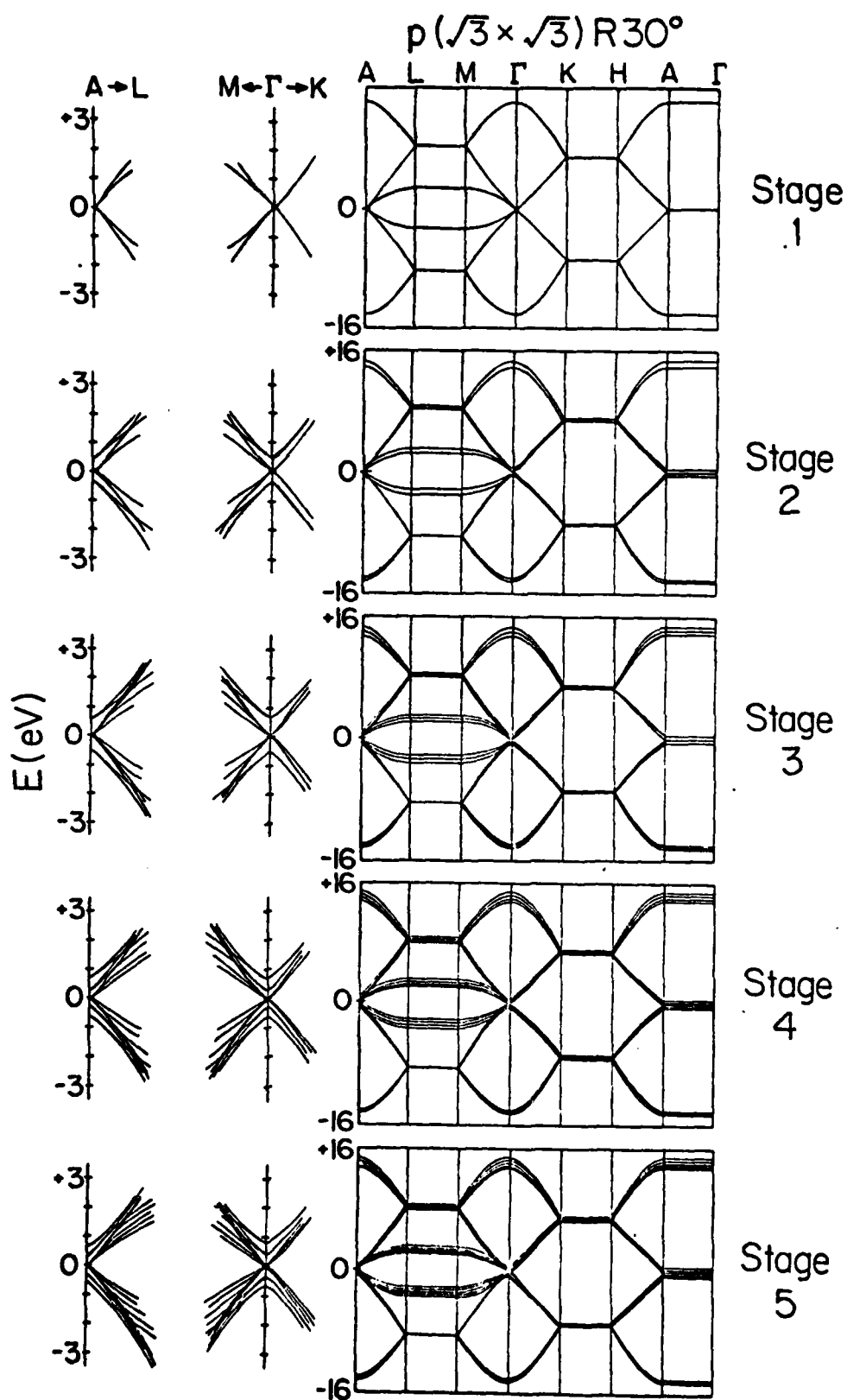


Fig. 4



Accepted June 3, 1980

R.H. Silsbee / m

PHENOMENOLOGICAL ELECTRONIC ENERGY BANDS  
IN GRAPHITE INTERCALATION COMPOUNDS

G. Dresselhaus<sup>†</sup> and S.Y. Leung<sup>\*</sup>

Massachusetts Institute of Technology, Cambridge, MA 02139

ABSTRACT

The electronic energy bands near the Fermi level for both donor and acceptor graphite intercalation compounds are modelled using a  $k_z$ -axis zone folded form of the SWMcC bands for pristine graphite. The effect of intercalation is included through terms for the intercalant and for the interaction between intercalant and graphite layers. Graphitic  $\pi$ -bands appropriate to both donor and acceptor compounds are presented.

Recent advances in the preparation and characterization of graphite intercalation compounds have given rise to detailed and accurate measurements relevant to the Fermi surface topology [1,2] and to the electronic structure [2,3]. Various authors [4,5] have stressed that even for low-stage compounds most of the electronic levels in an energy range of  $\sim \pm 10$  eV of the Fermi level are directly related to those in pristine graphite. Because of this close relation to pristine graphite, the theoretical models which have been discussed are often expressed in terms of single layer graphite bands [6,7]. The two-dimensional models for intercalated graphite [8] have been written to include charge transfer to the graphite and screening charge in the graphite bounding layers.

The first principles calculations for the stage 1 donor compounds  $C_6Li$  [9] and  $C_8K$  [10,11] have confirmed many of the above assumptions. These calculations also emphasize that a fully self-consistent one-electron band calculation does not require additional assumptions about charge transfer and screening charge density because such quantities can be calculated directly from the wave functions used in the calculation. Nevertheless, because of practical considerations related to the large number of atoms in the unit cell for the dilute compound, first principles band calculations cannot be carried out for the entire range of stages and intercalants for which experimental work has been reported. Therefore phenomenological models, such as the  $k_z$ -axis zone folded model developed in this paper, are needed to explain experimental data or to serve as an interpolation scheme between calculated  $\vec{k}$  points in first principles calculations and as an extrapolation scheme to high stage compounds.

The results presented in this paper represent a specialization of a more general c- and a-axis zone folded model presented elsewhere [12,13]. The general model shows that the form of the levels near the Fermi surface reduces to the Slonczewski-Weiss-McClure (SWMcC) form, independent of the in-plane order. The SWMcC effective Hamiltonian valid for  $\vec{k}_s$  on or near the HKH axis is written [14,15] as

$$H_0(\vec{k}_s) = \begin{vmatrix} E_1 & 0 & H_{13} & H_{13}^* \\ 0 & E_2 & H_{23} & -H_{23}^* \\ H_{13}^* & H_{23}^* & E_3 & H_{33} \\ H_{13} & -H_{23} & H_{33}^* & E_3 \end{vmatrix} \quad (1)$$

in which the  $\vec{k}_s$  dependence of the matrix elements is either the SWMcC Hamiltonian [14] or the full 3-dimensional Fourier expansion [16] of the interacting  $\pi$ -bands.

The SWMcC Hamiltonian is written [14] in a representation whose symmetrized Bloch functions are given by  $\psi_{11} = (a+a')/\sqrt{2}$ ,  $\psi_{21} = (a-a')/\sqrt{2}$ ,  $\psi_{31} = b$ ,  $\psi_{32} = b'$ .

These functions transform as the irreducible representations of the group of the  $\vec{k}_s$  wave vector at point  $\vec{k}_s$  and are

$$\begin{aligned}
 a(\vec{k}_s) &= \frac{1}{\sqrt{N}} \sum_{\vec{d}} e^{i\vec{k}_s \cdot \vec{d}} \psi_z(\vec{r} - \vec{d}) \\
 a'(\vec{k}_s) &= \frac{1}{\sqrt{N}} \sum_{\vec{d}} e^{i\vec{k}_s \cdot (\vec{d} + \vec{t}_{A'})} \psi_z(\vec{r} - \vec{d} - \vec{t}_{A'}) \\
 b(\vec{k}_s) &= \frac{1}{\sqrt{N}} \sum_{\vec{d}} e^{i\vec{k}_s \cdot (\vec{d} + \vec{t}_B)} \psi_z(\vec{r} - \vec{d} - \vec{t}_B) \\
 b'(\vec{k}_s) &= \frac{1}{\sqrt{N}} \sum_{\vec{d}} e^{i\vec{k}_s \cdot (\vec{d} + \vec{t}_{B'})} \psi_z(\vec{r} - \vec{d} - \vec{t}_{B'})
 \end{aligned} \quad (2)$$

where the origin is at atom A in the A plane and  $\vec{t}_{A'}$ ,  $\vec{t}_B$ ,  $\vec{t}_{B'}$  are vectors from the origin to the other atoms in the graphite unit cell. The intercalation compound is modelled using a  $k_z$ -axis zone folding technique. The Hamiltonian is written in terms of  $l$  pairs of graphite planes ABAB...AB, where the basic repeat distance is determined by the number of planes in the c-axis repeat distance of the intercalation compound, considering for the moment the intercalate layer to be indistinguishable from graphite. The zone-folded Hamiltonian is taken to be

$$H_{\text{folded}}(\vec{k}_s) = \begin{vmatrix} H_0(\vec{k}_s) & 0 & \dots & \dots \\ 0 & H_0(\vec{k}_s + \frac{\pi}{l c_0} \hat{z}) & & \\ \vdots & & \ddots & \\ \vdots & & & H_0(\vec{k}_s + \frac{l-1}{l} \frac{\pi}{c_0} \hat{z}) \end{vmatrix} \quad (3)$$

where each of the blocks is the 4x4 SWMcC Hamiltonian given by Eq. (1) and  $l=n+1$  for even stage or  $(n+1)/2$  for odd stage compounds, where  $n$  is the stage index. The basis functions for the folded Hamiltonian, Eq. (3), are given by Eq. (2), with the appropriate translations in  $\vec{k}$ -space, and  $c_0=3.35\text{\AA}$ .

In order to consider explicitly the effect of intercalation, the Hamiltonian given by Eq. (3) must be transformed to a layer representation which is written explicitly by

$$H_{\text{layer}}(\vec{k}_s) = U H_{\text{folded}}(\vec{k}_s) U^{-1} \quad (4)$$

where the unitary transformation is derived from the basis functions given in Eq. (2), yielding

$$U = \begin{vmatrix} \Omega_{0,0} & \Omega_{1,0} & \dots & \Omega_{\ell-1,0} \\ \Omega_{0,1} & \Omega_{1,1} & \dots & \Omega_{\ell-1,1} \\ \Omega_{0,2} & \Omega_{1,2} & \dots & \Omega_{\ell-1,2} \\ \vdots & \vdots & & \vdots \\ \Omega_{0,\ell-1} & \Omega_{1,\ell-1} & & \Omega_{\ell-1,\ell-1} \end{vmatrix} \quad (5)$$

where the  $4 \times 4$  matrix  $\Omega_{p,m}$  is given by

$$\Omega_{p,m} = \exp\left(\frac{-2\pi i m}{\ell}\right) \begin{vmatrix} \frac{1}{\sqrt{2}} & 0 & \frac{\gamma_p}{\sqrt{2}} & 0 \\ \frac{1}{\sqrt{2}} & 0 & -\frac{\gamma_p}{\sqrt{2}} & 0 \\ 0 & 1 & 0 & 0 \\ 0 & 0 & 0 & \gamma_p \end{vmatrix} \quad (6)$$

and  $\gamma_p = \exp(-\pi i p / \ell)$ . The resulting layer Hamiltonian is then written as

$$H_{\text{layer}}(\vec{k}_s) = \begin{vmatrix} H_{A_0 A_0} & H_{A_0 B_0} & \dots & \dots \\ H_{A_0 B_0}^\dagger & H_{B_0 B_0} & H_{B_0 A_1} & \dots \\ \vdots & H_{B_0 A_1}^\dagger & H_{A_1 A_1} & \dots \\ \vdots & \vdots & \vdots & \vdots \\ \vdots & \vdots & \vdots & H_{B_{\ell-1} B_{\ell-1}} \end{vmatrix} \quad (7)$$

in which the blocks  $H_{A_i A_j}$ ,  $H_{A_i B_j}$ ,  $H_{B_i B_j}$ , ... are  $2 \times 2$  matrices having layer subscripts.

The unitary transformation of  $H_{\text{folded}}(\vec{k}_s)$  does not change the eigenvalues of the Hamiltonian. Thus the energy bands from the folded SWMcC Hamiltonian in the layer representation of Eq. (6) are identical to the SWMcC energy bands. However, in the layer representation, the effect of intercalation is easily included by substitution of matrix blocks for the intercalate species in place of the appropriate graphite layer. For the odd stage  $n$  compounds, the resulting Hamiltonian is

$$H_{\text{GIC}}^{(n)} = \begin{vmatrix} H_{XX} & H_{XB_0} & H_{XA_1} & \dots & H_{XB_\lambda} \\ H_{XB_0}^\dagger & H_{B_0 B_0} & H_{B_0 A_1} & & \\ H_{XA_1}^\dagger & H_{B_0 A_1}^\dagger & H_{A_1 A_1} & & \\ \vdots & & & \ddots & \\ H_{XB_\lambda}^\dagger & & & & H_{B_\lambda B_\lambda} \end{vmatrix} \quad (8a)$$

where  $\lambda$  is written for  $(n-1)/2$ , and  $X$  denotes an intercalate layer. For the even stage compounds the effective Hamiltonian is

$$H_{\text{GIC}}^{(n)} = \begin{vmatrix} H_{XX} & H_{XB_0} & \dots & \dots & H_{XB_n} \\ H_{XB_0}^\dagger & H_{B_0 B_0} & & & \\ \vdots & \ddots & H_{A_\mu A_\mu} & H_{A_\mu X} & \\ \vdots & & H_{A_\mu X}^\dagger & H_{XX} & H_{XA_\nu} \\ \vdots & & & H_{XA_\nu}^\dagger & H_{A_\nu A_\nu} \\ & & & \ddots & \vdots \\ H_{XB_n}^\dagger & & & & H_{B_n B_n} \end{vmatrix} \quad (8b)$$

where  $\mu = n/2$  and  $\nu = (n/2) + 1$ . If the stacking of the intercalate layers is different in successive layers (e.g.  $\alpha, \beta, \gamma, \dots$ ), the Hamiltonian can be generalized by considering explicitly a larger unit cell and appropriate interaction terms to split the zone-folded levels.

In this paper we consider the implications of the form of Eq. (8a) and (8b) by an explicit diagonalization of these matrices, first for an "empty" lattice in which the intercalate layer is "vacuum" (i.e.  $H_{YX} = H_{XA_1} = H_{XB_j} \equiv 0$ ) and then for a generalized donor or acceptor compound in which a dispersionless intercalate layer interacts with the graphite bounding layer. Because of the non-equivalent bounding layer carbon sites, the Fourier expansion Hamiltonian for the intercalation compound includes a constant energy shift for the bounding graphite layer,  $\mu_0$ , as well as  $\vec{k}$ -dependent interaction terms. The results for a single parameter model are shown in Fig. 1. The case of the "empty lattice" ( $\mu_0 = 0$ ) is given in the center of each set. Results for a bounding layer energy shift of  $\mu_0 = 0.3\text{eV}$  are presented on the left side labeled acceptors, and for  $\mu_0 = -0.3\text{eV}$  on the right side labeled donors. The position of the intercalate level  $E_X$  is assumed to lie below the region of the SWMcC  $\pi$ -bands for acceptors upshifting the bounding layer energy levels. Correspondingly  $E_X$  is above the  $\pi$ -bands for donors giving a downshift to the bounding layer levels. The interaction of  $0.3\text{eV}$  was suggested by the preliminary analysis of Shubnikov-de Haas data [1,2]. The plots in Fig. 1 are made using the SWMcC band parameters for pristine graphite [17] given in Table 1 and a single interaction parameter  $\mu_0$ . The magnitude of  $\mu_0$  is expected to differ for each intercalant, but provided the in-plane intercalate density is independent of stage,  $\mu_0$  will also be independent of stage. Thus, the dispersion curves given in Fig. 1 for stages  $1 \leq n \leq 8$  depend on the introduction of a single parameter  $\mu_0$ .

The withdrawal of a graphite layer greatly reduces the dispersion of the bands in the  $k_z$  direction. Additional  $k_z$  dispersion can be introduced by inclusion of  $k_z$ -dependent terms in the intercalate-graphite bounding layer interaction. For stages  $n > 2$ , the near degeneracy of the  $E_3$  graphite levels shown for the "empty lattice" bands in Fig. 1 is partially lifted by  $\mu_0$  through non-rigid band shifts, though a number of the  $E_3$  levels still cluster and retain their near degeneracy. However, for stages  $n=1$  and 2, the effect of  $\mu_0$  is merely to produce a constant energy level shift, which is physically reasonable since in these cases there are only graphite bounding layers. Note that for higher stage compounds ( $n \geq 4$ ) in Fig. 1, both electron and hole pockets can be formed if the interaction energy is comparable with the Fermi energy shift.

Landau level transitions between the nearly degenerate  $E_3$  levels are observed in the magnetoreflexion spectra [3] which are well fit by the SWMcC model with small but measurable changes in the SWMcC band parameters upon intercalation. These modified values of the band parameters can then be used in applying Eqs. (8a) and (8b) to the interpretation of experimental data such as the de Haas-van Alphen effect. Though the parameter changes result in small perturbations of the SWMcC bands, near the HK axis, larger interactions

could occur in other regions of the Brillouin zone, e.g. the M point. The energy bands of Fig. 1 show extremal cross sectional areas at the H and K points [2] which can be calculated and compared with measured DHVA frequencies and effective masses. The band model of Eq. (8a,8b) is also amenable to Landau level calculations using either raising and lowering operator techniques [18] or semi-classical Bohr-Sommerfeld quantization [19], both of which have been applied to graphite.

The bands shown in Fig. 1 are all graphite  $\pi$ -bands. The levels represented by the intercalate Hamiltonian  $H_{XX}$  are not included in this presentation of results in order to show features of the graphite  $\pi$ -bands which are common to all intercalants. The intercalate block  $H_{XX}$  is eliminated from Eqs. (8a) and (8b) using the Löwdin summation. This gives the addition of a term  $-(H_{XA_i} H_{XA_j}) / (H_{XX} - \epsilon)$  to the larger block in Eq. (8) where  $\epsilon$  is the eigenvalue. The sign of this contribution is negative for donors when the intercalate layers are above  $\epsilon$  and positive for acceptors where the intercalate layers are below  $\epsilon$ . The Fermi level can be calculated by assuming explicitly the fractional charge transfer per intercalate atom or molecule. Incomplete charge transfer to the SWMcC bands implies that the intercalate bands are occupied or that in-plane zone-folding has resulted in the occupation of  $\pi$ -bands at other points in the zone such as the M-point [13]. These additional levels should then be included explicitly in Eqs. (8a,8b).

The electronic states associated with the intercalate layer can be explicitly incorporated in the  $H_{XX}$  block of the Hamiltonian,  $H_{GIC}^{(n)}$ , given in Eqs. (8a,8b). The alkali metal donor compounds require levels associated with s and p orbitals, whereas the acceptor compounds generally require the use of more localized electronic states. These considerations for the electronic levels in the pristine intercalate material suggest that donor compounds should exhibit more  $k_z$  dependence in the coupling blocks,  $H_{XB_0}$ , and more  $k_z$  dispersion than the acceptor compounds. The observed conductivity anisotropies in donors and acceptors is consistent with this basic difference in the intercalate electronic levels.

This simple extension of the phenomenological graphite Hamiltonian features the close relation between pristine graphite and the well-staged intercalation compounds. The model is based on a  $k_z$ -axis Brillouin zone-folding and makes no use of a-plane superlattice periodicity. The same Hamiltonian with no additional parameters can be used to model all stages (plots are shown in Fig. 1 for stages  $1 \leq n \leq 8$ ). The model can be used for the standard introduction of Landau level quantization and thus provides a direct way of applying quantum oscillatory phenomena to a quantitative determination of the electronic structure of intercalation compounds.

**Acknowledgments** - The authors wish to thank M. Shayegan and Prof. M.S. Dresselhaus for numerous discussions regarding this work. This work was supported by AFOSR grant #77-3391.

# REFERENCES

- † Francis Bitter National Magnet Laboratory, supported by the NSF.
- \* Department of Electrical Engineering and Center for Materials Science & Engineering
1. SUEMATSU, H., TANUMA, S. and HIGUCHI, K., *Physica* 99B, 420 (1980).
2. DRESSELHAUS, G., LEUNG, S.Y., SHAYEGAN, M. and CHIEU, T.C., *Synthetic Metals* (to be published).
3. MENDEZ, E., CHIEU, T.C., KAMBE, N. and DRESSELHAUS, M.S., *Solid State Commun.* 33, 837 (1980).
4. DRESSELHAUS, M.S., DRESSELHAUS, G. and FISCHER, J.E., *Phys. Rev.* B15, 3180 (1977).
5. EBERHARDT, W., MCGOVERN, I.T., PLUMMER, E.W. and FISCHER, J.E., *Phys. Rev. Lett.* 44, 200 (1980).
6. BLONOWSKI, J., NGUYEN, H.H., RIGAUX, C., VIEREN, J., LETOULLEC, R., FURDIN, G., HÉROLD, A. and MELIN, J., *J. Physique* 41, 47 (1980).
7. HOLZWARTH, N.A.W., *Phys. Rev.* B21, 3665 (1980).
8. PIETRONERO, L., STRÄSSLER, S., ZELLER, H.R. and RICE, M.J., *Phys. Rev. Lett.* 41, 763 (1978).
9. HOLZWARTH, N.A.W., RABII, S. and GIRIFALCO, L.A., *Phys. Rev.* B18, 5190 (1978).
10. INOSHITA, T., NAKAO, K. and KAMIMURA, H., *J. Phys. Soc. Japan* 43, 1237 (1977).
11. OHNO, T., NAKAO, K. and KAMIMURA, H., *J. Phys. Soc. Japan* 47, 1125 (1979).
12. DRESSELHAUS, G. and LEUNG, S.Y., *Extended Abstract of the 14th Biennial Conference on Carbon*, Penn. State Univ., p. 498 (1979).
13. DRESSELHAUS, G. and LEUNG, S.Y. (to be published).
14. MCCLURE, J.W., *Phys. Rev.* 108, 612 (1957).
15. DRESSELHAUS, G. and DRESSELHAUS, M.S., *Phys. Rev.* 140, A401 (1965).
16. JOHNSON, L.G. and DRESSELHAUS, G., *Phys. Rev.* B7, 2275 (1973).
17. MENDEZ, E., MISU, A. and DRESSELHAUS, M.S., *Phys. Rev.* B21, 827 (1980).
18. MCCLURE, J.W., *Phys. Rev.* 119, 606 (1960).
19. DRESSELHAUS, G., *Phys. Rev.* B16, 3602 (1974).



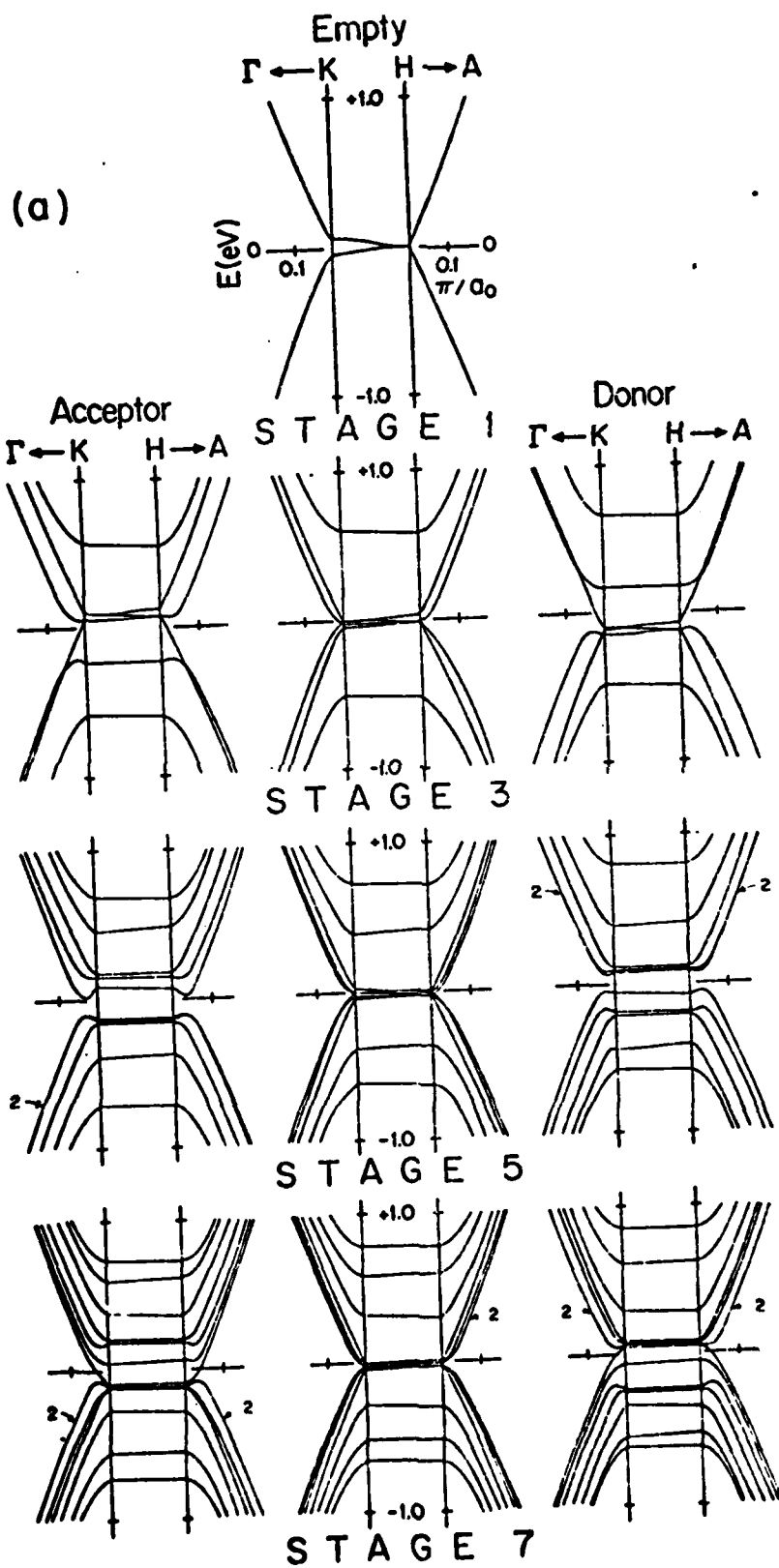
**Table 1** SMMC Band Parameters <sup>a)</sup>.

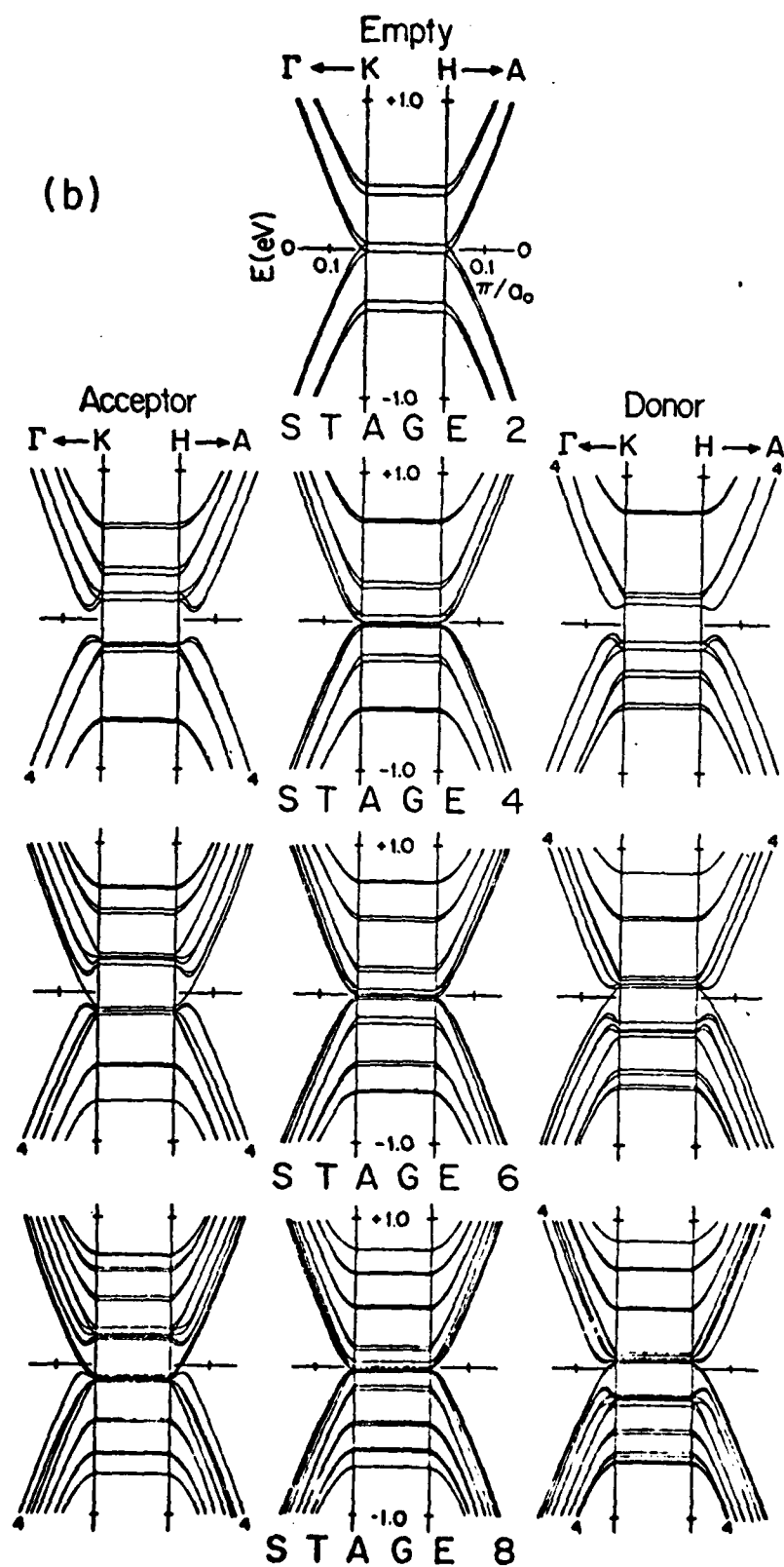
Band Parameters	Values (eV)
$\gamma_0$	3.16
$\gamma_1$	0.39
$\gamma_2$	-0.019
$\gamma_3$	0.30
$\gamma_4$	0.044
$\gamma_5$	0.038
$\Delta$	-0.008

<sup>a)</sup> See Ref. [17].

# Figure Captions

**Fig. 1**  $E(\vec{k})$  for graphite intercalation compounds along the edge of the hexagonal Brillouin zone where the K-point corresponds to  $k_z=0$ . The  $E(\vec{k})$  for the odd-stage compounds are plotted in (a) for stages  $n=1,3,5,7$  where the H-point corresponds to  $\pi/I_c$  where  $I_c$  is the repeat distance in the c-direction. The  $E(\vec{k})$  for the even stages is plotted in (b) for  $n=2,4,6,8$  where the H-point corresponds to  $\pi/2I_c$ . An intercalate graphite bounding layer interaction appropriate to donors is shown on the right hand side of the figure and that appropriate to acceptors is shown on the left. For each stage, the center panel is for the "empty lattice" with no graphite-intercalant interaction. Where degeneracies (or near degeneracies) occur, the number of levels is indicated. For the even stages the levels pair away from the HK axis except for the double pairings labeled 4.





# THE INTERRELATION OF SHUBNIKOV-DE HAAS, MAGNETOREFLECTION AND TRANSPORT PROPERTIES OF ALKALI METAL DONOR INTERCALATION COMPOUNDS

M.S. Dresselhaus<sup>†</sup>, G. Dresselhaus<sup>\*,\*</sup>, M. Shayegan<sup>~</sup> and T.C. Chien<sup>~</sup>

Massachusetts Institute of Technology  
Cambridge, Massachusetts 02139, USA

The  $k_z$ -axis zone folded Hamiltonian based on pristine graphite energy bands with an empty intercalate layer accounts for both observations of the Fermi surface made by the Shubnikov-de Haas technique, which show large changes with intercalation, and of the magnetic energy level structure by the magnetoreflexion technique, where very small changes are found. This model has implications for transport and optical properties for donor intercalation compounds.

Because of the unusual properties of graphite intercalation compounds and their close connection to the semiconductor superlattice structures now being fabricated by molecular beam epitaxy, graphite intercalation compounds have attracted attention in the semiconductor community. Analogous to the transport behavior observed for the semiconductor superlattice structures, the high electrical conductivity of graphite intercalation compounds is achieved by charge transfer from the intercalate layers where the mobility is low to the graphite layers where the mobility is very high. The superlattice structure created by molecular beam epitaxy growth is achieved in graphite intercalation compounds by the staging mechanism which results in intercalated graphite with sequential intercalant layers separated by  $n$  graphite layers where  $n$  denotes the stage. For intercalated graphite the staging periodicity is long range and is a dominant symmetry.

The electronic structure is determined by the basic symmetry of graphite as modified by the staging periodicity. This structure is here studied by the Shubnikov-de Haas effect for a determination of the Fermi surface and by the magnetoreflexion technique which is sensitive to the quantized electronic energy levels in a magnetic field. A phenomenological model based on crystal symmetry is used to interpret and to interrelate the experimental observations made by the two techniques. Application of the calculational techniques developed for the intercalated graphite superlattice structures to the semiconductor superlattice structures could be of significance.

Observation of only small changes in the electronic band parameters with intercalation suggests a theory for the electronic structure of intercalated graphite. The staging periodicity is modeled by a  $k_z$  folding of the energy bands and a perturbation by the intercalant at the proper  $k_z$  position. The interaction between the intercalant and the graphite layers is modeled by a perturbation theory. Results are shown in Fig. 1. The theory is compared to the experimental data in Fig. 2.

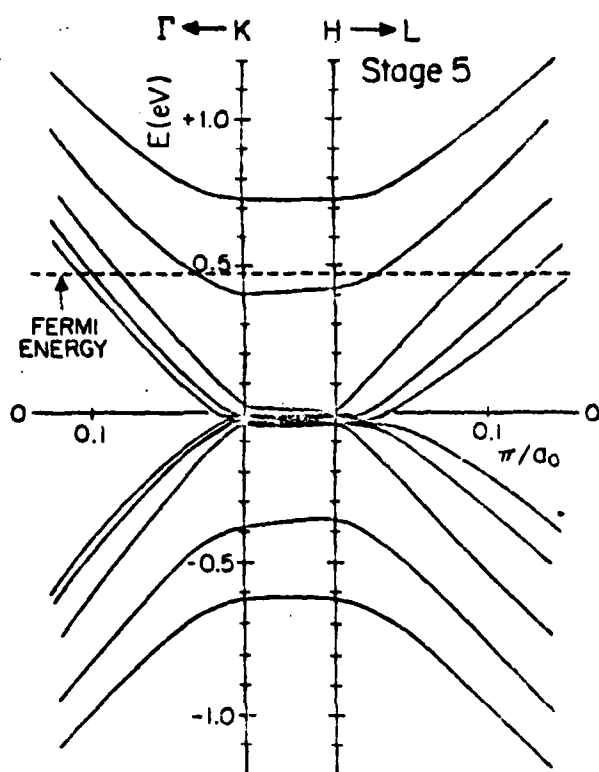


Fig. 1 Electronic band structure in the vicinity of the HK axis for a stage 5 "empty intercalate layer" model for a graphite intercalation compound. The Fermi energy is determined to fit the observed SdH frequencies. For the indicated Fermi level, four of the conduction bands are partially occupied and give rise to Fermi surfaces and carrier pockets.

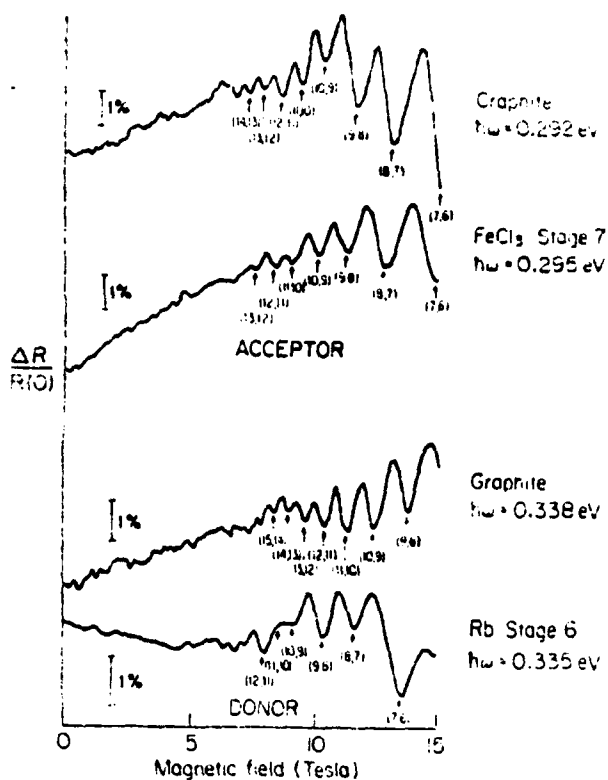


Fig. 2 Magnetoreflexion spectra using (+) circular polarization for an acceptor ( $\text{FeCl}_3$  stage 7) and for a donor compound (Rb stage 6) at the indicated photon energies. For comparison, traces for graphite are shown. The resonances are specified by quantum numbers for the initial and final states (Ref. 3).

interaction is neglected [2]. These results, shown for the 5 conduction and 5 valence bands near the H-K zone edge, demonstrate that intercalation greatly decreases the  $k_z$  dispersion. The placement of the Fermi level in Fig. 1 results in a partial occupation of the  $\pi$ -bands which gives rise to a  $z$ -dependent charge distribution.

Detailed information on the form of these energy bands is provided by the magnetoreflexion experiment which probes resonant transitions from occupied magnetic energy levels below the Fermi level  $E_F$  to unoccupied levels above  $E_F$ . Measurements have been made on well-staged donor (stages  $n \geq 6$ ) and acceptor (stage  $n \geq 4$ ) compounds [3], characterized by (00 $l$ ) diffractograms to establish their stage index and staging fidelity. Resonant structures observed in the magnetoreflexion spectra are identified with Landau level transitions between magnetic energy levels associated with the  $E_3$  bands which in graphite are degenerate at the K-point. The close similarity of the magnetoreflexion spectra in pristine graphite and in these donor and acceptor compounds indicates that the electronic structure of the  $\pi$ -bands near  $E_F$  remains highly graphitic upon intercalation.

Table 1 Results of analysis of magnetoreflexion experiments

Inter-calant	Stage	$m_c^*$	$m_v^*$	$(\gamma_0^2/\gamma_1)$
(HOPG)	$\infty$	0.056	0.084	25.1
AlCl <sub>3</sub>	8	0.056	0.076	26.0
	6	0.054	0.076	26.6
FeCl <sub>3</sub>	7	0.055	0.079	26.1
	5	0.054	0.075	26.6
Rb	6	0.045	0.065	31.7

Analysis of the observed spectra on the basis of a two-band model for the K-point valence and conduction bands yields the valence and conduction band effective masses  $m_v^*$  and  $m_c^*$ . Since the observed magnetoreflexion spectra in the intercalation compounds are well satisfied by the form of the Slonczewski-Weiss-McClure (SWMcC) energy level model for graphite, analysis of these data yields the SWMcC band parameter combination  $(\gamma_0^2/\gamma_1)$  which determines the Landau level

separation. A summary of typical results is given in Table 1, giving strong support for the close relation between the graphite  $\pi$ -bands in the intercalation compounds and in pristine graphite.

To study the Fermi surface, Shubnikov-de Haas (SdH) measurements of the transverse magnetoresistance have been made. Particular emphasis was given to measurements on encapsulated, well-staged alkali metal donor compounds [2]. The four-point method was used to study the a-plane transverse magnetoresistance in the temperature range  $1.4 < T < 4.2$  K and in magnetic fields up to 15 Tesla. Data acquisition was by computer, and the data were manipulated to obtain a Fourier power spectrum of resistance vs  $1/H$ , thereby yielding the frequencies of SdH oscillations, which are related to the extremal cross sections of the Fermi surface [2]. The Fourier power spectra for the SdH frequencies for potassium stages 2, 5 and 8 are shown in Fig. 3. Of particular significance is the stage dependence of the observed spectra, in agreement with results by Suematsu et al. [4]. A detailed study was made for several stage 5 samples and the observed SdH frequencies compared with predictions of the empty intercalate layer model of Fig. 1, with the Fermi level placed to fit the SdH frequencies. It should be noted that the empty intercalate layer model uses only graphite band parameters, which have been determined previously. Thus the good agreement obtained between the calculated and observed SdH frequencies in Table 2 gives strong support that the energy levels close to  $E_F$  are very similar to the basic  $\pi$ -bands of pristine graphite in agreement with the magnetoreflexion results discussed above. The large change in the SdH frequencies and their stage dependence is due to the stage dependence of the number of conduction and valence bands, of the  $k_z$ -axis zone-folding procedure and of the position of the Fermi level relative to the K-point band edge. It is of interest to note that light masses similar to those in pristine graphite are found for the small carrier pockets, with significantly larger masses for the larger carrier pockets which probably contribute more significantly to transport properties. It is furthermore likely that other carrier pockets of lower mobility occur elsewhere in the zone, thereby accounting for the proper charge transfer.

From the Shubnikov-de Haas results and the model for the energy bands we conclude that the transport properties of graphite intercalation compounds must be interpreted in terms of a multi-pocket model, with contributions from each of the occupied carrier pockets (see Fig. 1 and Table 2). Explicit use of an energy band model which can be applied to any stage and intercalant provides a basis for calculations of the transport properties for intercalated graphite.

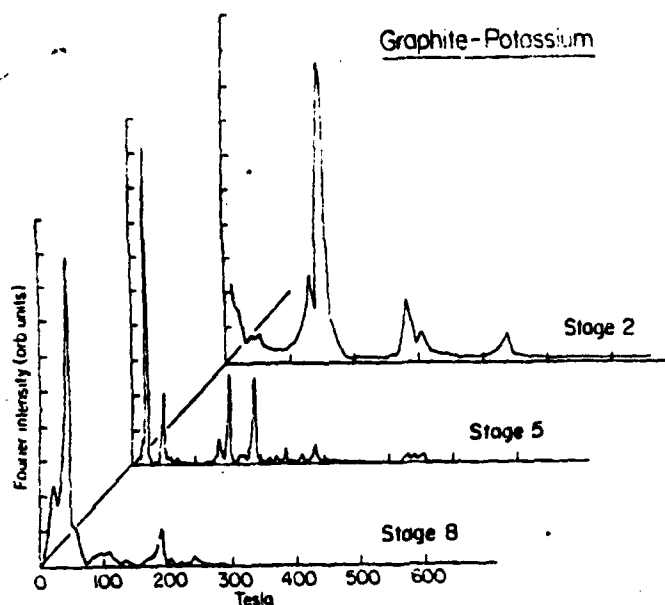


Fig. 3 Shubnikov-de Haas Fourier transform power spectra for stages 2, 5 and 8 graphite-K. These power spectra were obtained by a Fourier transform of an experimental resistivity vs  $1/H$  trace for magnetic fields  $H < 15$  Tesla. The peaks in the power spectra correspond to SdH frequencies, which are given in Tesla and the same scale is used for each stage.

Table 2 Fermi surface parameters associated with stage 5 graphite-K

Fermi Surface Parameters	K-point Band Designation			
	$K_1$	$K_2$	$K_3$	$K_4$
$m^*/m_0$	0.143	0.115	0.0828	0.0511
$n_i (x10^{20} \text{ cm}^{-3})$	2.36	1.76	0.975	0.138
SdH Frequencies				
Calculated (Tesla)	401	300	163	26.7
Observed (Tesla)	453 430	290 267 243	191 152 135	24 18

## References

- \* Supported by AFOSR grant #77-3391.
- + Center for Materials Science and Engineering, and Department of Electrical Engineering and Computer Science.
- \*\* Francis Bitter National Magnet Laboratory, supported by NSF.
- 1) G. Dresselhaus and S.Y. Leung: Solid State Commun. (in press).
- 2) G. Dresselhaus, S.Y. Leung, M. Shayegan and T.C. Chieu: Syn. Metals (to be published).
- 3) E. Mendez, T.C. Chieu, N. Kambe and M.S. Dresselhaus: Solid State Commun. 33 (1980) 837.
- 4) H. Suematsu, K. Higuchi and S. Tanuma: J. Phys. Soc. Japan 48 (1980) 1541.



Abstract Submitted  
for the New York Meeting of the  
American Physical Society  
March 24-28, 1980

Physical Review  
Classification Scheme  
Number 72.15.Gd

Bulletin Subject Heading  
Graphite Intercalation  
Compounds

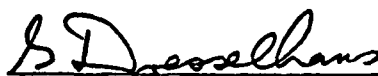
Electronic Energy Bands and Fermi Surfaces in Graphite Intercalation Compounds.<sup>†</sup> G. DRESSELHAUS,\* S.Y. LEUNG and M. SHAYEGAN, M.I.T.--A model for the electronic energy bands for graphite intercalation compounds is presented, based on the 3-dimensional Fourier expansion for the  $\pi$ -bands in pristine graphite. The model focuses both on staging periodicity which is treated by zone folding in the  $k_z$  direction and an in-plane superlattice which introduces an in-plane zone-folding. The effect of intercalation is treated in the Hamiltonian by the removal of a graphite layer and its replacement by an intercalate layer, resulting in a greatly reduced  $k_z$  dispersion with only minor changes in the in-plane dispersion. Graphite-intercalate interactions are introduced to yield the appropriate  $k_z$  dispersion indicated by experiment. This model is used to calculate extremal areas of the Fermi surface which are compared with SDH and DHVA experiments on low stage alkali metal compounds.

<sup>†</sup>Supported by AFOSR Grant #77-3391.

\*Francis Bitter National Magnet Lab, supported by NSF.

Prefer Regular Session

Submitted by



G. Dresselhaus  
Room 13-3017, M.I.T.  
Cambridge, MA 02139

Abstract Submitted  
for the New York Meeting of the  
American Physical Society  
March 24-28, 1980

Physical Review  
Classification Scheme  
Number 72.15.Gd

Bulletin Subject Heading  
Graphite Intercalation  
Compounds

Angular Dependence of SdH Frequencies in  
Alkali-Metal Graphite Intercalation Compounds.<sup>†\*</sup>  
M. SHAYEGAN and G. DRESSELHAUS<sup>†</sup>, M.I.T.-- The different  
stage dependence of the Fermi surface reported for  
donor and acceptor compounds has been a matter of  
interest and controversy. We report the angular  
dependence ( $\theta$ =angle between magnetic field and c-axis)  
for Shubnikov-de Haas (SdH) frequencies  $\Omega_0$  (Tesla) in  
well-staged (stages  $n \leq 4$ ) graphite-K and graphite-Rb  
compounds. The observed  $\Omega_0$  for potassium stage 2 are  
135T, 150T, 280T and 310T, with the main  $\Omega_0$  at 150T.  
The  $\theta$  dependence of these  $\Omega_0$  is consistent with a  
cylindrical Fermi surface along the c-axis. Rubidium  
samples show significantly different features.  
Rubidium stage-2 has its main  $\Omega_0$  at 28T with two  $\Omega_0$  of  
lower intensity at 220T and 260T. The  $\theta$  dependence  
for these  $\Omega_0$  is not compatible with cylindrical Fermi  
surfaces. Comparison is made to DHVA frequencies for  
graphite-K compounds reported by Tanuma et al. The  
results for K and Rb donor intercalants is contrasted  
and compared with observations in acceptor compounds.

<sup>†</sup>Supported by AFOSR grant #77-3391.

\*Work done at National Magnet Lab, sponsored by NSF.

<sup>†</sup>Francis Bitter National Magnet Lab, supported by NSF.

Prefer Regular Session

Submitted by

---

M. Shayegan  
Room 13-3029, M.I.T.  
Cambridge, MA 02139

by

BRUCE LEONARD HEFLINGER

Submitted to the Department of Electrical Engineering and Computer Science  
on November 28, 1979, in partial fulfillment of the requirements  
for the Degree of Doctor of Philosophy.

## ABSTRACT

Raman spectroscopy has been used to study Br-Br bond stretch modes, both for bromine adsorbed on Grafoil between  $-120$  and  $-133^{\circ}\text{C}$ , and for bromine in the gas phase above a room temperature pyrolytic graphite sample. The low temperature spectra include broad (FWHM  $\sim 24$   $\text{cm}^{-1}$ ) peaks at  $269$  and  $277$   $\text{cm}^{-1}$ , and a narrower peak ( $\sim 4$   $\text{cm}^{-1}$ ) at  $274$   $\text{cm}^{-1}$ . These three peaks, which are seen individually at different temperatures and bromine pressures, are tentatively correlated with the pressure/temperature adsorbed phase diagram from Lander and Morrison's LEED study. The data do not cover a sufficient range of pressures and temperatures to make a positive identification of the observed modes with the adsorbed phases.

At excitation wavelengths shorter than  $5100$  Angstroms, the room temperature Raman spectra are featureless at all bromine pressures studied. In particular, the expected Br-Br stretch modes corresponding to adsorbed  $\text{Br}_2$  molecules at gas pressures near the bromine-graphite intercalation threshold ( $18$  Torr) are not observed.

At excitation wavelengths longer than  $5100$  Angstroms, sharply resonant room temperature Raman spectra are observed. Relatively simple spectra excited by argon and krypton laser lines are identified as arising when the photon energy matches the energy separation between a level of the  $1\Sigma_g^+$  ground state and a level of the  $3\Pi_{0u}^+$  excited state. Dye laser spectra over the range  $5722$   $\text{\AA}$  to  $6360$   $\text{\AA}$ , which are much more complex, are nevertheless shown to arise from the same source.

A background chapter surveys the literature concerning bromine intercalation and adsorption on graphite, as well as resonant scattering from rotational energy levels of  $\text{Br}_2$  in the gas phase.

An experimental chapter discusses the equipment used in the light scattering experiments.

An experiment is proposed to study fluorescence from resonant absorptions, in order to deduce the energies of high rotational-vibrational levels of the ground state.

THESIS SUPERVISOR: Mildred S. Dresselhaus

TITLE: Abby Rockefeller Mauzé Professor of Electrical Engineering, and  
Director of the Center for Materials Science and Engineering

# MAGNETOREFLECTION AND SHUBNIKOV-DE HAAS EXPERIMENTS

## ON GRAPHITE INTERCALATION COMPOUNDS

M. S. Dresselhaus<sup>†</sup>, G. Dresselhaus<sup>\*</sup>, M. Shayegan<sup>†</sup> and T.C. Chieu<sup>†</sup>

Massachusetts Institute of Technology  
Cambridge, Massachusetts 02139

U.S.A.

### 1. Introduction

Graphite intercalation compounds represent a class of compounds with many similarities to the superlattice semiconductors prepared by molecular beam epitaxy. Intercalated graphite has recently attracted considerable attention because the addition of an intercalant can dramatically change the electronic properties of the host graphite material. For example, with the addition of  $\text{AsF}_5$ , an intercalation compound with room temperature conductivity comparable to that of copper can be achieved [1], while the addition of an alkali metal can result in a superconductor [2]. Similar to the behavior in modulation-doped superlattices, high conductivity in intercalated graphite is achieved by a charge transfer from the intercalate layer, where the mobility is low, to the high mobility graphite layers.

High magnetic fields allow use of the magnetoreflexion technique to obtain detailed information on the electronic dispersion relations within a few hundred meV of the Fermi level [3,4], and use of the Shubnikov-de Haas effect and related quantum oscillatory phenomena to provide information on the Fermi surface [5-8]. Initially it seemed difficult to reconcile the results obtained by these two high field techniques because the magnetoreflexion experiment provided strong evidence that the electronic structure near the Fermi level remained highly graphitic upon intercalation, while the Shubnikov-de Haas experiment indicated that large changes in the Fermi surface occur through intercalation. Using a recently-developed phenomenological model for the electronic structure of intercalated graphite [9], consistency between the magnetoreflexion and Shubnikov-de Haas results is demonstrated. This model also provides a basis for the calculation of the magnetic energy level structure which is needed to explain the magnetoreflexion spectra in detail.

Graphite intercalation compounds are prepared by the insertion of atomic or molecular layers of a different chemical species between layers of the graphite host material [10]. In this insertion or intercalation process, the layer structure of graphite is almost completely preserved because of the strong intraplanar binding in graphite, and likewise the intercalate layer is closely related to a layer in the parent solid. Structurally, graphite intercalation compounds exhibit the remarkable phenomenon called staging, whereby the intercalate layers are periodically arranged in a matrix of graphite layers and are characterized by a stage index  $n$ , denoting the number of graphite layers between consecutive intercalate layers. This staging symmetry is the dominant symmetry of these intercalation compounds and results in a

superlattice structure similar to that prepared in semiconductors by the molecular beam epitaxy technique. Staging is widespread among graphite intercalation compounds and well-staged samples can be prepared up to high stage ( $n \approx 10$ ). The stage determination and the c-axis repeat distance  $c$  are obtained from (00 $\lambda$ ) x-ray diffractograms. Because of the strong stage dependence found for the Shubnikov-de Haas (SdH) frequencies in the donor intercalation compounds in this work, it is necessary to carry out the measurements on single-staged samples. By careful preparation of well-staged compounds it is possible to achieve the resonance condition  $\omega_c \tau \gg 1$  required for the observation of Landau level phenomena. For both the magnetoreflexion and Shubnikov-de Haas studies, the samples were prepared by the two-zone growth technique [11] and the stage index was determined from (00 $\lambda$ ) x-ray diffractograms.

## 2. Magnetoreflexion Experiments

The magnetoreflexion measurements were made at nearly normal incidence to the c-face of the intercalated graphite samples using the Faraday geometry with magnetic fields in the range  $0 < H < 15$  Tesla [4]. Magnetoreflexion traces were taken at constant photon energy in the range  $0.1 \text{ eV} < \hbar\omega < 0.5 \text{ eV}$ , using circularly polarized light obtained with a gold-wire grid and a CsI Fresnel rhomb. Measurements were made using a cold finger dewar operating at 4.2K.

The observed magnetoreflexion spectra are in most cases qualitatively similar to those of pristine graphite, but show differences with regard to resonant magnetic fields and in some cases also differences in resonant line-shapes. Illustrative spectra are shown in Fig. 1 for an acceptor compound

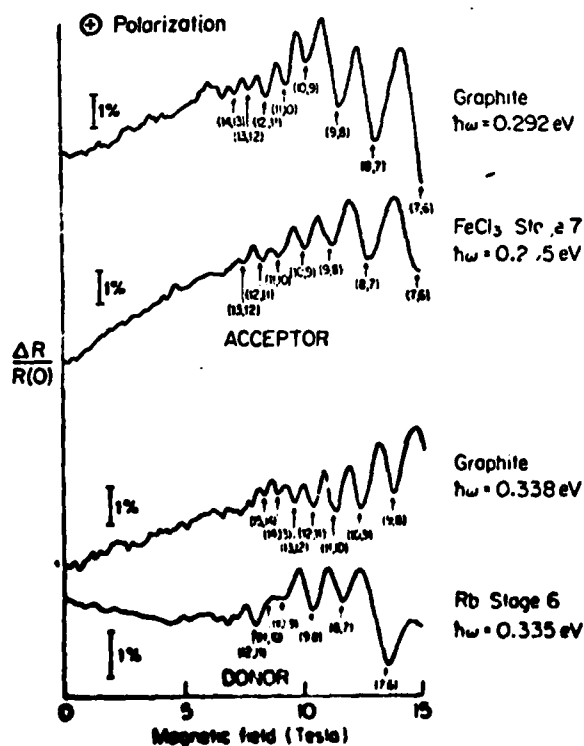


Fig. 1 Magnetoreflexion spectrum using (+) circular polarization for an acceptor compound (FeCl<sub>3</sub> stage 7) at a photon energy  $\hbar\omega = 0.295 \text{ eV}$  and for a donor compound (Rb stage 6) at  $\hbar\omega = 0.335 \text{ eV}$ . For comparison, traces for graphite are shown at comparable photon energies. The resonances are specified by the quantum numbers for the initial and final states.

(FeCl<sub>3</sub> stage 7) and a donor compound (Rb stage 6). For comparison, spectra are also included for pure graphite at similar photon energies. Each structure in Fig. 1 is identified with a K-point Landau level interband transition, specified by the quantum numbers for the initial and final states. For all compounds that have been studied, the resonant magnetic field for a given transition shifts to increasingly lower fields with increasing intercalate concentration for both (+) and (-) senses of circular polarization. The shifts of the resonant magnetic fields for a given transition are much larger for donor compounds than for acceptors of comparable stage. The intensity of the resonances (magnitude of the percent reflectivity change) is reduced with respect to that in graphite because of a reduction in relaxation time and an increase in the magnitude of the zero field reflectivity  $R(0)$ . For example, at a photon energy of  $\hbar\omega \sim 0.2$  eV,  $R(0)$  is found to be  $\sim 0.7$ ,  $0.8$ ,  $0.9$  respectively for pristine graphite, graphite-FeCl<sub>3</sub> stage 7, and graphite-Rb stage 6.

Resonant Landau level transitions are observed and are analyzed by taking spectra over a wide range of photon energies. A summary of such results for a typical intercalation compound is shown in Fig. 2, in which a comparison with results for pristine graphite is included. From this analysis it is

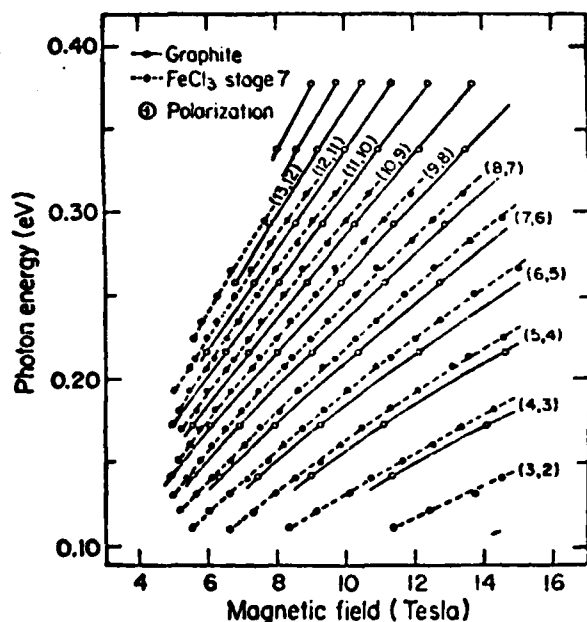


Fig. 2 Summary of resonant magnetic fields "fan chart" for photon energies in the range  $0.110 < \hbar\omega < 0.320$  eV for a FeCl<sub>3</sub> stage 7 sample using (+) circularly polarized radiation. To emphasize the similarities but measurable differences, a comparison of the results for this compound and for graphite is presented in the same photon energy range.

shown that for graphite intercalation compounds with stages  $n \geq 4$ , the electronic structure within a few hundred millivolts of the Fermi level is well described by the graphite  $\pi$ -bands, with modifications to the band parameters that can be measured quantitatively.

At constant  $\hbar\omega$ , the data in Fig. 2 and in "fan charts" constructed for other samples, are well explained by a simple two-band model approximation. Nevertheless, the mass parameters determined from such a model exhibit some dependence on  $\hbar\omega$ , since the Landau level transitions in Fig. 2 show departures from a linear dependence between  $\hbar\omega$  and resonant magnetic field. Therefore the comparison between masses for the intercalated and pure graphite samples is made at a common reference point, taken at the K-point band edge, and found by taking  $\hbar\omega \rightarrow 0$ . The results for the valence and conduction band

masses  $m_c^*$  and  $m_v^*$  thus obtained are given in Table 1 for a number of different samples. We note that in all cases, the mass parameters in the inter-

Table 1 Results of analysis of magnetoreflexion experiments

Intercalant	Stage	$m_c^*$	$m_v^*$	$(\gamma_0^2/\gamma_1)$
(HOPG)	$\infty$	0.056	0.084	25.1
AlCl <sub>3</sub>	8	0.056	0.076	26.0
	6	0.054	0.076	26.6
FeCl <sub>3</sub>	7	0.055	0.079	26.1
	5	0.054	0.075	26.6
Rb	6	0.045	0.065	31.7

calation compounds differ from the masses in graphite by only a few percent, with significantly larger changes in  $m_c^*$  and  $m_v^*$  occurring in the donor Rb compound than in acceptors of comparable stage.

Analysis of the magnetoreflexion spectra in Fig. 2, and in "fan charts" obtained for other samples with  $n \geq 4$  show that these spectra can be explained by dispersion relations which have the same form as the three-dimensional Slonczewski-Weiss-McClure (SWMcC) band model for graphite, but with modified values of the band parameters. Included in Table 1 are values for the SWMcC band parameter combination  $\gamma_0^2/\gamma_1$ , which is directly related to the reduced effective mass  $m^*$  [4].

Magnetoreflexion resonances such as in Fig. 1 are not observed below a certain photon energy, the cutoff energy  $E_x$ , which depends on both stage and intercalate species. The cutoff of K-point interband transitions below  $E_x$  is interpreted as due to the introduction of carriers by the intercalant, resulting in a shift in Fermi level  $E_F$ . Because of the Pauli exclusion principle, interband Landau level transitions are made from occupied valence to unoccupied conduction states. The lowering of  $E_F$  caused by the introduction of holes in acceptor-type compounds leads to a cutoff of Landau level transitions as  $E_F$  drops below the extremum of the magnetic subbands for the initial state. With increasing intercalate concentration,  $E_F$  moves to lower energies, therefore increasing the magnitude of  $E_x$ . In donor-type compounds the introduction of electrons causes  $E_F$  to rise, leading to the cutoff of interband transitions as  $E_F$  rises above the extremum of the magnetic subbands for the final state. Analysis of the measured cutoff photon energies yields the shift in the Fermi level relative to the K-point band edge  $|E_F - E_{3,K}^0|$ . Results for several intercalants and stages are presented in Fig. 3, where the + sign in  $E_F - E_{3,K}^0$  is for donors and the - sign for acceptors. Of significance is the much larger shift in the Fermi level in donor compounds relative to acceptor compounds of similar stage, indicating a significantly larger charge transfer in the case of donor compounds. To carry out a complete analysis of the magnetoreflexion spectra, it is necessary to use Landau levels for intercalated graphite, and this is discussed below in Section 5.

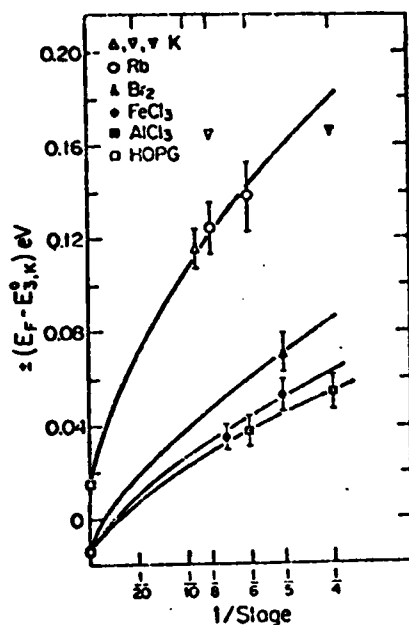


Fig. 3 Dependence on reciprocal stage ( $1/n$ ) of the Fermi level measured relative to the K-point band edge for several intercalants. The + sign for  $(E_F - E_{3,K}^0)$  applies to the donor compounds and the - sign to the acceptors. For all intercalants, the graphite value is obtained in the limit  $(1/n) \rightarrow 0$  and is denoted by open squares. The open triangle  $\nabla$  is a Shubnikov-de Haas result from the present work and the closed triangle  $\blacktriangledown$  is from magnetic susceptibility results of DISALVO ET AL [12].

### 3. Shubnikov-de Haas Experiments

Having established that the electronic levels near the Fermi level are closely identified with the graphite  $\pi$ -bands, it is of interest to explore the effect of intercalation on the Fermi surface. In this connection Shubnikov-de Haas (SdH) and other quantum transport experiments have been reported on a wide variety of graphite intercalation compounds [5-8]. The multitude of experimental results suggest that with careful sample preparation and characterization, a complete set of frequencies associated with each stage of a given intercalation system can be obtained. A number of careful experiments have already been reported. Perhaps the most complete set of data has been obtained for the graphite-K system where SUMATSU ET AL [6] give results for stages  $n = 1, 3, 4$  and we for  $n = 4, 5, 8$ . Also, results for graphite-Rb compounds have been previously reported, showing that the Fermi surfaces are not only stage-dependent, but also vary from one alkali metal intercalant to another.

To obtain quantitative information on the stage dependence of these Fermi surfaces, it is important to work with well-staged and characterized samples. Since the Fermi surfaces for the alkali metal compounds with the intercalants K and Rb are stage-dependent, staging fidelity is essential for obtaining reproducible experimental results for different samples of the same stage index. Because of the instability of alkali-metal samples in the presence of air and moisture, the samples are encapsulated in ampoules and sample handling is done in an Argon-filled dry box (<1 ppm oxygen content). The stage of the samples was determined using (002) x-ray diffraction profiles both before and after the SdH experiments, confirming that the samples were single-staged and that no desorption had occurred during the measurements.

The four-point method was used to study the in-plane transverse magnetoresistance in the temperature range  $1.4 \leq T \leq 4.2$  K and in magnetic fields up to 15 Tesla. The leads were attached to the sample using conducting epoxy. The sample was then inserted in a helium-filled ampoule and stycaast was used to seal the ampoule. The angular dependence of the SdH oscillations could then be measured by rotating the sample around the direction of the current.



such that  $\vec{I} \perp \vec{H}$  for all angles, and hence transverse magnetoresistance was always measured. Data acquisition was by computer, and the data were manipulated to obtain a Fourier power spectrum of resistance vs.  $1/H$ , thereby yielding the frequencies of SdH oscillations. These frequencies are related to the extremal cross sections of the Fermi surface. The Fourier power spectra for the SdH frequencies for stages 4, 5, 8 graphite-potassium are presented in Fig. 4.

During the course of these studies, a great deal of care was given to ensure the fidelity and reproducibility of the data. For this reason, the experiment was performed on five potassium stage 5 samples and on one of these, the measurements were repeated several weeks later after attaching new leads. While x-ray profiles after each experimental step confirmed that the samples retained their single stage identity, the magnetoresistance oscillations and the relevant Fourier power spectra revealed nearly identical traces for these stage 5 samples. Measurements done on potassium samples with different stages or on rubidium samples, however, showed distinctly different SdH frequencies. In all cases the SdH frequencies were very different from those found in pristine graphite. Hence our conclusion is that there is a unique set of SdH frequencies and Fermi surfaces associated with each stage and donor intercalant (K, Rb). SUEMATSU ET AL [6] have also shown stage dependent de Haas-van Alphen frequencies in stages 3 and 4 graphite-potassium compounds.

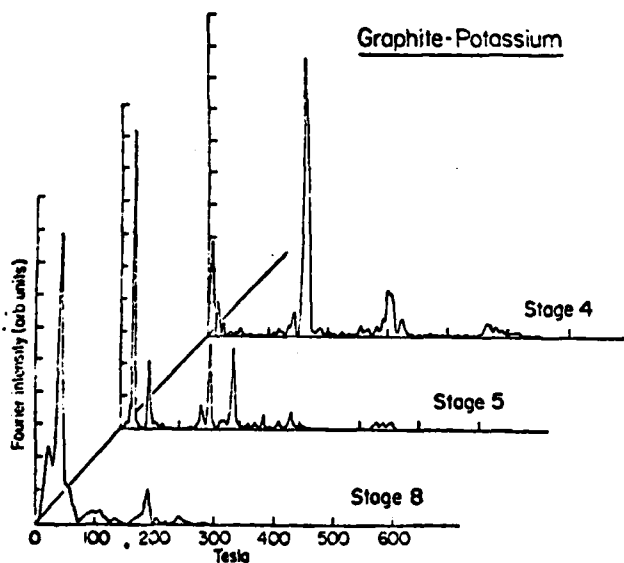


Fig. 4 Shubnikov-de Haas Fourier Transform Power Spectra for stages 4, 5 and 8 graphite-K. These power spectra were obtained by a Fourier transform of an experimental resistivity vs  $1/H$  trace for magnetic fields  $H < 15$  Tesla. The peaks in the power spectra correspond to SdH frequencies, which are given in Tesla and the same scale is used for each stage.

Poorly-staged samples also give distinct SdH frequencies. In fact more frequencies are found in mixed than in single-staged samples. Samples showing the greatest stage fidelity also show the simplest SdH spectra. The effect of mixed staging introduces additional frequencies associated with the minority phase and shifts the Fermi level to some intermediate value between those corresponding to the pure stage values. This shift in Fermi level is most sensitively observed in the very low frequency cross-sections where a small change in Fermi level can result in large shifts in frequency. There is also some indication that different in-plane intercalate densities will yield shifts in Fermi level. In fact, a detailed interpretation of the SdH spectra is expected to provide a critical test for any model of the electronic structure for these materials.

Measurements of the angular dependence of the Shubnikov de Haas frequencies (shown in Fig. 5) suggest that the Fermi surface is segmented into

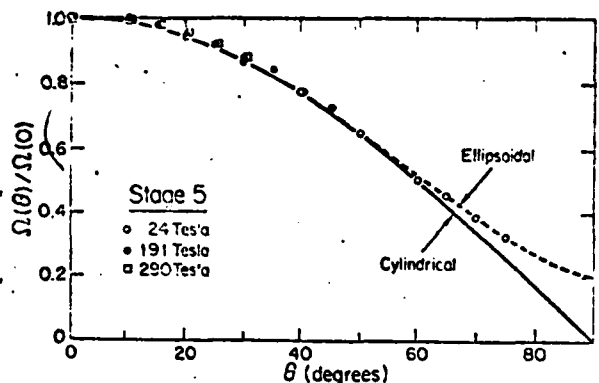


Fig. 5 Angular dependence  $\Omega(\theta)/\Omega(0)$  of several dominant SdH frequencies where  $\theta=0$  corresponds to  $H \parallel c$ -axis and the indicated frequency values are for  $\nu=0$ . The 290, 191 and 24 T frequencies are not observed above  $\sim 30^\circ$ ,  $\sim 45^\circ$  and  $\sim 75^\circ$ , respectively. The angular dependence of the 290 T and 191 T frequencies is within experimental error given by a  $\cos \theta$  dependence (solid line), characteristic of a cylindrical Fermi surface, while the 24 T frequency exhibits departures from the  $\cos \theta$  dependence at large angles.

cylindrical rings. Deviations from two-dimensional behavior is measured by small departures from the cylindrical angular dependence and by the observation of doublet SdH frequencies (Fig. 4) which indicate different cross-sectional areas at the K and H points in the Brillouin zone.

#### 4. Application of Energy Band Model

To interpret these Shubnikov-de Haas results a band model appropriate to a range of intercalate stages is necessary. Such a model for the electronic dispersion relations  $E(\mathbf{k})$  for graphite intercalation compounds is already available in terms of a Hamiltonian based on the SWMcC three-dimensional model for the graphite  $\pi$ -bands [9]. In this model the  $c$ -axis superlattice periodicity is included through a  $k_z$ -axis zone-folding of the energy levels. A unitary transformation then transforms the matrix Hamiltonian into a layer representation. For a stage  $n$  compound,  $n$  graphite layers are retained and the  $(n+1)$ st layer is replaced as a first approximation by an empty intercalate layer and for more quantitative results by an intercalate layer which interacts with the adjacent graphite bounding layers. In the "empty intercalate layer" model, the matrix Hamiltonian depends only on the graphite band parameters, and these are already known from previous experiments on pristine graphite. The magnetoreflexion experiment provides revised values for some of these band parameters, as modified by the intercalation process. Intercalant-specific interactions between the intercalant and the graphite bounding layer can then be introduced to obtain the final dispersion relations.

This model for the electronic dispersion relations has been applied to the interpretation of the observed SdH frequencies. Since the most complete set of experimental data is available for stage 5 graphite-K, the application of the energy band model is made for this case. Thus in Fig. 6 are shown the electronic dispersion relations for the five valence and five conduction  $\pi$ -bands appropriate to a stage 5 intercalation compound. The empirical position of the Fermi level  $E_F$  shown in Fig. 6 is adjusted to yield the best fit to the experimental SdH frequencies, in this case corresponding to four partially occupied conduction bands. The Fermi surface parameters obtained from this model are listed in Table 2, including calculated and observed SdH frequencies  $\Omega(0)$  for  $H \parallel c$ -axis, the cyclotron mass  $m^*/m_0$  at  $E_F$ , the trigonal warping anisotropy listed as  $k_1/k_2$ , and the electron density  $n_i$  for each carrier pocket. The values for  $k_1/k_2$  in Table 2 suggest that trigonal warping is

AD-A091 858

MASSACHUSETTS INST OF TECH CAMBRIDGE CENTER FOR MATE--ETC F/6 7/4  
ELECTRONIC AND OPTICAL PROPERTIES AND MODELING OF INTERCALATED --ETC(U)  
SEP 80 M S DRESSSELHAUS, G DRESSSELHAUS AFOSR-77-3391

UNCLASSIFIED

AFOSR-TR-80-1065

NI

2  
1  
1  
1

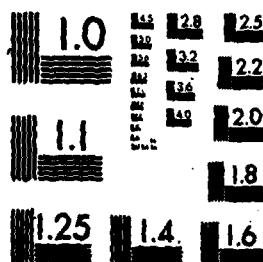


END  
DATE  
FILMED  
1-84  
DTIC

551F1E

2 OF 2.

ADA  
09108



MICROCOPY RESOLUTION TEST CHART  
NATIONAL BUREAU OF STANDARDS-1963-A

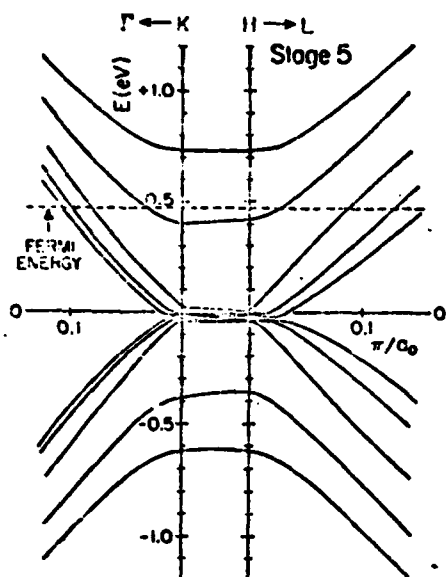


Fig. 6 Electronic band structure in the vicinity of the HK axis near the Fermi level for a stage 5 "empty intercalate layer" model for a graphite intercalation compound. The Fermi level is determined to fit the observed SdH frequencies. For the indicated Fermi level four of the conduction bands are partially occupied and give rise to Fermi surfaces and carrier pockets.

Table 2 Fermi surface parameters associated with stage 5 graphite-K

Fermi Surface Parameters	K-point Band Designations			
	$K_1$	$K_2$	$K_3$	$K_4$
$m^*/m_0$	0.143	0.115	0.0828	0.0511
$n_1 (\times 10^{20} \text{ cm}^{-3})$	2.36	1.76	0.975	0.138
Calculated SdH Frequencies $\Omega(0)$	401	300	163	26.7
Observed $\Omega(0)$ (Tesla)	453 430	290 267 243	191 152 135	24 18
Trigonal Warping Anisotropy $k_1/k_2$	0.68	0.77	0.91	1.00

important for the larger cross-sectional areas with heavier masses, whereas the smaller light mass cross-sections are circular. The generally good agreement of the observed SdH frequencies with the empty intercalate layer model of Fig. 6 suggests that the effect of intercalant-graphite bounding layer interactions can be treated as a perturbation and evaluated by fitting the model quantitatively to the observed SdH frequencies. It should be noted that the volumes of the carrier pockets for the four occupied bands in Fig. 6 correspond to a charge transfer of  $\approx 0.3$  electrons per intercalant into these carrier pockets, suggesting that other carrier pockets could be present elsewhere in the Brillouin zone.

### 5. Landau Level Calculation

The empty intercalate layer model used to calculate the Fermi surface can

also be applied to compute the Landau levels. The results of such a calculation are shown in Fig. 7 for a stage 3 intercalation compound. For a

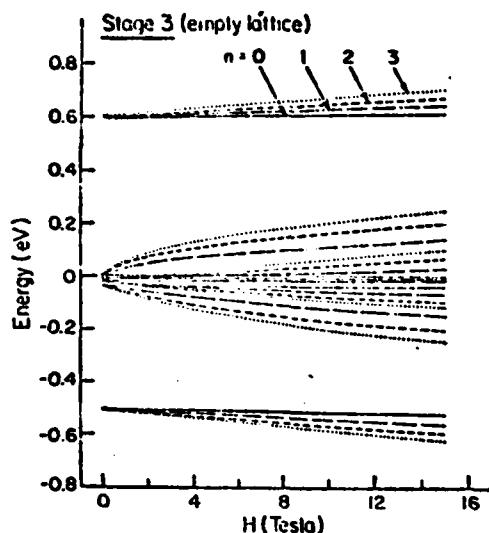


Fig. 7 Magnetic field dependence of the four lowest quantum number Landau levels at  $k=0$  for a stage 3 graphite intercalation<sup>2</sup> compound, calculated on the basis of an 'empty intercalate layer' model. The middle set of levels correspond to the  $E_3$  levels of graphite while the upper and lower sets correspond respectively to the  $E_1$  and  $E_2$  levels.

stage 3 compound, model calculations yield three conduction bands and three valence bands, such that two of the three conduction and valence bands lie close to each other in the vicinity of the HK axis, leaving one higher-lying conduction band and one lower-lying valence band. (See Fig. 6 where the levels for a stage 5 compound are shown.) The near-degeneracy of the four bands for the case of stage 3 results in magnetic level crossings as shown in Fig. 7. In this calculation the trigonal warping is also neglected ( $\gamma_3=0$ ) and only linear  $\kappa$  terms in the off-diagonal magnetic Hamiltonian are retained. Under these assumptions the Landau levels can be calculated exactly and the usual optical selection rules apply ( $\Delta n=\pm 1$ ). The central set of levels in Fig. 7 correspond to the K and H point transitions between the pristine graphite  $E_3$  bands, including levels arising from  $k_z$ -axis zone folding. On the other hand, the upper and lower Landau levels of Fig. 7 are associated with the  $E_1$  and  $E_2$  graphite bands. Landau level transitions involving these bands are analogous to the H-point transitions in pristine graphite.

Assuming that the Fermi level in a stage 3 donor compound lies between the central and upper group of magnetic energy levels (see Fig. 7), additional sets of Landau level transitions are predicted, corresponding to the excitation of an electron from the central set of levels to the upper set. Such excitations require a photon energy of  $\sim 0.6$  eV which is in excess of the photon energies employed to date in the magnetoreflexion experiments on intercalated graphite. The Landau level calculation itself is vital for the detailed analysis of the magnetoreflexion experiment with regard to identification of the observed resonant structures, selection rules for Landau level transitions and lineshape analysis for determination of the resonant point within the experimental linewidth. To carry out such a detailed analysis it is necessary to include explicitly the interaction between the intercalant and the graphite bounding layers. In turn, such an analysis provides a sensitive method for the experimental determination of the magnitude of these interaction parameters.

The Shubnikov-de Haas oscillations in the conductivity are also related to the Landau levels shown in Fig. 7. However, for those cross sections with fast frequencies where trigonal warping (see Table 2) is important, it

is necessary to also include explicitly the trigonal warping parameter  $v_3$  and higher terms in  $\kappa$  in order to make a quantitative fit to be experimental SdH frequencies. A systematic fit of both Shubnikov-de Haas and magneto-reflection data for a single series of compounds is now underway and is expected to result in precise determination of the interaction between the intercalant and the graphite bounding layers.

## 6. Acknowledgements

We gratefully acknowledge S. Y. Leung for valuable discussions and Mr. L. Rubin and Dr. R. L. Aggarwal of the Francis Bitter National Magnet Laboratory for technical assistance and AFOSR Grant #77-3391 for support of this research.

† Center for Materials Science and Engineering and Department of Electrical Engineering and Computer Science

\* Francis Bitter National Magnet Laboratory, supported by the National Science Foundation

1. G.M.T. Foley, C. Zeller, E.R. Falardeau and F.L. Vogel, Solid State Commun. 24, 371 (1977).
2. Y. Koike, H. Suematsu, K. Higuchi and S. Tanuma, Physica 99B, 503 (1980).
3. D.D.L. Chung and M.S. Dresselhaus, Solid State Commun. 19, 227 (1976); Physica 89B, 131 (1977).
4. E. Mendez, T.C. Chieu, N. Kambe and M.S. Dresselhaus, Solid State Commun. 33, 837 (1980).
5. A.S. Bender and D.A. Young, J. Phys. C. Solid State Phys. 5, 2163 (1972).
6. H. Suematsu, K. Higuchi and S. Tanuma, J. Phys. Soc. Japan 48, 1541 (1980).
7. I. Rosenman, F. Batallan and G. Furdin, Phys. Rev. B20, 2373 (1979).
8. G. Dresselhaus, S.Y. Leung, M. Shayegan and T.C. Chieu, Synthetic Metals (in press).
9. G. Dresselhaus and S.Y. Leung, Solid State Commun. (in press).
10. A. Hérolde, Physics and Chemistry of Materials with Layered Structures (ed. F. Lévy), Reidel, Dordrecht, Holland 6, 323 (1979).
11. D.E. Nixon and G.S. Parry, J. Appl. Phys. 1, 291 (1968).
12. F.J. DiSalvo, S.A. Safran, R.C. Haddon, J.V. Waszczak, and J.E. Fischer, Phys. Rev. B20, 4883 (1979).